Zinc oxide nanocomposites of selected polymers: Synthesis, characterization and corrosion inhibition studies on mild steel in HCl solution

TW Quadri

orcid.org/0000-0003-4845-6448

Dissertation submitted in fulfilment of the requirements for the degree *Master of Science in Chemistry* at the North-West University

Supervisor: Prof EE Ebenso
Co-supervisors: Dr LO Olasunkanmi
Dr OE Fayemi

Graduation May 2018

Student number: 28293622

NWU®
NORTH-WEST UNIVERSITY
NOORDWES-UNIVERSITEIT
UNIBESITI YA BOKONE-BOPHIRIMA

DECLARATION

I hereby declare that the work presented in this dissertation entitled "Zinc oxide nanocomposites of selected polymers: Synthesis, characterization and corrosion inhibition studies on mild steel in HCl solution" submitted to the Department of Chemistry, North-West University, Mafikeng Campus in fulfilment of the requirements for the degree of Master of Science in Chemistry was compiled and written by me under the supervision of Prof. Eno E. Ebenso and has not been included in any other research work submitted previously by any other student at the North-West University or any other University. Sources of my information are acknowledged in the reference pages.

.....

Taiwo Wasiu Quadri

DEDICATION

I dedicate this dissertation to the Godhead – God the Father, God the Son and God the Holy Spirit. I thank the *"I AM THAT I AM"* through whom I can say *"I am what I am"*. He has given me inestimable life, unmerited grace and uncommon favour to start and successfully complete this project.

ACKNOWLEDGEMENTS

First and foremost, I would like to specially thank my amiable supervisor and mentor, Prof. Eno E. Ebenso. Words will not suffice to thank you for your motivation, patience and support all the way. Thank you sir for your outstanding fatherly role, intellectual input and impact, and undeniable moral support ever since I became your student. The thought of you alone is a motivation and drive to move on. I am indeed grateful to you sir.

I would like to also specially thank my co-supervisors, Dr. Lukman O. Olasunkanmi and Dr. (Mrs.) Omolola E. Fayemi. You have both shown me immeasurable support both academically and otherwise in ways I cannot describe. You have both played the roles of mentors, parents and guardians to me.

I would also like to appreciate the National Research Foundation and the North-West University for their financial supports towards the completion of my MSc. programme.

My sincere appreciation also goes to all staff members of the Chemistry Department of North-West University (Mafikeng campus), in particular Mr. Kagiso Mokalane and Mr. Sizwe Loyilane. I would like to appreciate Dr. Anine Jordaan of Chemistry Department, North West University (Potchefstroom campus). I also want to acknowledge the support of colleagues and members of the MaSIM Research Group among which are Mashuga Motsie, Henry Nwankwo, Gnanapragasam Raphael, Katlego Masibi, Palesa Tsele.

My acknowledgements would be incomplete without a word of appreciation to Prof. O. S. Oyediran and the entire Tidings family. Thank you sir for the all-time care, love, support, motivation and advice you have generously offered. Many thanks also to my spiritual family, members and leaders of Deeper Life Campus Fellowship in Lagos and South Africa.

I say thanks to my family and friends. I sincerely appreciate my parents and siblings for their unalloyed love, support and prayers. My load of friends in various countries of the world have been wonderful companions and friends indeed though separated by distance. You have given worthwhile encouragement and prayers along the journey. You are all appreciated without exception.

ABSTRACT

Corrosion inhibition potentials of polyethylene glycol (PEG), polyvinylpyrrolidone (PVP) and polyacrylonitrile (PAN) and their zinc oxide (ZnO) nanocomposites were evaluated for mild steel in 5 % HCl solution. The ZnO-polymer nanocomposites were synthesized and characterized using Fourier transform infrared (FTIR) spectroscopy, ultraviolet visible (UV-vis) spectroscopy, thermogravimetric analysis (TGA) and transmission electron microscopy (TEM) techniques. The FTIR and UV-vis spectra suggested successful formation of the polymer-ZnO nanocomposites. The TGA curves revealed that each of the synthesized polymer nanocomposites is more thermally stable than the corresponding parent polymer. The surface morphologies of the ZnO nanoparticles obtained from TEM study revealed that the nanomaterials were rod-like in shape with an estimated size of 50 – 75 nm. Corrosion inhibition efficiencies were obtained from potentiodynamic polarization (PDP), linear polarization resistance (LPR) and electrochemical impedance spectroscopy (EIS) measurements. The electrochemical results showed that both the selected polymers and their ZnO nanocomposites inhibit mild steel corrosion in 5 % HCl. The protection performances of the polymers and their polymer nanocomposites were compared and the results showed that the polymer nanocomposites exhibited higher inhibition efficiency than the polymers alone. The results of potentiodynamic polarization studies revealed that both the polymers and their ZnO nanocomposites are mixed-type inhibitors. The EIS results suggested that the polymers and their zinc oxide nanocomposites inhibit mild steel corrosion in 5 % HCl solution by adsorbing on mild steel surface to form protective film. Anticorrosion potentials of the selected polymers and their ZnO nanocomposites were also proven by scanning electron microscopy (SEM). The adsorption studies show that the polymers and the ZnO nanocomposites obeyed Langmuir adsorption isotherm.

Key Words: HCl solution; Mild steel; EIS; Polarization; Polymers; Polymer nanocomposites; Langmuir adsorption isotherm

LIST OF ABBREVIATIONS

Ag/AgCl	Silver/silver chloride
AFM	Atomic force microscopy
CTAB	Cetyltrimethyl ammonium bromide
CeO_2	Cerium oxide
DMF	Dimethylformamide
DMS	Molecular dynamic simulations
EDAX	Energy dispersive x-ray analysis
EDS	Energy dispersive x-ray spectroscopy
EIS	Electrochemical impedance spectroscopy
Fe_2O_3	Iron II oxide
Fe_3O_4	Iron III oxide
$Fe(OH)_2$	Ferrous hydroxide
FTIR	Fourier transform infrared spectroscopy
GNP	Gross national product
GPC	Gel permeation chromatography
H_2SO_4	Sulphuric acid
HCl	Hydrochloric acid
IE	Inhibition efficiency
KBr	Potassium bromide
KCl	Potassium chloride
NaOH	Sodium hydroxide
NACE	National association of corrosion engineers
NMR	Nuclear magnetic response spectroscopy

PAN	Polyacrylonitrile
PANI-PAAm/Fe_3O_4	Magnetite-containing polyaniline-polyacrylamide nanocomposite
PDMAEMA-PU	Poly(dimethylaminoethylmethacrylate)-b-polyurethane-b-poly (dimethylaminoethylmethacrylate)
PDP	Potentiodynamic polarization
PEG	Polyethlyene glycol
PIn	Polyindole
PNVP-PU	Poly(N-vinylpyrrolidone)-b-polyurethane-b-poly (N-vinylpyrrolidone)
PPG/AgNPs	Polypropylene glycol/silver nanoparticles
PVP	Polyvinylpyrrolidone
SDBS	Sodium dodecyl benzene sulfonate
SEM	Scanning electron microscopy
SiC	Silicon carbide
TEM	Transmission electron microscopy
TERP-1	Oligopolymer derived from α-naphthol (N), formaldehyde (F) with aniline
TERP-2	Oligopolymer derived from paraaminobenzoic acid
TERP-3	Oligopolymer derived from sulphanilic acid
TGA	Thermogravimetric analysis
TiO_2	Titanium oxide
UV-vis	Ultraviolet visible spectroscopy
$Zn(NO_3)_2.6H_2O$	Zinc nitrate hexahydrate
ZnO	Zinc oxide

LIST OF SYMBOLS

ac	Alternating current
b_a	Anodic Tafel slope
b_c	Cathodic Tafel slope
^oC	Temperature in degree Celsius
C_{dl}	Double-layer capacitance
CPE	Constant phase element
ε	Dielectric constant
ε_o	Permittivity of free space
eV	Electron volt
E^o	Standard electrochemical potential
E	Electrochemical potential
E_a	Activation energy
π	Pi
F	Faraday constant
h	Hour
Hz	Hertz
K	Kelvin
kJ mol^{-1}	Kilo Joule per mole
kV	Kilovolt
M	Molar
mM	Millimolar
min	Minute
mL	Millilitre

mV	Millivolt
nm	Nanometre
mdd	Milligrams per square decimetre per day
mmpy	Millimetres per year
mpy	Mils per year
ppm	Parts per million
R	Universal gas constant
R_{ct}	Charge transfer resistance
R_p	Polarization resistance
R_s	Solution resistance
s	Second
% wt	Percentage weight
ω	Angular frequency
W	Warburg impedance

LIST OF FIGURES

LIST OF TABLES

TABLE OF CONTENTS

CHAPTER 1

INTRODUCTION

1.1 HISTORICAL BACKGROUND OF CORROSION

Corrosion is as old as the earth itself. Since ancient times, corrosion has continually affected the quality of the daily life of man and his technical progress. It is an inevitable and undesirable occurrence which destroys the beauty and lustre of materials and reduces their lifespan. Corrosion is commonly called rust in iron and is known to man by other names such as degradation, deterioration or destruction. Corrosion occurs in metals, as well as in plastics, ceramics and composites [1].

Several renowned scientists, philosophers and writers have made invaluable observations and contributions on corrosion and its effects in their works. Earliest among them was Herodotus (fifth century BC) who proposed the protection of iron with tin. Also, a Roman Philosopher, Pliny the elder (AD 23-79) wrote extensively about the degradation of iron in his essay "*Ferrum Corrumpitar*". In 1819, Thenard discovered the electrochemical nature of corrosion process. A decade later, Hall established that iron will only rust in the presence of oxygen. In later years, Michael Faraday made more contributions that became very useful when he discovered a quantitative relationship between chemical action and electric current. His first and second laws of electrolysis became the basis for calculating the rate of corrosion of metals. Over the years, several researchers, organizations and institutions have continued to make great contributions to the study of corrosion with the aim of minimizing the effects of corrosion using various techniques [1, 2].

1.1.1 DEFINITION OF CORROSION

The word "corrosion" originates from Latin. The Latin word *rodere* means "gnawing," and *corrodere* means "gnawing to pieces" [2]. Corrosion is a naturally occurring phenomenon commonly defined as deterioration of metal caused by reaction with the surrounding environment [1]. Such surrounding environment could be water, moisture in air, acids, bases, salts, aggressive metal polishes and other corrosive solids and chemicals. Corrosion remains a worldwide scientific and industrial problem as it affects the metallurgical, chemical, construction and oil industries [1-4]. Figures 1.1 and 1.2 represent cases of corrosion related to oil industry and transportation.

Figure 1.1: Oil pipeline corrosion [5]

Figure 1.2: Corrosion effect in a train [6]

Fontana [7] defined corrosion as the destruction or deterioration of a material as a result of its reaction with its environment. Thus, corrosion is not only limited to metals but also extends to all natural and synthetic materials such as ceramics, polymers, papers, glasses and wood. Corrosion of metals can be said to be the loss of useful intrinsic properties such as malleability, ductility, density, electrical conductivity and optical reflectivity by metal due to attack of the environment [8]. Amongst many metals, corrosion is experienced strongly in iron and steel. This is because the oxide that is formed during the oxidation process does not hold firmly to the surface of the metal, which makes it to erode off the metal surface quite easily [9, 10].

Corrosion can be alternatively understood by comparing it with extraction of metals from the earth. Large amounts of energy are expended when structural metals such as iron, aluminium, zinc are extracted from their ores or natural state. These extracted metals can be said to be in a metastable state and tend to lose their energy by reverting to compounds more or less similar to their original state. The transformation of these metals from the metastable state to a more energetically stable state is referred to as the corrosion process [10].

1.1.2 CONSEQUENCES OF CORROSION

The consequences of corrosion cut across several aspects of human life. Corrosion is known to adversely affect health, safety, economy, culture and technology. These aforementioned consequences of corrosion are discussed below [1, 7, 10]:

Health effects: Human beings continuously make use of metals and metal products. These include the metal piercing on their bodies. The other well-known example is the application of metallic utensils and cutleries such as pots, plates, cups and spoons by human beings. When these metallic utensils and cutleries are affected by corrosion, human health can be at high risk.

Safety effects: Most transportation systems are made of metals and these include cars, trains, airplanes and ships. If any of the metals that are used in the construction of these transport systems experience corrosion failure, the passengers may be at risk of an accident. Metals are also heavily used in construction of buildings and bridges and if these metals corrode, the safety of the people using the facility is not guaranteed.

Economic effects: The economy of each and every country has significant contribution from the industries in that country. Many of these industries make use of metal products to construct the transportation and storage of their industrial products. For instance, gas and petroleum industries use metals for their fluid carrying pipes and tanks. These industries spend a huge sums of money to minimize corrosion in order to avoid economic loss due to metal corrosion.

Cultural effects: The statues of our heroes such as political or social heroes are often constructed from metallic products. These statues are considered to be very important in the

national life as they are held in high esteem. Since those statues are made from metals, they are susceptible to corrosion attack and therefore impact the cultural beliefs of that nations.

Technological effects: Technological gadgets, devices and equipment are often constructed from metallic products. These include electricity power stations and solar energy systems. When these materials are exposed to corrosive environments such as high temperatures or pressures, the technological effect is experienced.

1.1.3 COST OF CORROSION

The cost of corrosion is enormous. There are several direct and indirect costs incurred as a result of corrosion. Below are some major cost effects of corrosion [1, 10]:

i. Reduction of metal thickness leading to loss of mechanical strength and structural failure or breakdown. When the metal is lost in localized zones, leading to a crack-like structure, very considerable weakening may result from quite a small amount of metal loss.
ii. Leaking containers, storage tanks, water and oil transportation lines and fuel tanks cause significant loss of product and may generate severe accidents and hazards.
iii. Loss of time in availability of profit-making industrial equipment.
iv. Reduced value of goods due to deterioration of appearance.
v. Corrosion products may contaminate chemicals, pharmaceuticals, dyes and packaged goods with direct consequences to consumers.
vi. Perforation of vessels and pipes allowing escape of their contents and possible harm to the surroundings.
vii. Loss of technically important surface properties of a metallic component. These could include frictional and bearing properties, ease of fluid flow over a pipe surface, electrical conductivity of contacts, surface reflectivity or heat transfer across a surface.
viii. Mechanical damage to valves and pumps or blockage of pipes by solid corrosion products cause loss of efficiency.
ix. Added complexity and expense of equipment which needs to be designed to withstand a certain amount of corrosion, and to allow corroded components to be conveniently replaced.

x. Nuclear hazards like the Chernobyl disaster of 1986 is a practical example of transport of radioactive corrosion products in water which are fatal to human, animal and biological life.

Countries worldwide spend a large financial expenditure to combat the effects of corrosion. Studies on the cost of corrosion undertaken by several countries including the United States, United Kingdom, Japan, Australia, Kuwait, Finland, Sweden, Germany, India and China revealed that the annual corrosion costs ranged from about one to five percent of the Gross National Product (GNP) of each nation [12]. In South Africa, the research conducted by the Council for Mineral Technology group showed that the direct cost of corrosion to the South African economy was R130-billion per annum in 2004. This cost is expected to increase with advancement in technology and metals utilization. Intensive studies and researches conducted on the prevention of corrosion. Literature revealed that corrosion prevention is more cost-effective than repairing gadgets, equipment and structures damaged by corrosion [13].

1.1.4 CLASSIFICATION OF CORROSION

Corrosion can be classified in different ways. A classification based on environment is given below [7]:

1. Chemical or Dry Corrosion

This type of corrosion takes place in the absence of a liquid phase or above the dew point of the environment. The corrodents are usually vapours and gases. Dry corrosion is often associated with high temperature. A good example is the attack on stainless steel by furnace.

2. Electrochemical or Wet Corrosion

Wet corrosion takes place in the presence of a liquid. It usually involves an aqueous solution or electrolyte. This is the most common type of corrosion. A good example is corrosion of turbine blade by water.

1.1.5 FORMS OF CORROSION

Corrosion of metal mainly has two forms; uniform and localized. Uniform corrosion is accountable for the greatest tonnage of metal degraded though it is easier to control. Localized

forms of corrosion are unpredictable and more difficult to control than general corrosion [14]. The different forms corrosion takes are described below [1, 2, 7, 10]:

General Corrosion: This is the simplest and most common type of corrosion. It is also known as uniform attack. It is characterized by a chemical or electrochemical reaction which occurs at a uniform rate over the entire exposed surface of a metal. The metal becomes thinner and eventually experiences failure. An example is a piece of iron immersed in dilute sulphuric acid [7].

Galvanic corrosion: This is also referred to as two-metal or bimetallic corrosion. It occurs when two dissimilar metals in electrical contact are immersed in a corrosive environment. The more active metal acts as the anode while the more noble metal acts as the cathode. Galvanic corrosion is more pronounced at the junction of the two dissimilar metals and the intensity of the attack decreases with increasing distance from the junction [2, 7].

Crevice corrosion: This is a localized corrosion which occurs within crevices and shielded areas on metal surfaces exposed to corrosive materials. This form of corrosion is connected with small volumes of stagnant solution trapped in lap joints, gasket surfaces, surface deposits, clamps, fastener heads. This form of corrosion is sometimes called deposit or gasket corrosion [2, 7, 15].

Filiform corrosion: Filiform corrosion is a special case of crevice corrosion which occurs under painted or plated surfaces when moisture finds it way under them. For instance, products below coatings of paints, rubber, lacquer, paper etc. are often affected. The components of the material is weakened and the surface appearance is also affected thereby reducing the sale potential of the material [1, 10].

Pitting: Pitting is a form of extremely localized attack that results in holes or pits in the metal. These holes may be small or large in diameter, but in most cases they are relatively small. Pits are sometimes isolated or so close together that they look like a rough surface. Pitting is one of the most destructive forms of corrosion [2, 16].

Intergranular corrosion: This form of localized corrosion occurs with alloys when potential difference exist between the grain and the grain boundary. This results in the disintegration of

the alloy and loss of its strength. Intergranular corrosion can be caused by impurities at the grain boundaries, enrichment of one of the alloying elements or depletion of one of the elements in the grain-boundary areas [2, 15, 16].

Erosion corrosion: Erosion corrosion is caused by increase in the rate of attack on a metal because of the relative motion between a corrosive medium and the exposed metal surface. This rapid motion causes mechanical wear effects. The metal is removed from the surface as dissolved ions or it forms solid corrosion products which are mechanically swept from the metal surface. Erosion corrosion is characterized in appearance by grooves, gullies, waves, rounded holes and valleys. It is also called impingement corrosion [2, 7, 15].

Stress corrosion cracking: Stress-corrosion cracking involves material cracking caused by the combined influence of tensile stress and a specific corrosive environment. During stress-corrosion cracking, the metal or alloy may be virtually unaffected over most of its surface, while fine cracks progress through it [2, 10, 16].

Exfoliation: This a more intense form of intergranular corrosion that results in the accumulation of corrosion products in grain boundaries leading to removal of metals as layers from an alloy. It occurs mostly in wrought products such as high-strength aluminium. Examples can be found in Zn-Mg-Cu and Al-Zn-Mg-Cu alloys [1, 15].

Dealloying: Dealloying otherwise known as selective leaching is the removal of one element from a solid alloy by corrosion processes. It is an uncommon form of corrosion found in copper alloys, cast iron and some other alloys. It occurs when the alloy loses the active component of the metal and retains the most corrosive resistant component as a porous "sponge" on the metal surface. Common examples are dezincification (selective removal of zinc metal from brass) and graphitization (selective removal of graphite from grey cast iron) [1, 2, 15].

Corrosion fatigue: Corrosion fatigue is a special case of stress corrosion caused by the combined effects of cyclic or fluctuating stress and a corrosive medium. This results in a sharp reduction in the fatigue limit of the metal parts which are dynamically loaded in the corrosive environment [1, 2, 10].

Fretting corrosion: This form of corrosion is a combination of wear and corrosion. It is increased by the relative movement between contacting surfaces when they are subjected to minute amplitude oscillations. Fretting corrosion occurs when the oscillatory motion between the surfaces in contacts are in the tangential direction. Examples of vulnerable components are shrink-fits, smoking rivets, bolted parts, press fits and spines [2, 7].

Microbiological corrosion: Microbiological corrosion is caused by the activities of various micro-organisms such as bacteria, algae, fungi etc. Conventional corrosion control techniques and use of biocides can be employed in the inhibition of microbial corrosion [17].

Figure 1.3 gives a general illustration of the various forms of corrosion that can occur in metals.

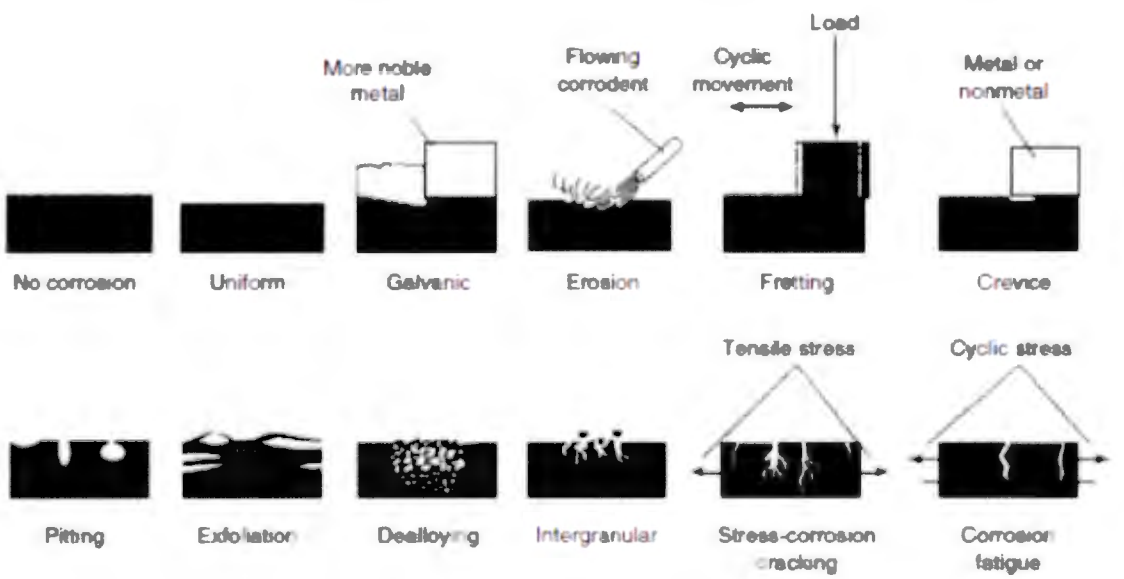

Figure 1.3: Illustration of common forms of corrosion [10]

1.1.6 RATE OF CORROSION

The process of corrosion involves weight loss of the corroding material. This loss per unit time is often expressed as the rate of corrosion. The rate of corrosion can also be defined as the speed or kinetics at which metals corrode in a particular medium [1]. The corrosion rate of a material is dependent upon the nature of the material and the environmental conditions [15]. There are materials that are incapable of producing a passive film and others that are capable.

The rate of corrosion in those substances that have the ability to form a passive film is much slower when compared to those that do not have the ability to produce the passive film. When a thin protective layer oxide (passive film) is formed on the surface of the metal, the phenomenon is known as passivation.

The rate at which the corrosion occurs is of great importance and is usually expressed in one of these two ways:

- Weight loss per unit area per unit time, usually mdd (milligrams per square decimetre per day).
- Decrease in thickness per unit time i.e., rate of penetration or the thickness of metal lost. This may be expressed in American units, mpy (mils per year) or in metric units or mmpy (millimetres per year).

The important factors which may influence the corrosion process include the position of the metal in the galvanic series, purity of the metal, relative area of the anode and cathode, nature of the surface film, temperature, pH, nature of dissolved gases and salts, flow velocity etc. [8].

1.1.7 MECHANISM OF CORROSION

Corrosion is generally caused by an electrochemical inhomogeneity in metal or its environment. When in contact with an electrolyte, metals corrode when areas of higher free energy or potential behave as anodes and those of lower free energy or potential behave as cathodes, thereby creating a corrosion cell. Metal ions are produced at the anode and dissolve into the electrolyte. The electrons pass through the metal to the adjacent cathode areas where they react with the environment. This flow of electrons from the anode to cathode and the associated charge transfer through the electrolyte from the cathode to the anode constitute the corrosion current. The corrosion rate is, therefore, associated with the corrosion current. The process of corrosion can be represented by the following reactions [5, 18].

(1) **Anodic reaction**: The electrochemical reaction at the anode or metal dissolution can be written as

$$M \rightarrow M^{n+} + n\, e^{-} \qquad (1.1)$$

The released electrons migrate to the cathode through the metal producing corrosion current.

(2) **Cathodic reaction:** The nature of the reaction at the cathode (in which the electrons released in anodic dissolution are consumed) depends upon the nature of the environment. The most common cathodic reactions that are encountered in corrosion are as follows:

(A) Oxygen reduction (Acid solution)

$$O_{2\,(g)} + 4H^{+} + 4\,e^{-} \rightarrow 2H_2O \qquad (1.2)$$

(B) Oxygen reduction (Neutral or basic solution)

$$O_{2\,(g)} + H_2O_{\,(l)} + 2\,e^{-} \rightarrow 2\,(OH)^{-} \qquad (1.3)$$

(C) Hydrogen evolution

$$2\,H^{+}_{\,(aq)} + 2\,e^{-} \rightarrow H_{2\,(g)} \qquad (1.4)$$

(D) Metal ion reduction: Metal ions present in solution may be reduced:

$$M + e^{-} \rightarrow M^{(n-1)+} \qquad (1.5)$$

This can occur only if there is a high concentration of M^{n+} ions. In this reaction, the metal ion decreases its valence state by accepting an electron.

(E) Metal deposition: Metal may be reduced from an ionic to a neutral metallic state:

$$M^{n+} + e^{-} \rightarrow M \qquad (1.6)$$

Hydrogen evolution is common since acidic media are frequently encountered. Oxygen reduction is also common since any aqueous solution in contact with air is capable of promoting this reaction. Metal ion reduction and metal deposition are less common reactions. These partial reactions can be used to understand most of the corrosion processes; for example, corrosion of plain mild steel in water (Figure 1.4).

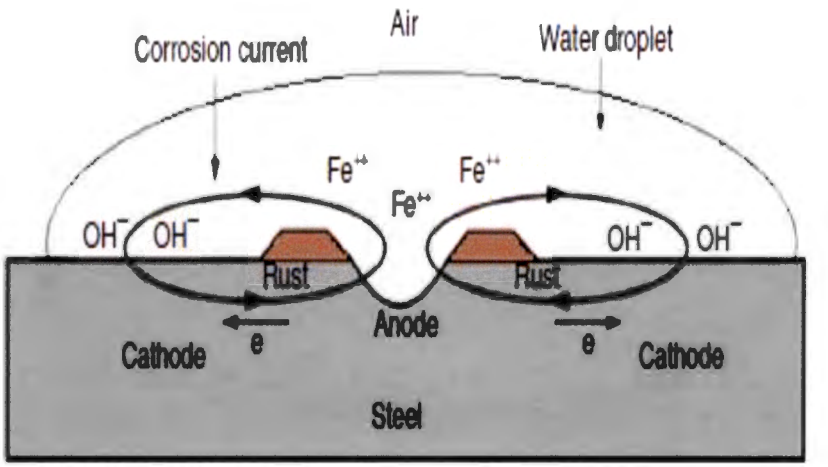

Figure 1.4: Electrochemical processes involved in the formation of rust [18]

The corrosion process occurs in two steps. In the first stage, areas covered by a water droplet are precluded from oxygen supply and become anodic compared to the other areas that are freely exposed to air. Thus, plain mild steel, in contact with any electrolyte, low in dissolved oxygen will be anodic with respect to plain mild steel, in contact with electrolyte, rich in dissolved oxygen. A principal reason for this is that in an area with water rich in oxygen the following reaction will take place:

$$O_{2\,(g)} + 2H_2O_{\,(l)} + 4\,e^- \rightarrow 4\,OH^- \qquad (1.7)$$

This is a cathodic reaction because it absorbs electrons. There will be a greater amount of oxygen available near the edge of the water droplet and this area will become cathodic with hydroxyl ions that are formed. The electrons will be supplied from another part of the metal where there is less oxygen and so such areas act as anodes. At the anodic area under the centre of the water droplet, electrons will be generated by the reaction:

$$Fe \rightarrow Fe^{2+} + 2\,e^- \qquad (1.8)$$

The Fe^{2+} cations will move through the electrolyte toward the cathode and the $(OH)^-$ anions will tend to move toward the anode. Migration of the oxidative product (Fe^{2+}) from the anode and the reduction product (OH^-) from the cathode occurs until they combine to form ferrous hydroxide.

$$Fe + 2H_2O + O_2 \rightarrow 2Fe^{2+} + 4\,OH^- \rightarrow Fe(OH)_2 \qquad (1.9)$$

Ferrous hydroxide ($Fe(OH)_2$) precipitates, due to its insolubility, from the oxygenated aqueous solution and settles as deposit near the cathode area. In the second stage, at the outer surface of the $Fe(OH)_2$ layer, access to dissolved oxygen converts the ferrous hydroxide to insoluble and the hydrous ferric hydroxide as follows:

$$2Fe(OH)_2 + ½\ O_2 + 2H_2O \rightarrow 2Fe(OH)_3 \qquad (1.10)$$

Reddish brown ferric hydroxide, $Fe(OH)_3$, is known normally as red rust which forms in the initial stages of corrosion and gradually changes to ferric oxy-hydroxide, FeOOH. Different forms of ferric oxy-hydroxides are also termed as red rust. When $Fe(OH)_3$ is dehydrated it becomes ferric oxide:

In the case of limited oxygen supply, this reaction results in the formation of black magnetite (Fe_3O_4). Once a rust deposit has formed on the steel surface, the area under the porous deposit will become oxygen deficient and, hence, anodic compared to the bare steel. In addition, the rust layers are not protective because they are permeable to air and water. Therefore, the dissolution of steel can continue, unobserved, below the layer of rust [18-20].

1.1.8 KINETICS AND THERMODYNAMICS OF CORROSION

Kinetics of Corrosion

The kinetics of corrosion gives helpful information on how the rate of corrosion proceeds in a medium at a given time. The basic reactions which takes place during corrosion produce and consume electrons which can be quantified as electrical current.

More information on the electrochemical behaviour of metals in corrosive media can be generated through the influence of temperature on the kinetic process of corrosion. Arrhenius law shows the existing relationship between the rate constant of chemical reactions and the temperature [21].

$$k = Ae^{-E_a / RT} \qquad (1.11)$$

where: k = rate constant

A = pre-exponential factor

R = universal gas constant

E_a = activation energy

T = absolute temperature

According to Equation 1.11, the rate of corrosion should increase when the temperature increases, and E_a and A may vary with temperature.

The rate of corrosion can be determined in different ways depending on the electrochemical technique employed in the experiment. If the popular gravimetric method (weight loss) is used, Equation 1.12 can be used directly.

$$\rho = \left(\frac{\Delta w}{St} \right) \tag{1.12}$$

where: ρ = corrosion rate

Δw = average weight loss of the material

S = total area of the of the material

t = immersion time

Thermodynamics of Corrosion

The process of corrosion can best be explained in terms of the stability of the chemical species and reactions associated therein. Therefore, the thermodynamic concept is important in understanding the corrosion process. However, the rates of corrosion cannot be predicted through thermodynamics calculations. One of the great advantages of thermodynamics is that it can be used to calculate the theoretical activity of a given metal when the composition of the medium is known.

The concept of spontaneous and non-spontaneous reactions is also vital in the study of corrosion processes. Corrosion processes are known to be spontaneous processes. For a reaction to occur spontaneously, the free energy of that particular reaction should have a negative value [21]. Corrosion involves both oxidation and reduction half reactions. The overall free energy for the redox reaction is negative. The standard free energy of the cell reaction ΔG^0 under standard conditions can be calculated as;

$$\Delta G^0 = -nF\Delta E^0 \qquad (1.13)$$

where ΔG^0 = standard free energy change

n = number of exchanged electrons

F = Faraday constant

ΔE^0 = standard energy change in the reaction

Studies indicate that the values of ΔG^0 of around –20 kJ mol^{-1} or lower imply physical adsorption (physisorption) and those around –40 kJ mol^{-1} or higher imply chemical adsorption (chemisorption) for a particular corrosion process [21, 22]. Chemisorption is a process in which the interactions involved are covalent in nature and the type of layer that results is monolayer [21]. Physisorption is a process that involves weak Van der Waals intermolecular interactions that result in multilayer products [21, 22]. Also, while chemisorption is an irreversible process, physisorption is a reversible one.

From the electrochemical measurements, other thermodynamics quantities such as the adsorptive enthalpy, ΔH^0_{ads} can be derived. The Van't Hoff equation can be utilized for this purpose.

$$\ln K = -\frac{\Delta H^0{}_{ads}}{RT} + Cons\tan t \qquad (1.14)$$

where K is the adsorption constant.

The value of the ΔH^0_{ads} obtained from this equation can also be ascertained using the Gibbs-Helmholtz equation.

$$\left[\frac{\partial\left(\Delta G^0{}_{ads}/T\right)}{\partial T}\right]_P = -\frac{\Delta H^0{}_{ads}}{T^2} \qquad (1.15)$$

The other thermodynamic quantity that can be deduced is the standard entropy, ΔS^0_{ads} through the use of the thermodynamic basic Equation 1.16.

$$\Delta G^0_{ads} = \Delta H^0_{ads} - T\Delta S^0_{ads} \quad (1.16)$$

The equilibrium constant (K_{eq}) for the reaction can be calculated using Equation 1.17 below;

$$RTln\, K_{eq} = -\Delta G° = nF\Delta E° \quad (1.17)$$

1.1.9 CORROSION CONTROL METHODS

Corrosion is a destructive and unavoidable process with negative effects on individuals, industries and the nation. Hence, the possible prevention and effective control of corrosion plays a significant role in economics and safety [23, 24]. There are several practical methods which can be employed in corrosion control. These methods are broadly based on [10]:

- Selection of material
- Modification of metals
- Modification of design
- Application of inhibitors
- Modification of corrosive medium
- Modification of surface

The choice of method(s) to employ in controlling corrosion between these possibilities is dependent on economic considerations, appearance, environment and safety. Among all these methods, the use of corrosion inhibitors has been found to be the most practical, easiest, economical and efficient means of corrosion control [25-27].

1.2 INHIBITORS AND INHIBITION

1.2.1 DEFINITION OF CORROSION INHIBITORS

The process of retarding or controlling corrosion of metal is known as corrosion inhibition. According to Norman [28], the definition of corrosion inhibitor favoured by the National Association of Corrosion Engineers is: a substance which retards corrosion when added to an environment in small concentrations. It is established that inhibitors function in one or more ways to control corrosion [29];

- by adsorption of a thin film onto the surface of a corroding material,

- by inducing the formation of a thick corrosion product, or
- by changing the characteristics of the environment resulting in reduced aggressiveness.

Corrosion inhibitors may be organic or inorganic compounds, and they are usually dissolved in aqueous media. Some of the most effective inorganic inhibitors are chromates, nitrites, silicates, carbonates, phosphates and arsenates. The organic inhibitors include amines, heterocyclic nitrogen compounds, sulphur compounds such as thioethers, thioalcohols, thioamides, thiourea and hydrazine. The campaign for environmental safety has led to drastic reduction in the use of chromates and zinc salts as corrosion inhibitors due to their toxicity. Nowadays, they are largely been replaced by organic inhibitors [25, 30]. Most of these organic inhibitors possess electronegative functional groups and pi-electrons in triple or conjugated double bonds. The presence of heteroatoms (such as O, N, S, P) as well as aromatic rings in their structures serves as centres for adsorption. Their molecular structure, molecular size and mass, presence of heteroatoms and adsorptive tendencies have been found to be responsible for their effectiveness as corrosion inhibitors [31-33].

Some of the practical criteria for the selection of corrosion inhibitors from the great variety of inorganic and organic compounds with ability to retard corrosion properties are not only their inhibition performance but also their safety of use, ready availability, economic constraints, inertness, environmental friendliness, solubility in the medium of application and compatibility with other chemicals in the system [34-37].

Inhibitors have a wide range of applications. The types of environment that can be modified include aqueous, partly aqueous and gaseous. Aqueous are often at near neutral pH range such as natural water, cooling water systems and in acidic range such as acid pickling to remove rolling scale as well as in the production and refinery of oil and gas. The major industries involved with the usage of corrosion inhibitors are the oil and gas industry, the petroleum refining industry, the chemical industry, heavy industrial manufacturing industry, water treatment facilities and the product additive industries [38].

1.2.2 TYPES OF INHIBITORS

Corrosion inhibitors can be classified based on their chemical functionality. The most common types of inhibitors are anodic, cathodic and mixed type. These inhibitors work differently depending on the type and nature of material under consideration.

Anodic inhibitors: Anodic inhibitors are generally used in near-neutral solutions where sparingly soluble corrosion products, such as oxides, hydroxides, or salts, are produced. These inhibitors retard the dissolution of metal at the anodic site by forming passivating films. Anodic inhibitors are often called passivators. In the situation of low concentrations of anodic inhibitor, corrosion becomes accelerated instead of being retarded. Examples of these inhibitors are chromates, nitrites, phosphates, tungstates etc. [39].

Cathodic inhibitors: These inhibitors inhibit corrosion by either decreasing the reduction rate (cathodic poisons) or by selective precipitation on the cathode (cathodic precipitators).
The cathodic inhibitors take either one of these three mechanisms [35, 39];

i. Cathodic poisons: These are substances that reduce the rates of cathodic reactions by resisting hydrogen recombination and discharge. However, cathodic poisons increase the tendency of exposing the metal to hydrogen-induced cracking.
ii. Cathodic precipitates: These are substances which increase the alkalinity at cathodic sites and form insoluble precipitates on the surface of the metals. Examples are carbonates of calcium and magnesium.
iii. Oxygen scavengers: These are substances that inhibit corrosion by reacting with oxygen so as to remove it from the corrosive environment. Examples are sulphite and hydrazine.

Mixed type inhibitors: These inhibitors simultaneously reduce the rate of anodic and cathodic reactions. The potential shift is smaller and the direction of the shift is determined by the relative size of the anodic and cathodic sites. The advantage of mixed-type inhibitors over others is that they regulate both the anodic and cathodic reactions and hence are safer to apply [39].

1.2.3 GREEN CORROSION INHIBITORS

There is no clear-cut and widely accepted definition of "environmental friendly" or "green" corrosion inhibitors. In general practice, corrosion inhibition studies have become oriented towards the safety of human, animals and the environment. Green corrosion inhibitors are known to be biodegradable and free from heavy metals and toxic substances. These eco-friendly corrosion inhibitors which range from rare earth metals to organic compounds are being used as suitable replacement of toxic inhibitors. Natural products such as plant extracts and animal proteins have been reported as excellent corrosion inhibitors. Inorganic compounds

such as lanthanide, cerium and samarium salts have been exploited as corrosion inhibitors [38]. Recent explorations of environmentally benign compounds have led to utilization of polymers and polymer nanocomposites as corrosion inhibitors of many metals in different corrosive environments. This is due to their eco-friendliness, low cost, easy availability, non-toxicity and inhibitive ability [32, 40].

1.2.4 MECHANISM OF CORROSION INHIBITION

Corrosion mechanism entails the adsorption of inhibitor molecules onto the metal surface. Adsorption is a surface phenomenon in which molecules adhere to the surface of the metal thereby forming a protective layer. Organic corrosion inhibitors found to possess one or more polar functions (with O, N, S and P atoms) have shown to be efficient anticorrosion compounds, as well as heterocyclic compounds containing polar groups and π – electrons. The polar function is usually regarded as the active centre for the establishment of adsorption process. Adsorption of polymeric inhibitors on the surface of the metal is controlled by the residual charge on the metal and inhibitor properties such as the charge density, adsorption active centres in the molecule, the molecular weight, the mode of adsorption and the formation of metallic complexes [38, 39]. Generally, the efficiency of the inhibitors performance can be determined by the extent to which the molecules of the inhibitors adhere to the metal surface or by their remaining in the corrosive media for corrosion protection. However, the incorrect utilization and wrong application of inhibitors could lead to an increase in the rate of corrosion [27].

The two common types of adsorption classification based on its mode of adsorption are chemisorption and physisorption. For effective adsorption of an inhibitor on a metal surface to take place, the forces of attraction between the metal and the inhibitor must be greater than that between the metal and water [2].

Physisorption or physical (electrostatic) adsorption: This is the result of existing weak electrostatic attractive forces between inhibiting organic ions or dipoles and the charged metal surface. The interaction occurring between physically adsorbed inhibitors and the metal surface is rapid but are easily removed from the metal surface. Increase in temperature results in desorption of physically adsorbed inhibitor on the metal surface. Physisorption has low activation energy and is relatively independent of temperature. The enthalpy of physisorption

can be measured by monitoring the rise in temperature of a sample of known heat capacity. Also, the enthalpy values are usually in the range of of 0 kJ mol^{-1} to 20 kJ mol^{-1} [2, 21, 22].

Chemisorption: This process involves a direct and stronger contact between the adsorbed inhibitor and the metal surface. In chemisorption, charge transfer occurs from the inhibitor molecule to the metal surface to form a coordinate bond-type. The process is slower than physisorption and possesses higher activation energy. It is specific for metals and is not completely reversible. The enthalpy values are greater than in physical adsorption and are usually above 20 kJ mol^{-1} [2, 21, 22].

Factors that could affect adsorption include the nature of corrosion inhibitor and the metal, the surface area of adsorbent, activation of adsorbent, amount of the inhibitor and reaction conditions such as temperature, pressure and pH. Adsorption is usually described through isotherms. Various adsorption isotherms have been proposed to model the type of adsorption taking place between the inhibitor molecules and the metal surface. The common adsorption isotherms are Langmuir, Freundlich, Temkin, Frumkin, Flory Huggins [41-43].

1.2.5 PROBLEM STATEMENT

Metals constitute a great part of construction material elements in agricultural equipment, oil and gas, petrochemical, medical services, process and allied industries. In these industries, the metallic material as a result of interaction with its surrounding environment loses its strength and properties over a period of time. As a result, the material cannot perform the intended function effectively and reliably [4, 8]. Corrosion of mild steel has numerous consequences and has been considered a matter of serious concern to experts in both academia and industries [26].

The use of inhibitors has been identified as one of the most cost-effective and easiest methods of repressing metal corrosion. Organic compounds are extensively used as corrosion inhibitors. The recent campaigns for environmental protection and the use of eco-friendly materials have heightened the development of environmentally benign compounds as corrosion inhibitors [18, 24, 25]. Many polymers have been identified as potential eco-friendly corrosion inhibitors [18, 44]. Some major problems that still limit the use of polymers as inhibitors of metal corrosion include their limited solubility in common aqueous corrosive environments and desorption at high temperatures. Incorporation of metal/metal oxide nanoparticles into the backbone of

polymers has been reported as a means of improving their protection efficiency [45]. A review of corrosion literatures revealed that polymer-metal oxide nanocomposites tested for corrosion inhibition are effective inhibitors of mild steel in corrosive media [35, 45-47].

This research is therefore conceptualized as a continuation of the efforts to design more eco-friendly polymer-metal oxide nanocomposites as inhibitors of metal corrosion in major aqueous environments. The sets of polymer-metal oxide nanocomposites selected for this work have not been used as inhibitors for mild steel corrosion in 5 % HCl solution in any previous study.

1.2.5 AIM AND OBJECTIVES OF THE STUDY

The aim of this study is to synthesize, characterize and study the corrosion inhibition of ZnO nanocomposites of polyethylene glycol (PEG), polyvinylpyrrolidone (PVP) and polyacrylonitrile (PAN) on mild steel in acidic media.

The specific objectives of the study are to:

i. synthesize and characterize polymer-ZnO nanocomposites using Fourier transform infrared (FTIR) spectroscopy, ultraviolet visible (UV-vis) spectroscopy, thermogravimetric analysis (TGA) and transmission electron microscopy (TEM).
ii. study the electrochemical corrosion of mild steel in acidic medium using potentiodynamic polarization (PDP), linear polarization resistance (LPR) and electrochemical impedance spectroscopy (EIS) techniques.
iii. assess the inhibitive effects of the newly synthesized polymer-ZnO nanocomposites on mild steel corrosion in the acidic medium.
iv. predict the mechanism(s) of corrosion inhibition by the polymer-ZnO nanocomposites and their mode of adsorption on the steel surface.
v. study the surface morphologies of mild steel surface before and after immersion in the aggressive environments without and with the synthesized polymer-ZnO nanocomposites.

CHAPTER 2

LITERATURE REVIEW

2.1.1 HISTORICAL BACKGROUND OF POLYMERS

The word "*polymer*" is derived from two Greek words, *poly* meaning "many" and *meres* meaning "parts." In other words, a polymer is a long-chain molecule (macromolecule) that is composed of a large number of repeating units of identical structure. The repeating units are derived from some simple reactive molecules called monomers and are connected by covalent bonds. Polymerization is the process by which polymers are formed from respective monomers [48, 49]. Some polymers such as proteins, cellulose, gum arabic and silk, are found in nature, while a vast majority including polystyrene, polyethylene, polyacrylamide and nylon, are produced by synthetic routes.

The history of polymer science and technology may be traced back to the mid-nineteenth century. In the 1830s, Charles Goodyear discovered the process of vulcanization that transformed the sticky latex of natural rubber into a useful elastomer for tyre use. In 1847, Christian F. Schönbein discovered that reacting cellulose with nitric acid will produce cellulose nitrate as product. This cellulose nitrate was used in the 1860s as the first man-made thermoplastic, celluloid. Leo Hendrik Baekeland produced Bakelite (phenol–formaldehyde resin) in 1907. In 1912, a protective coating resin, Glyptal (unsaturated-polyester resin) was developed by General Electric.

By the 1930s, research efforts at DuPont in the United States had led to the production of a wide variety of new man-made polymers including synthetic rubber, nylon and Teflon. By 1938, Dow had produced polystyrene in commercial quantities for the first time and in 1939, low-density polyethylene was manufactured by scientists at ICI in England. Frantic efforts were made during World War II to develop new polymeric materials, especially synthetic rubber because of the shortage in supply of Hevea rubber. In the 1950s, Karl Ziegler and Giulio Natta independently developed a family of stereospecific transition-metal catalysts that made possible the commercialization of polypropylene as a major commodity plastic. The 1960s and 1970s witnessed the development of a number of high-performance engineering plastics polymers that could compete favourably with more traditional materials, such as metals, for automotive and aerospace applications. These included polycarbonate, poly(phenylene oxide), polysulfones, polyimides, aromatic polyamides and other high-temperature rigid-chain polymers. More recently, specialty polymers with electrically conducting, photo-conducting, and liquid-crystalline properties have appeared for a variety of applications [48].

2.1.2 CLASSIFICATION OF POLYMERS

Thousands of different polymers have been synthesized and more will be manufactured in the future to meet the industrial needs of man. Basically, all polymers have been placed to one group or the other based on the broad classification shown below in Figure 2.1 [48, 49]:

1. **The origin or source:** Based on origin, polymers can either be naturally occurring from both plants and animal. They could also be formed from further chemical reactions of these naturally occurring polymers or artificially synthesized by man in laboratory or industry.

2. **The structure:** Polymers could be known to possess long and straight chain having high melting points and density, or with some branches in its chain with characteristic low melting point and density. Polymers can also be said to compose of bi-functional and tri-functional monomers with strong covalent bonds between the different long and straight chains.

3. **The mode of polymerization:** Elastomers are classified based on the mode of polymerization as polymers with elastic ability like rubber. The polymer chains in elastomers are connected by weak intermolecular forces which makes it easy for stretching when moderate stress is applied. Fibres are thread forming solids having stronger intermolecular forces between their chains than elastomers and can withstand stress. Thermoplastic polymers have the ability to repeatedly soften on heating and harden on cooling. Thus, they can be easily converted into any desired shape on heating. Thermosets are polymers which become hard on heating and infusible because of extensive crosslinking of the polymer bonds.

4. **The molecular forces:** While some polymers are formed by the repeated addition of monomers possessing double or triple bonds, others are formed by repeated condensation between two different bi-functional or tri-functional monomers.

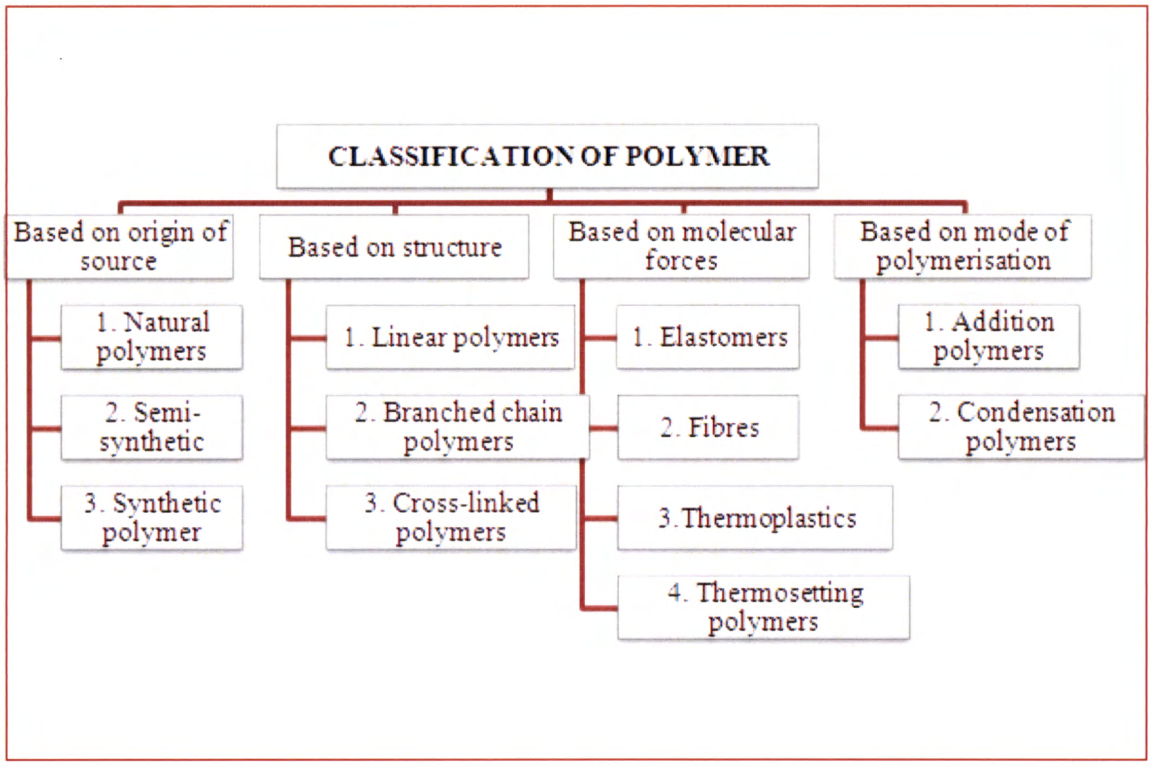

Figure 2.1: Classification of polymers

2.1.3 PROPERTIES OF POLYMERS

Polymers have distinct and unique properties that make them widely applicable in several industries. In the field of corrosion, recent interest has developed in the application of polymers as corrosion inhibitors of metals in different media because of several properties they possess. Polymers are generally odourless and have low cost of production. Most of them are highly soluble in water and polar solvents. They have high tensile strength, flexibility, thermal stability and can be easily processed. They are also resistant to chemicals such as oil, grease and solvents. Polymers have also been found to possess unique functional groups such as -OH, -NH_2, -COOH and oxygen, nitrogen atoms in their chain which enables the formation of complexes with metal ions and on the metal surface [44, 50]. These complexes occupy a large area, thereby blanketing the surface and protecting the metal from corrosive ions present in the aqueous solution. The availability of multiple adsorption centres, excellent film forming and adhesive properties, and the eco-friendliness of polymers make them suitable replacement for inorganic and organic corrosion inhibitors. Inorganic inhibitors such as chromates, nitrates etc. and organic corrosion inhibitors have been widely used in industrial operations such as pickling, cleaning and acidizing to protect metals because they show significant inhibition

efficiency. However, most of them are costly and environmentally unsafe to both man and the environment unlike polymers [44, 51-53].

Polymers have a wide range of industrial applications like food and agriculture, pharmaceuticals, medicine, paint, textiles, paper, constructions, adhesives, coatings, water treatment and many others [54]. Polymers have also been used in the production of consumer goods such as plastics. Figure 2.2 below shows the chemical structures of some common synthetic polymers which are been explored as corrosion inhibitors.

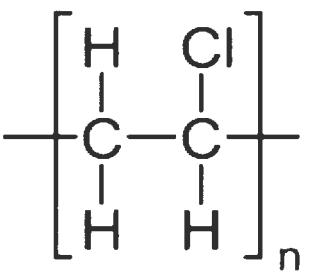

Polyvinyl chloride

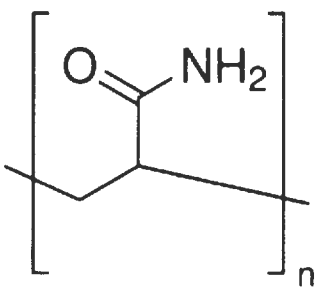

Polyacrylamide

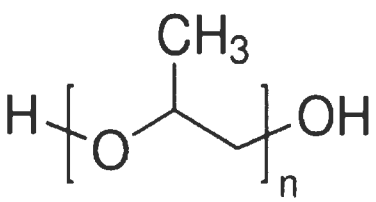

Polypropylene glycol

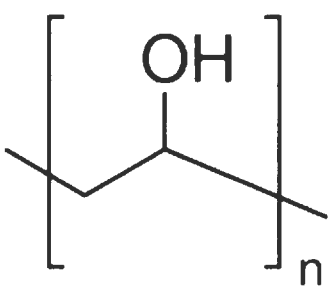

Polyvinyl alcohol

Figure 2.2: Structures of some common synthetic polymers used as corrosion inhibitors

Synthetic water-soluble polymers are macromolecules that can dissolve or disperse well in water, and thus, modify the physical properties of aqueous systems. These polymers which usually have repeating units contain hydrophilic groups that are substituents or are incorporated into the backbone. The hydrophilic groups may be non-ionic, anionic, cationic or amphoteric [54].

This present study employs synthetic water-soluble polymers and polymer nanocomposites as corrosion inhibitors of mild steel in acid medium. PEG is an uncharged, hydrophilic, linear polymer available in a wide range of molecular weights. It has been found to be non-toxic, having low cost of production and has been employed in the synthesis of polymeric nanoparticles. Its excellent solubility in aqueous medium, thermal stability coupled with its ease of forming nanocomposite with inorganic oxides makes it a polymer of interest in various field of corrosion research [54-56].

Another important water-soluble polymer is PVP which is found to be a bulky, odourless polymer. It is also eco-friendly, cheap and has excellent solubility in water and other non-aqueous liquids. PVP has chelating properties with metals due to its high charge density which makes it have wide applications in aqueous or polar organic solutions. The wide variety of usable solvents is due to the presence of imide, methylene and carbonyl groups in PVP. Based on these properties, the anticorrosion potentials of PVP has been tested for different mild steel in different media [57, 58].

PAN is a well-recognized synthetic thermoplastic polymer with varied applications in the industry. However, it is relatively insoluble in water. PAN has shown interesting properties such as ease of synthesis, mechanical strength, easy accessibility, non-toxicity, electrochemical stability and thermal stability which makes it considered for corrosion inhibition study [59-61].

2.1.4 ZINC OXIDE NANOPARTICLES

Metal oxide nanoparticles are of special interest due to their diverse mechanical, structural, thermal, electronic, magnetic and optical properties. Zinc oxide is grouped under II-IV semiconductors and has a broad energy band (3.37 eV) and a high exciton bond energy (60 meV) at room temperature [62]. Among the wide variety of metal oxide nanoparticles, it is one of the most promising because of its unique properties such as thermal and mechanical stability at room temperature, good physical and chemical stability, environmental friendliness, abundant availability and low cost. Recently, research efforts are geared towards improving the properties of polymeric materials by incorporating ZnO nanoparticles into the polymer backbone. These nanoparticles generally tend to form complexes with the polymer chains thereby increasing the physical properties of the polymer nanocomposites. ZnO nanoparticles have also been found to improve the thermal behaviour of polymers [60, 63].

2.1.5 POLYMER NANOCOMPOSITES

Nano, a Greek word for "dwarf" deals with structures having a size range of 1-100 nanometres [64]. The field of nanotechnology is one that has gained more attention in virtually all areas of current research and development. Among such areas of research where nanotechnology is applicable is corrosion inhibition of metals. Polymer nanocomposites are a special class of materials having unique properties and wide applications in diverse research areas [65].

Polymers have shown promising inhibiting ability, although several factors have stood as setbacks to their applications as metal corrosion inhibitors. These include moderate inhibition efficiency, insolubility in the environment of application and desorption at high temperatures [45]. Among the modifications employed to overcome these enumerated setbacks are copolymerizing, crosslinking, blending, and combination with substances that exert synergistic effect. Most recently, inorganic nanofillers are incorporated into the backbone of polymers to form polymer nanocomposites in a bid to enhance their properties and corrosion resistance ability [45, 66].

A polymer nanocomposite can be defined as a polymer-nanofiller system in which the inorganic filler is on a nanometric scale at least in one dimension and it can be a polymer/nanoparticles blend or a hybrid. The composite interconnection can be based on a secondary force or physical entanglement [67]. The polymer/nanofiller-hybrid, in turn, is formed when the polymer and the nanoparticles are covalently bonded. The covalent bond can be formed during the in-situ polymerization (the monomer or the growing polymer chain can react with the filler particle), or during the composite processing.

2.1.6 POLYMERS AS CORROSION INHIBITORS

Umoren et al. [68] investigated the efficiency of chitosan as a corrosion inhibitor for mild steel in 0.1 M HCl using electrochemical measurements and spectroscopic analyses. The results revealed that chitosan was an excellent inhibitor of corrosion in mild steel. The inhibition efficiency increased with a rise in temperature up to 96 % at 60 °C and then drops to 93 % at 70 °C, while it slightly increased with an increase in chitosan concentration. Tafel plots showed that chitosan behaved as a mixed inhibitor. Impedance results indicated that chitosan was adsorbed on the metal/solution interface. Adsorption of chitosan was found to be in agreement with Langmuir adsorption isotherm model. Chemical adsorption was the proposed mechanism

for corrosion inhibition considering the trend of protection efficiency with temperature. The calculated kinetic and thermodynamic parameters and the proposed mechanism correlated well.

Polyurethane based tri-block co-polymers namely poly(N-vinylpyrrolidone)-b-polyurethane-b-poly (N-vinylpyrrolidone) (PNVP-PU) and poly(dimethylaminoethylmethacrylate)-b-polyurethane-b-poly (dimethylaminoethylmethacrylate) (PDMAEMA-PU) were synthesized by Kumar et al. [69]. Nuclear magnetic response (NMR) spectroscopy and gel permeation chromatography (GPC) methods were used in characterizing the synthesized compounds. The corrosion inhibitive ability of the co-polymers was studied on mild steel in 0.5 M sulphuric acid using electrochemical measurements, surface analysis, quantum chemical calculations and molecular dynamic simulations (DMS). Results showed that the inhibitors exhibited mixed-type effect and adsorbed on the mild steel surface. The inhibition efficiency increased with increase in concentration and decreased with increasing temperature. The two studied co-polymers obeyed Langmuir adsorption isotherm and followed physisorption and chemisorption adsorption modes. Surface analyses using scanning electron microscopy (SEM) and atomic force microscopy (AFM) confirmed inhibition by formation of film protection on the mild steel surface by the corrosion inhibitors. Quantum chemical calculations and molecular dynamic simulations studies corroborated experimental results.

Verma et al. [70] synthesized three oligopolymers derived from α-naphthol (N), formaldehyde (F) with aniline (TERP-1), paraaminobenzoic acid (TERP-2) and sulphanilic acid (TERP-3) and investigated their anticorrosion potential of mild steel in 1 M HCl using electrochemical impedance spectroscopy (EIS), potentiodynamic polarization, linear polarization and gravimetric methods. The three polymers performed as excellent inhibitors of corrosion in acid medium with inhibition efficiencies above 90 % at 50 ppm concentration. The order of inhibition efficiency of the studied oligopolymers are TERP-3 > TERP-2 > TERP-1 which is best explained in terms of presence of the various substituents in the phenyl moiety. Inhibition concentration of the studied inhibitors increased with increasing concentration. The Tafel curves revealed that the studied oligopolymers acted as mixed-type inhibitors. The inhibition efficiencies obtained from the four electrochemical techniques employed showed good agreement. Adsorption on mild steel by the inhibitors followed Langmuir adsorption isotherm. Based on the values of activation energy and other calculated thermodynamic parameters, it was concluded that the adsorption on the mild steel was spontaneous and exothermic.

John et al. [71] assessed the inhibition of mild steel corrosion in aerated acid mixture of 0.05 N H_2SO_4 and 0.5 N HCl solutions by polyvinylpyrrolidone (PVP) and polyethylene glycol (PEG) using potentiodynamic polarization, linear polarization, electrochemical impedance spectroscopy, adsorption, and surface morphological studies. The presence of PEG and PVP decreased the double-layer capacitance and increased the charge-transfer resistance. Inhibition efficiency increased significantly with increase in the additives concentration. The inhibitor polymers adsorbed on the metal surface obeying Langmuir adsorption isotherm model. Both PEG and PVP were found to be good inhibitors of mild steel corrosion in acidic medium and act as mixed type inhibitors. Surface analyses revealed that PVP offered better protection to mild steel surface than PEG.

Polyvinylpyrrolidone, polyacrylamide and their blends have been studied as corrosion inhibitors of aluminium in HCl in the temperature range 30 °C - 60 °C using weight loss, hydrogen evolution and thermometric techniques by Umoren and Ebenso [72]. It was reported that the inhibition efficiencies increased with increasing inhibitors concentration but decreased with increase in temperature in both polymers with PVP acting as a better inhibitor. Corrosion rates increased with temperature and decreased in the presence of the polymeric inhibitors. The blending of the polymers led to increased inhibitive effect which was optimum at the blending ratio (PVP:PA) of 3:1. 97 % inhibition efficiency was obtained from the optimum blending ratio from the thermometric method. The adsorption models of the inhibitors on the aluminium followed Freundlich, Temkin and Flory-Huggins isotherms. Kinetic and thermodynamic parameters proposed physiosorption and spontaneous adsorption of the inhibitors onto aluminium.

Alaoui et al. [73] studied the effect of temperature on the efficiency of polyvinyl alcohols for the corrosion of carbon steel in 1 M HCl using a series of techniques such as weight loss, polarization and electrochemical impedance spectroscopy (EIS). The studied compounds exhibited a very good inhibiting performance. The results showed that the inhibition efficiency increased with the concentration of the inhibitors and depended on its temperature and immersion time. The adsorption of the studied polymers complied with the Langmuir adsorption model at all studied temperatures. Comprehensive adsorption (physisorption and chemisorption) was proposed.

Mobin and Khan [74] investigated the corrosion inhibition behaviour of polyethylene glycol alone and in the presence of surfactants sodium dodecyl benzene sulfonate (SDBS) and

cetyltrimethyl ammonium bromide (CTAB) on mild steel in 0.1 M H_2SO_4 in temperature range of 30 °C - 60 °C using weight loss method, solvent analysis of iron ions, scanning electron microscopy (SEM), energy dispersive x-ray analysis (EDAX), atomic force microscopy (AFM) and determination of kinetic/thermodynamic parameters. The inhibition efficiency (IE) of PEG increased with increasing concentration but decreased with increasing temperature. The addition of little quantity of the surfactants synergistically improved the corrosion inhibition of PEG. Surface morphology of the corroded mild steel specimen showed the existence of an adsorbed protective film on the surface. Langmuir adsorption isotherm was obeyed.

2.1.7 POLYMER NANOCOMPOSITES AS CORROSION INHIBITORS

Core/shell nanocomposites of zinc oxide nanoparticles surrounded by a shell of polyacrylamide was prepared using in-situ emulsion polymerization technique. Morsi et al. [47] employed potentiodynamic polarization and electrochemical impedance spectroscopy for corrosion of carbon steel in the presence of ZnO/PAM.NCs. Corrosion inhibition efficiency increased as the ZnO nanoparticles ratio increased. Scanning electron micrographs of carbon steel surface immersed in HCl in the presence of the nanocomposites showed less damage confirming the observed high corrosion protection. ZnO/PAM.NC10 was also found to display a broad spectrum antimicrobial activity with the inhibition zones in the range of 15 – 22 mm. ZnO/PAM.NC10 demonstrated a higher antibacterial activity for the Gram-positive than for the Gram-negative bacteria and exhibited lower minimum inhibitory concentrations and minimum bactericidal concentrations for the Gram negative bacteria than the Gram positive bacteria. This suggests its prospect as inhibitor of microbial corrosion.

El-Mahdy et al. [75] synthesized silica/polyacrylamide nanocomposite using dispersion radical polymerization technique. Silica/polyacrylamide nanocomposite of various concentrations was tested as corrosion inhibitor of mild steel in 1 M HCl using electrochemical techniques. The nanocomposite behaved as a mixed type inhibitor and formed an inhibitive layer on the metal surface. The inhibition efficiency increased with increase in concentration of silica/polyacrylamide nanocomposite. It was found that the silica/polyacrylamide nanocomposite inhibited the corrosion of steel better than silica alone.

Geethanjali and Subhasshini [76] developed a novel method for synthesizing magnetite-containing polyaniline-polyacrylamide nanocomposite (PANI-PAAm/Fe_3O_4). The synthesized nanocomposite was characterized and tested as corrosion inhibitor of mild steel in acidic

medium using electrochemical and spectroscopic techniques. The plotted polarization curves results obtained showed that the inhibitor affected both anode and cathodic reactions. The corrosion rate subsided by increase in the concentration of the inhibitors. The results obtained from Tafel plots and the Nyquist plots were in good agreement. Adsorption isotherm for the process obeyed Langmuir.

Trung and Huyen [77] synthesized nanocomposites of polyindole (PIn) and TiO_2 by in-situ polymerization. The morphology of nanoparticles was studied by scanning electron microscopy (SEM) and transmission electron microscopy (TEM). The chemical structure of the PIn was characterized by FTIR and Raman spectra. The thermal analysis showed that the stability of the polymers in the nanocomposites were stable at about 600 °C. The corrosion performance of the nanocomposites was investigated and showed that the nanocomposite was an effective inhibitor of mild steel.

Solomon et al. [45] synthesized a novel polypropylene glycol/silver nanoparticles (PPG/AgNPs) composite in-situ using natural honey as the reducing and capping agent. PPG/AgNPs proved to be an effective inhibitor of corrosion for mild steel in 0.5 M H_2SO_4 with a maximum inhibition efficiency of 94 % by 1000 ppm PPG/AgNPs at 333 K from weight loss studies. Adsorption of the inhibitor molecules to the metal surface was by chemisorption and follows Temkin adsorption model. Tafel plots revealed the composite acted as a mixed-type inhibitor. The SEM, EDS and water contact angle images confirmed the formation of PPG/AgNPs protective film on the mild steel surface.

Sasikumar et al. [78] reported the chemical synthesis of the nanocomposites of aniline and CeO_2 nanoparticles by in-situ polymerization. Morphological characterizations were performed using various surface analysis techniques. The inhibition potential of the synthesized nanocomposite was tested against corrosion of mild steel in 0.5 M HCl using different electrochemical techniques. Potentiodynamic polarization results revealed the inhibitor acted a mixed type inhibitor and impedance results indicated the adsorption of the nanocomposites film on the mild steel surface. The inhibition performance of inhibitor was found to increase almost linearly with concentration. Spectroscopic analyses were used to confirm the formation of a protective film adsorbed on the mild steel.

CHAPTER 3

EXPERIMENTAL MATERIALS AND METHODS

3.1 MILD STEEL AND MILD STEEL PRE-TREATMENT

Mild steel with the chemical composition (in wt %) of C = 0.17, Mn = 0.46, Si = 0.26, S = 0.017, and P = 0.019 and, balance Fe was used for all the studies. For all electrochemical studies, mild steel coupon was cut into 1 cm × 1 cm and embedded in a Teflon holder using epoxy resin, exposing a surface area of 1 cm^2. Mild steel surface was mechanically abraded on Struers MD Piano 220 (size: 200 diameter) mounted on Struers LaboPol-1 machine to remove traces of epoxy resin from the surface. The surface was then polished with SiC paper of graded grit sizes ranging from 600 to 1200 to achieve a mirror-shining surface. Mild steel surface was then washed with water, degreased in acetone and then washed with water again, and finally dried. All electrochemical experiments were conducted with freshly surface pre-treated mild steels.

3.2 REAGENTS

Hydrochloric acid of 32 % assay was commercially obtained from Promark Chemicals, South Africa, and diluted with distilled water to prepare the 5 % HCl solution used for all the experiments. $Zn(NO_3)_2.6H_2O$ and all the polymers (PEG, PVP and PAN) used in this study were purchased from Sigma-Aldrich Chemicals. NaOH was purchased from Merck Chemicals.

3.3 SYNTHESIS OF THE POLYMER-ZnO NANOCOMPOSITES

3.3.1 SYNTHESIS OF ZINC OXIDE NANOPARTICLES

Zinc nitrate, $Zn(NO_3)_2.6H_2O$ was used as a precursor in preparing zinc oxide nanoparticles using chemical methods [79]. NaOH was dissolved in deionized water to a concentration of 1.0 M and the resulting solution was heated, under constant stirring to the temperature of 70 °C. After achieving this temperature, solution of 0.5 M $Zn(NO_3)_2.6H_2O$ was added slowly (dripped for 1 h) into the glass flask containing the NaOH aqueous solution under continual stirring. The temperature of the reaction was constantly maintained at 70 °C throughout the experiment.

The suspension formed with the dropping of 0.5 M $Zn(NO_3)_2.6H_2O$ solution to the alkaline aqueous solution was kept stirred for 2 h in the temperature of 70 °C. The material formed was filtered and washed several times with deionized water. The washed sample was dried in the oven at 65 °C for several hours [79].

3.3.2 SYNTHESIS OF POLYMER NANOCOMPOSITES

Polymer nanocomposites of PEG, PVP and PAN were prepared by mixing aqueous solutions of the polymers and ZnO nanoparticles. Firstly, different concentrations (100 ppm, 300 ppm, 500 ppm, 700 ppm and 1000 ppm) of the polymers were prepared in 5 % HCl. Secondly, the respective concentrations of the polymer solution were used to prepare 1 mM ZnO nanoparticles solution. In the case of relatively insoluble PAN, it was initially dissolved in small quantities of dimethylformamide (DMF) before mixing with ZnO nanoparticles.

The names and structures of the polymers used in this study are shown in Figure 3.1 below.

Name of inhibitor	Molecular structure	Chemical formula	Molecular weight
Polyethylene glycol	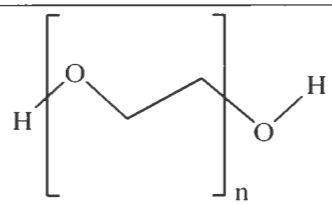	$C_{2n}H_{4n+2}O_{n+1}$	3,350 g/mol
Polyvinylpyrrolidone	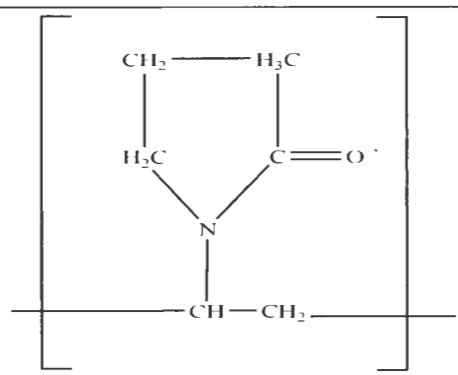	$(C_6H_9NO)_n$	10,000 g/mol
Polyacrylonitrile	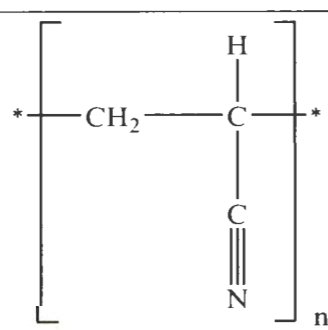	$(C_3H_3N)_n$	150,000 g/mol

Figure 3.1: Chemical structures of (a) Polyethylene glycol (b) Polyvinylpyrrolidone (c) Polyacrylonitrile

3.4 SPECTROSCOPIC, THERMAL AND SURFACE MORPHOLOGICAL ANALYSES

- **FTIR Analysis:** Fourier transformed infrared (FTIR) spectra of ZnO nanoparticles, PEG, PVP, PAN and their respective ZnO nanocomposites were recorded by Fourier transformed infrared spectrophotometer (Agilent Technology, Cary 670 series FTIR spectrometer, USA). The FTIR spectrum ranged from 4000 to 500 cm^{-1}.

- **UV-visible Measurements:** UV-visible spectra analyses of the ZnO nanoparticles, PEG, PVP, PAN and their respective ZnO nanocomposites were observed using a UV-vis spectrophotometer (Agilent Technology, Cary 300 series UV-vis spectrometer, USA) from 250 to 700 nm using a dual beam operated at a resolution of I nm with a scan rate of 200 nm/min at room temperature.

- **TEM Analysis:** The morphological analysis of the shape and size of ZnO nanoparticles and the synthesized nanocomposites were done using transmission electron microscopy (TEM). The drop of the inhibitors and the nanoparticles was loaded on carbon-coated copper grid and allowed to dry for an hour. The TEM micrograph images of the nanoparticles and synthesized nanocomposites were obtained and recorded.

- **TGA Analysis:** Thermogravimetric analysis (TGA) was carried out on the ZnO nanoparticles, PEG, PVP, PAN and their respective ZnO nanocomposites using an STA 1500 instrument. The TGA was conducted from 25 to 700 °C at a heating rate of 10 °C min^{-1} under nitrogen gas.

- **SEM Analysis:** The mild steel specimens were immersed in 5 % HCl without and with 1000 ppm of PEG, PVP, PAN and their respective ZnO nanocomposites for a period of 24 h and then taken out. Thereafter, the specimens were rinsed with double distilled water, degreased in acetone and finally dried in a desiccator. Scanning electron microscopy (SEM) analyses of the surfaces were carried out at an accelerating voltage of 15 kV on Microtrac Semtrac scanning electron microscope equipment.

3.5 ELECTROCHEMICAL MEASUREMENTS

The electrochemical measurements were performed on the Autolab Potentiostat Galvanostat 302N from Metrohm equipped with a three-electrode system. The Metrohm was driven by the Nova 1.10.1.9 software. The three-electrode cell used comprised Ag/AgCl with 3 M KCl as the reference electrode, platinum electrode as the counter electrode and a freshly prepared mild steel with a shining surface of 1 cm^2 surface area as the working electrode. The electrochemical system was maintained for a period of 1800 s in order to allow it to reach the steady open circuit potential (OCP) before each measurement. Potentiodynamic polarization measurements were carried out after 1800 s of immersing the mild steel in the aggressive solutions by sweeping the potential between -250 and +250 mV vs the OCP with scan rate of 1 mV/s. The electrochemical impedance spectroscopy (EIS) measurements were conducted at the OCP by analyzing the frequency response of the electrochemical setup in the range of 100 kHz to 0.1 Hz at 10 mV amplitude. All measurements were carried out under aerated unstirred conditions at 303 K. Figure 3.2 shows an image of the Autolab equipment used in carrying out the electrochemical measurements.

3.5.1 POTENTIODYNAMIC POLARIZATION (PDP) MEASUREMENTS

The PDP method was employed to obtain the relevant electrochemical parameters such as the corrosion potential, corrosion density, anodic and cathodic Tafel slopes. Corrosion inhibition efficiency (IE_i) was calculated from the Tafel polarization experiments as

$$IE_i = \frac{i^0_{corr} - i^i_{corr}}{i^0_{corr}} \times 100 \qquad (3.1)$$

where i^o_{corr} and i^i_{corr} are corrosion current densities in the absence and presence of inhibitors respectively.

3.5.2 ELECTROCHEMICAL IMPEDANCE SPECTROSCOPY (EIS)

EIS study was also conducted to study the corrosion of mild steel in 5 % hydrochloric acid. The electrochemical parameters such as the charge transfer resistance, capacity of double layer, the constant phase element constant and exponents were obtained and used to calculate the inhibition efficiency from the equation given below:

$$IE_z = \frac{R_{ct} - R^0{}_{ct}}{R_{ct}} \times 100 \qquad (3.2)$$

where, R_{ct} and $R^0{}_{ct}$ are the charge transfer resistances in the presence and absence of inhibitor respectively.

Figure 3.2: Autolab setup for electrochemical measurement

CHAPTER 4

RESULTS AND DISCUSSION

4.1 CHARACTERIZATION TECHNIQUES

4.1.1 FOURIER TRANSFORM INFRARED (FTIR) SPECTROSCOPY

Fourier transform infrared (FTIR) spectroscopy is an effective technique that provides qualitative information about the presence of certain functional groups in a molecule, composition of the product and the type of interactions existing between the polymers and the nanocomposites [80]. Figure 4.1 represents the FTIR spectra of PEG, PVP, PAN, ZnO nanoparticles and the synthesized polymer-ZnO nanocomposites taken at room temperature from 4000 cm^{-1} to 500 cm^{-1}.

Several significant modes of vibration can be observed from the FTIR spectra. The absorption band at 531 cm^{-1} is attributed to the Zn-O stretching vibration. The broad band observed around 3378 cm^{-1} is due to the O-H stretching vibration. IR bands at 1382 cm^{-1} and 1507 cm^{-1} correspond to symmetric and asymmetric stretching modes C=O bond. [81]. The presence of distinct sharp peak at 531 cm^{-1} in the ZnO spectrum confirms the formation of ZnO nanocrystals [82].

The IR spectrum of PEG-ZnO nanocomposite shows a band at 2883 cm^{-1}, which is due to C-H stretching vibrations of PEG 3350. A weak broad band is observed in the range 3200-3550 cm^{-1}, which can be attributed to the hydroxyl group present in PEG-ZnO. The band at 2930 cm^{-1} is attributed to C-H stretching. The weak broad band at around 1346 cm^{-1} is attributed to C-O-H bending vibration. The band at 842 cm^{-1} corresponds to the long polymeric chain bending in the nanocomposite and the one at 1108 cm^{-1} corresponds to C-O stretching vibration. It is observed that the band at 542 cm^{-1} indicates the presence of ZnO in the composite. This is in agreement with previous reports in literature [83-85].

In the IR spectrum of PVP-ZnO, the broad absorption band observed at 3100-3600 cm^{-1} is assigned to the O-H stretching vibration of the moisture content in the nanocomposite. Also, the broad band obtained in the range 2821-3028 cm^{-1} is attributed to the stretching mode of C-H. The band at 1655 cm^{-1} is ascribed to the C=O stretching mode on the PVP molecule in the composite. The bands at 1429 cm^{-1} and 1282 cm^{-1} are due to bending vibration of methylene ($-CH_2$) groups in the pyrrole ring of PVP and the stretching vibration band of nitrile (-C-N)

respectively. The band obtained for PVP at 1661 cm^{-1} due to C=O stretching band reduced to 1655 cm^{-1} in the composite and the peak at 1748 cm^{-1} disappeared. This is due to the interaction of the carbonyl oxygen with the zinc ion. The peak observed at 544 cm^{-1} is due to the Zn-O stretching in the nanocomposite. The results suggest successful formation of PVP-ZnO [83, 86].

The spectrum of PAN-ZnO shows absorption bands at 2937 cm^{-1} and 1451 cm^{-1}, which are both attributed to the stretching vibration of C-H. The peak at 2244 cm^{-1} is due to C-N stretching vibration of nitrile, and the stretching vibration of C=O appeared at 1738 cm^{-1}. The band at 1219 cm^{-1} is for the skeletal C-C vibrations in PAN molecules. The weak broad band around 3280 cm^{-1} indicates O-H stretching due to the hydroxyl group. The appearance of a band at 547 cm^{-1} indicates the formation of PAN-ZnO nanocomposite due to the Zn-O stretching band present [87, 88].

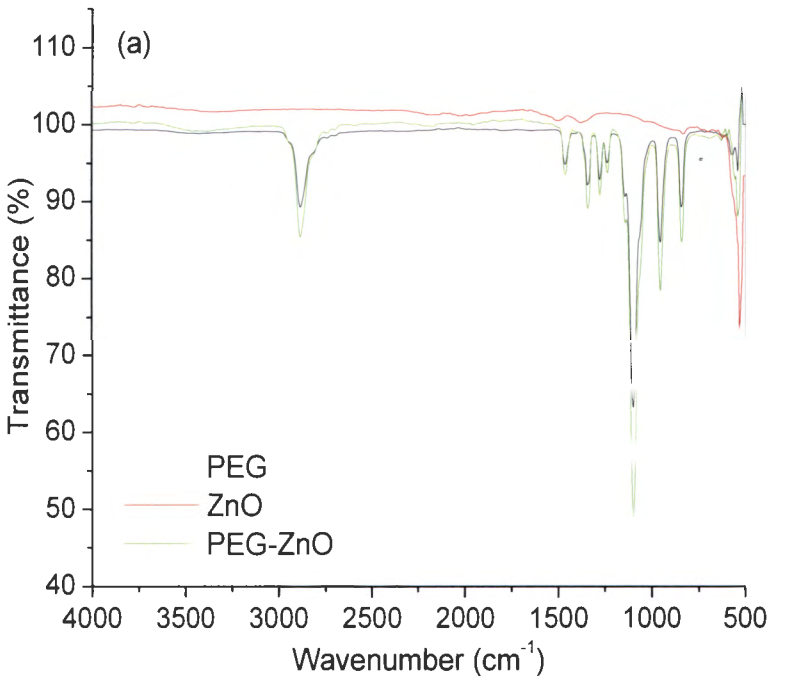

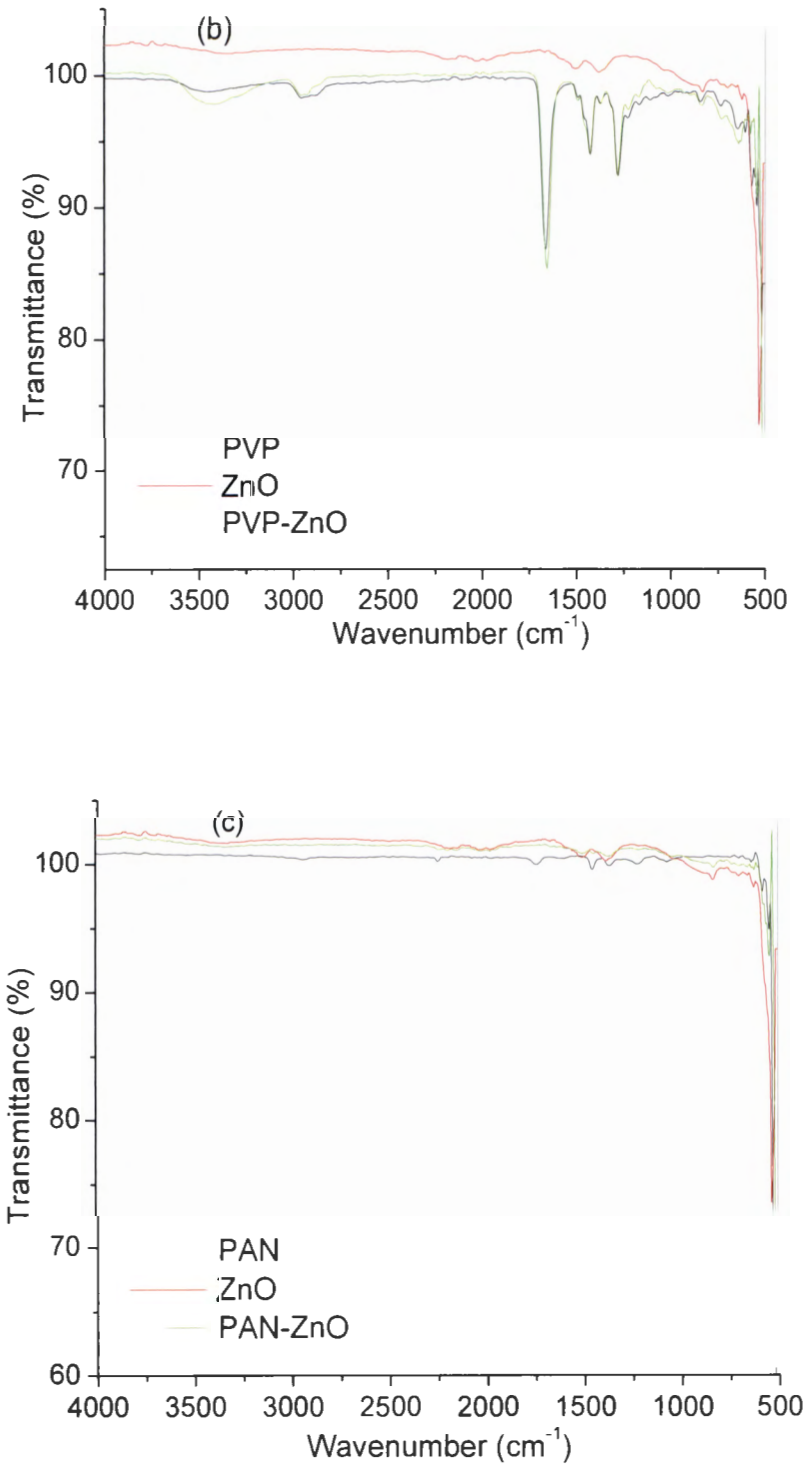

Figure 4.1: FTIR spectra of (a) PEG, ZnO and PEG-ZnO (b) PVP, ZnO and PVP-ZnO (c) PAN, ZnO and PAN-ZnO

4.1.2 ULTRAVIOLET-VISIBLE (UV-vis) SPECTROSCOPY

Further vital information on the chemical interaction between the ZnO nanoparticles and the polymers and their optical properties are obtained by employing ultraviolet visible absorption (UV-vis) spectroscopy [89]. Figure 4.2 shows the UV-vis absorption spectra for the ZnO nanoparticles, PEG, PVP, PAN and their ZnO nanocomposites. All the compounds had a powerful absorption at a wavelength range from 200 to 380 nm (UV region) [90].

The UV-vis absorption spectrum of ZnO nanoparticles exhibits excitonic peak with absorbance intensity at wavelength of 275 nm. A strong peak observed at about 372 nm is characteristic of ZnO nanoparticles and indicates the uniformity or monodispersed nature of the nanoparticle size. For ZnO having a wide band gap of 3.37 eV, an absorption peak of about 358 nm is expected [79, 89]. PEG has an absorbance peak of 275 nm and the incorporation of ZnO into the polymer slightly red shifted the absorbance peak to 276 nm. Another peak was observed at 368 nm. The interaction existing between PEG and the ZnO nanoparticles is responsible for the observed shift [85].

The UV-vis spectrum of PVP showed an absorbance peak of 265 nm with π-π^* transitions of the carbonyl group. The intercalation of ZnO shifted the peak to 276 nm and a new peak appeared at 367 nm. This can be attributed to the presence of ZnO in the nanocomposites which makes the composite absorb more light. This successfully confirms the formation of PVP-ZnO [91].

A characteristic absorption peak of 274 nm was observed for PAN which corresponds to C≡N π absorption [92]. The UV-vis spectrum of PAN-ZnO appeared at 276 nm. The red shift for the PAN-ZnO nanocomposite is attributed to the interaction of the ZnO nanoparticles with the cyanide group of PAN [93].

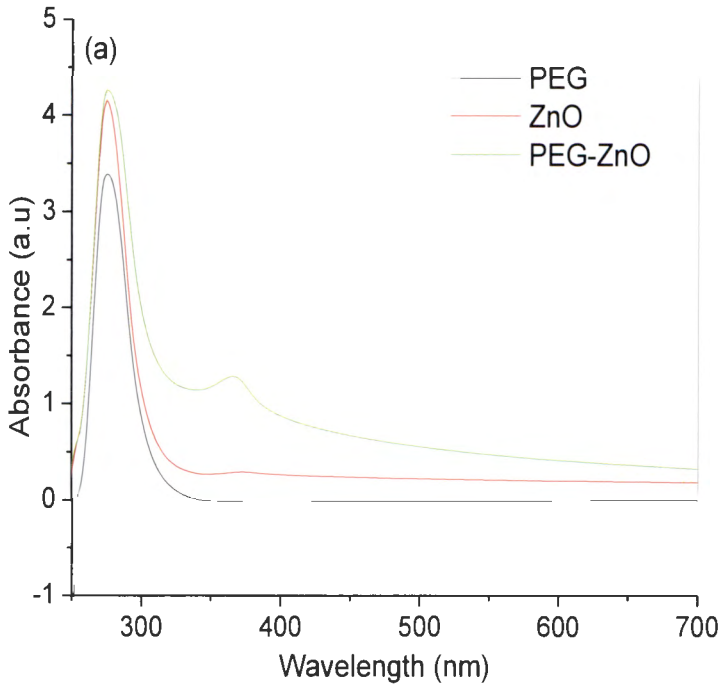
(a)
PEG
ZnO
PEG-ZnO
Absorbance (a.u)
Wavelength (nm)
5
4
3
2
1
0
-1
300
400
500
600
700

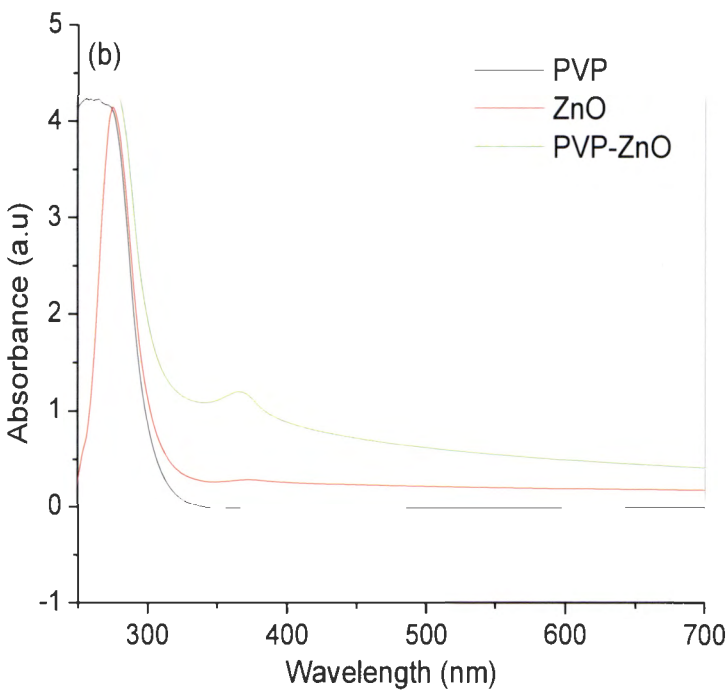
(b)
PVP
ZnO
PVP-ZnO
Absorbance (a.u)
Wavelength (nm)
5
4
3
2
1
0
-1
300
400
500
600
700

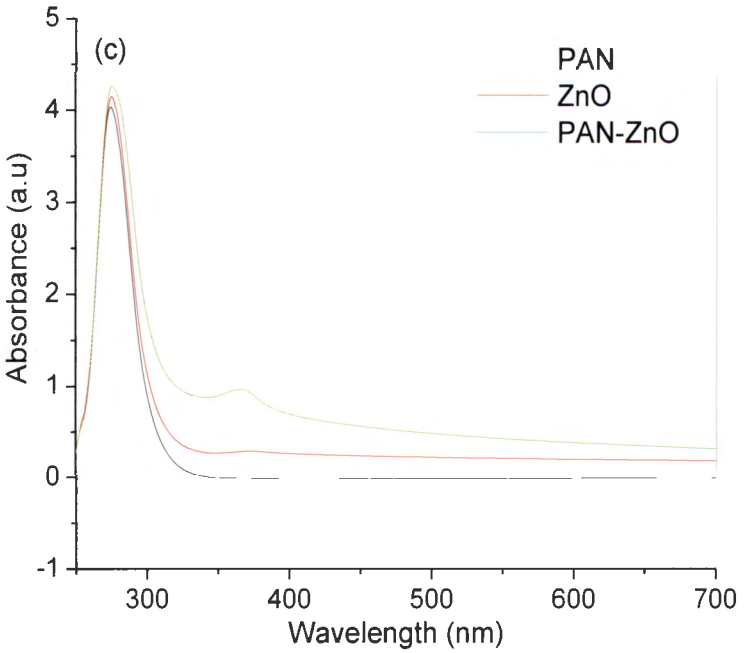

Figure 4.2: Uv-visible spectra of (a) PEG, ZnO and PEG-ZnO (b) PVP, ZnO and PVP-ZnO (c) PAN, ZnO and PAN-ZnO

4.1.3 THERMOGRAVIMETRIC ANALYSIS (TGA)

Thermogravimetric analysis (TGA) is a reliable tool to determine the thermal behaviour of substances, thermal degradation and weight loss as a function of temperature [94]. The TGA profiles of the synthesized ZnO nanoparticles, polymers and polymer nanocomposites are shown in Figure 1.3.

The TGA profile of ZnO nanoparticles shows a total weight loss of 1.5 % within the first 200 °C corresponding to loss of water. There is a rapid weight loss amounting to additional 3 % loss between 200 °C and 285 °C due to decomposition of ZnO in its present phase (probably the wurtzite phase). There is an indication of phase transition (possibly from wurtzite to zinc blende phase) at about 285 °C. It lost some weight after the transition but the weight loss thereafter is not as rapid as in the first 300 °C. No significant decomposition occurs above 492 °C up to 700 °C. This implies that when $Zn(OH)_2$ was heated, it converted into ZnO nanoparticles and became stable above 492 °C [95].

Figure 4.3(b) shows the TGA profile of PEG-ZnO to have an initial weight loss of 4.19 % at about 212 °C which is attributed to the elimination of water and volatile solvents. This is accompanied by a rapid weight loss of 73.16 % at 530 °C. PEG was almost completely thermally decomposed at about 420 °C. At 650 °C, the residue of PEG-ZnO was about 23 % while PEG was less than 1.00 %. This confirms that the presence of ZnO nanoparticles in PEG-ZnO nanocomposites improves the thermal stability of the polymer [96].

PVP-ZnO demonstrated three stages of weight loss. At the first stage, there was 8.13 % weight loss from room temperature to 308 °C which is attributed to the loss of residual solvent present in the nanocomposite. The second stage had a weight loss of 76.80 % which started at 308 °C and ended at about 502 °C due to the decomposition of PVP chains. Finally, an insignificant loss of about 1.00 % occurred at 641 °C and it is expected that the only change at this stage is in the crystal structure. It is observed that the PVP was completely decomposed at 641 °C leaving only the carbon residue. From the thermal behaviour of PVP observed in the curve, it is seen that an initial weight loss of 4.71 % occurred at 270 °C followed by a significant weight loss of 90.38 % between 270 °C and 464 °C which represents the decomposition of the polymer. PVP-ZnO nanocomposite is more thermally stable compared to PVP and this can be attributed to the higher chain compactness due to the interaction between the PVP and ZnO nanoparticles [97].

For PAN, 1.40 % weight loss was observed at 268 °C, attributed to the loss of moisture, low molecular weight oligopolymers and dehydrogenation. This is followed by a rapid weight loss of 32.00 % between a temperature range of 267 and 350 °C. The third stage of 23.08 % weight loss occurred at about 485 °C leading to reduction in the weight of PAN. The PAN-ZnO nanocomposite had weight losses of 2.24 % at 267 °C at the first stage, 21.81 % at 324 °C and 18.17 % at 485 °C at the third stage. It is observed that while the total weight loss of 56.48 % was recorded in PAN at about 485 °C, the nanocomposite containing ZnO nanoparticles had a reduced weight loss of 42.22 % at the same temperature with a higher residue. These results reveal that the presence of the ZnO nanoparticles in the polymer backbone reduced weight loss and promoted the formation of a thermally stable structure due to the bonding existing between them [87, 98].

The fact that ZnO improved thermal stability of the polymers could lead to the suggestion that the polymer-ZnO nanocomposites would be more useful during high temperature industrial processes where corrosion needs to be inhibited.

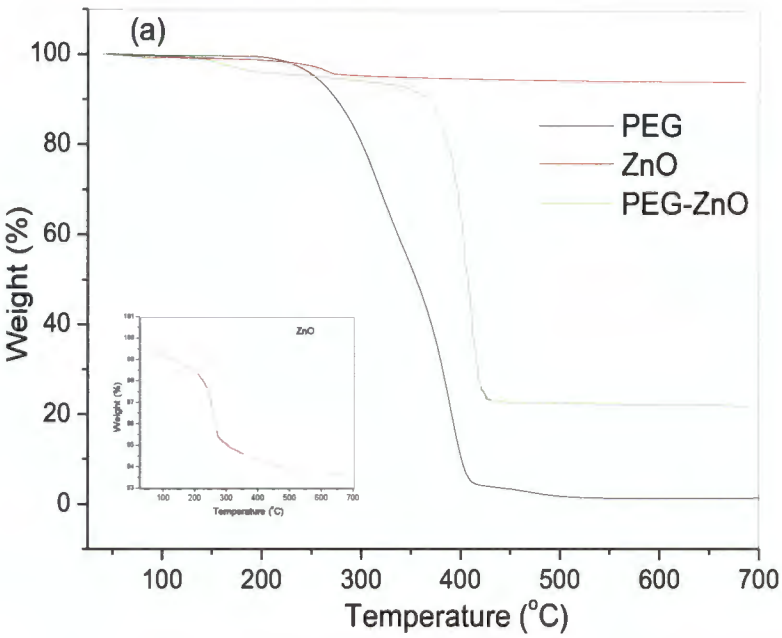
(a)
PEG
ZnO
PEG-ZnO
Weight (%)
Temperature (°C)
100
80
60
40
20
0
100
200
300
400
500
600
700
ZnO
Weight (%)
Temperature (°C)

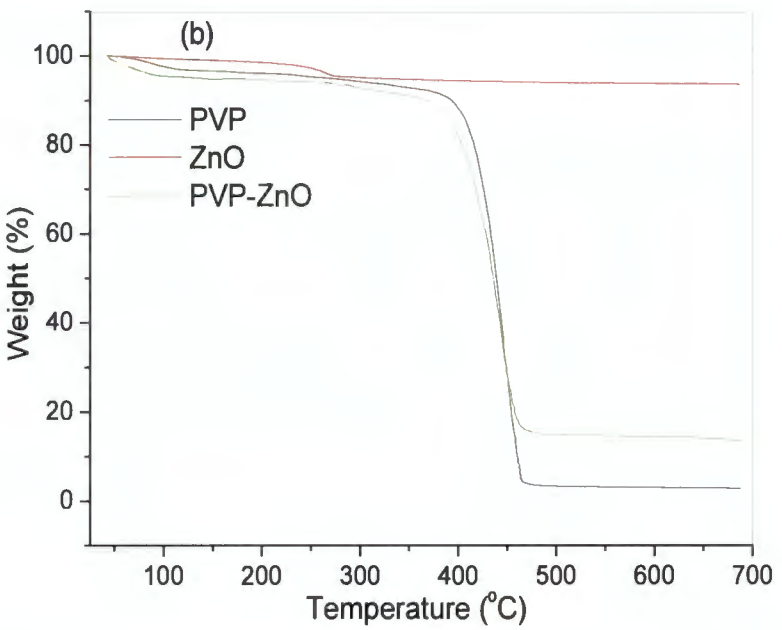
(b)
PVP
ZnO
PVP-ZnO
Weight (%)
Temperature (°C)
100
80
60
40
20
0
100
200
300
400
500
600
700

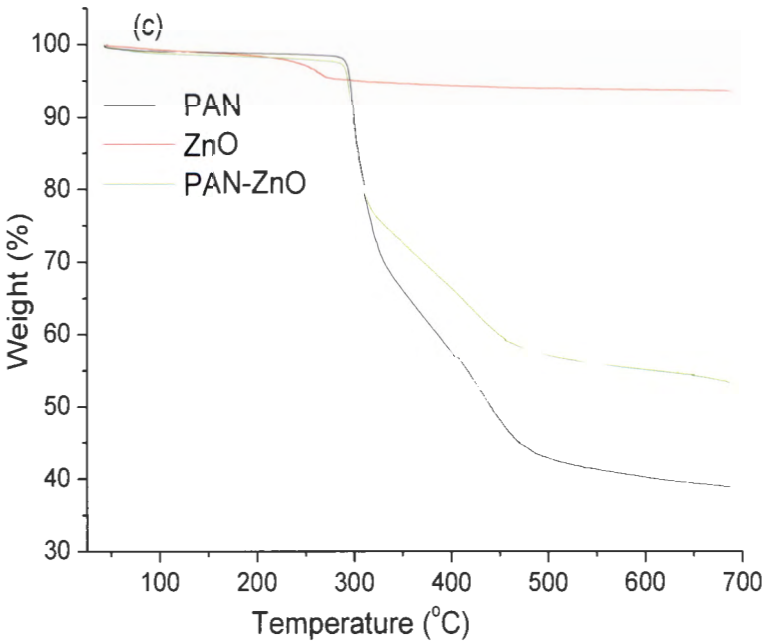

Figure 4.3: Thermogravimetric analysis curves of (a) PEG, ZnO and PEG-ZnO (b) PVP, ZnO and PVP-ZnO (c) PAN, ZnO and PAN-ZnO

4.1.4 TRANSMISSION ELECTRON MICROSCOPY (TEM)

Transmission electron microscopy (TEM) provides visual information on the surface morphology of the ZnO nanoparticles and the polymer-ZnO nanocomposites. The surface morphologies of the ZnO nanoparticles and polymer nanocomposites were examined using TEM and the results are shown in Figure 4.4.

The TEM image for the ZnO nanoparticles as presented in Figure 4.4(a) shows the ZnO nanoparticles are crystalline and rod-like in shape. The sizes of the ZnO nanoparticles are in the range of 50 – 75 nm. The presence of aggregated ZnO is evident from the TEM image. Figure 4.4(b-d) shows that the ZnO nanoparticles are incorporated inside the matrix of PEG, PVP and PAN. The shapes of the polymer nanocomposites are also rod-like. The light areas represent the polymers while the dark spots may be due to the aggregation of the ZnO nanoparticles in the nanocomposites. The size range for the nanocomposites is also 50 – 75 nm. The images confirm the successful formation and synthesis of ZnO nanoparticles and ZnO nanocomposites [89, 99, 100].

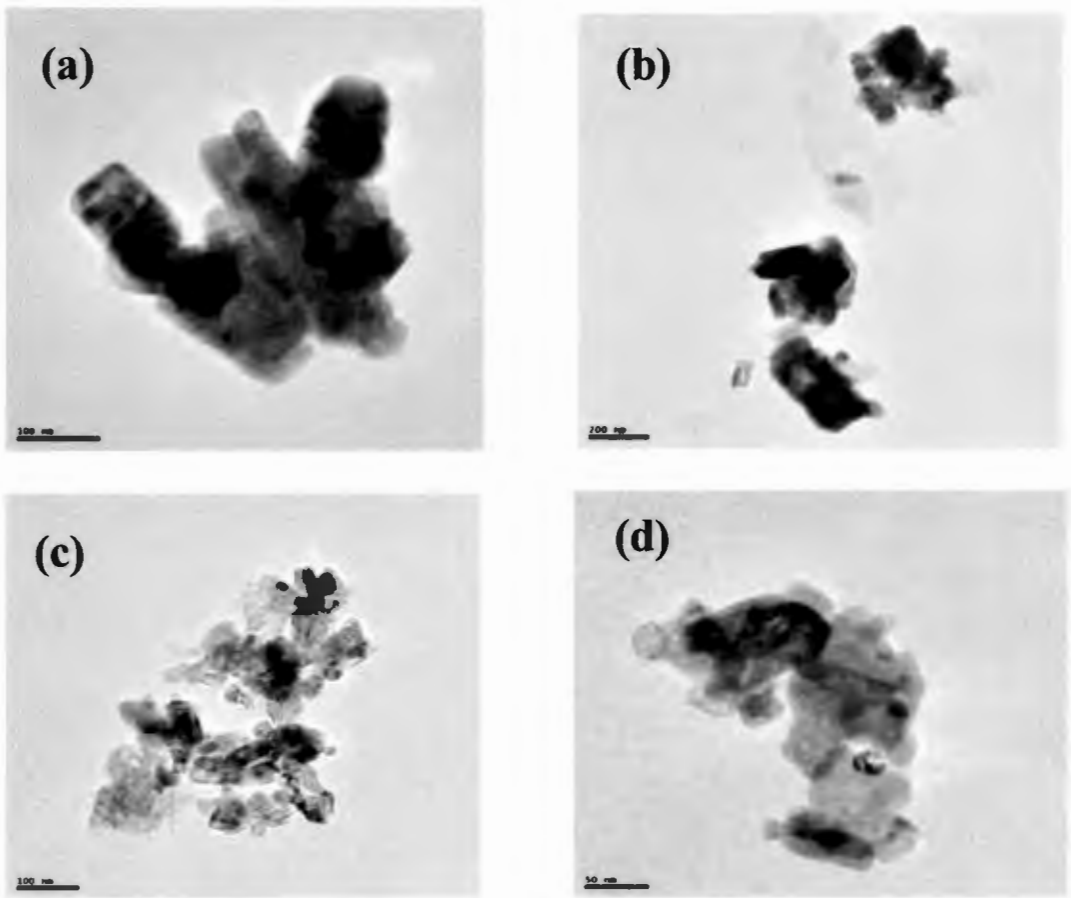

Figure 4.4: TEM images of (a) ZnO nanoparticles (b) PEG-ZnO (c) PVP-ZnO (d) PAN-ZnO

4.2 ELECTROCHEMICAL MEASUREMENTS

4.2.1 POTENTIODYNAMIC POLARIZATION (PDP)

Potentiodynamic polarization measurements were carried out to gain insight into the kinetics of the anodic and cathodic reactions. Tafel polarization curves were obtained from potentiodynamic polarization experiments on mild steel in 5 % HCl in the presence and absence of different concentrations of PEG, PVP, PAN and their respective polymer-ZnO nanocomposites at 303 K and the results are shown in Figures 4.5 – 4.7.

The inhibition efficiency was calculated using Equation 4.1:

$$IE_i = \frac{i^0_{corr} - i^i_{corr}}{i^0_{corr}} \times 100 \qquad (4.1)$$

where, i^{o}_{corr} and i^{i}_{corr} are corrosion current densities in the absence and presence of studied inhibitors respectively.

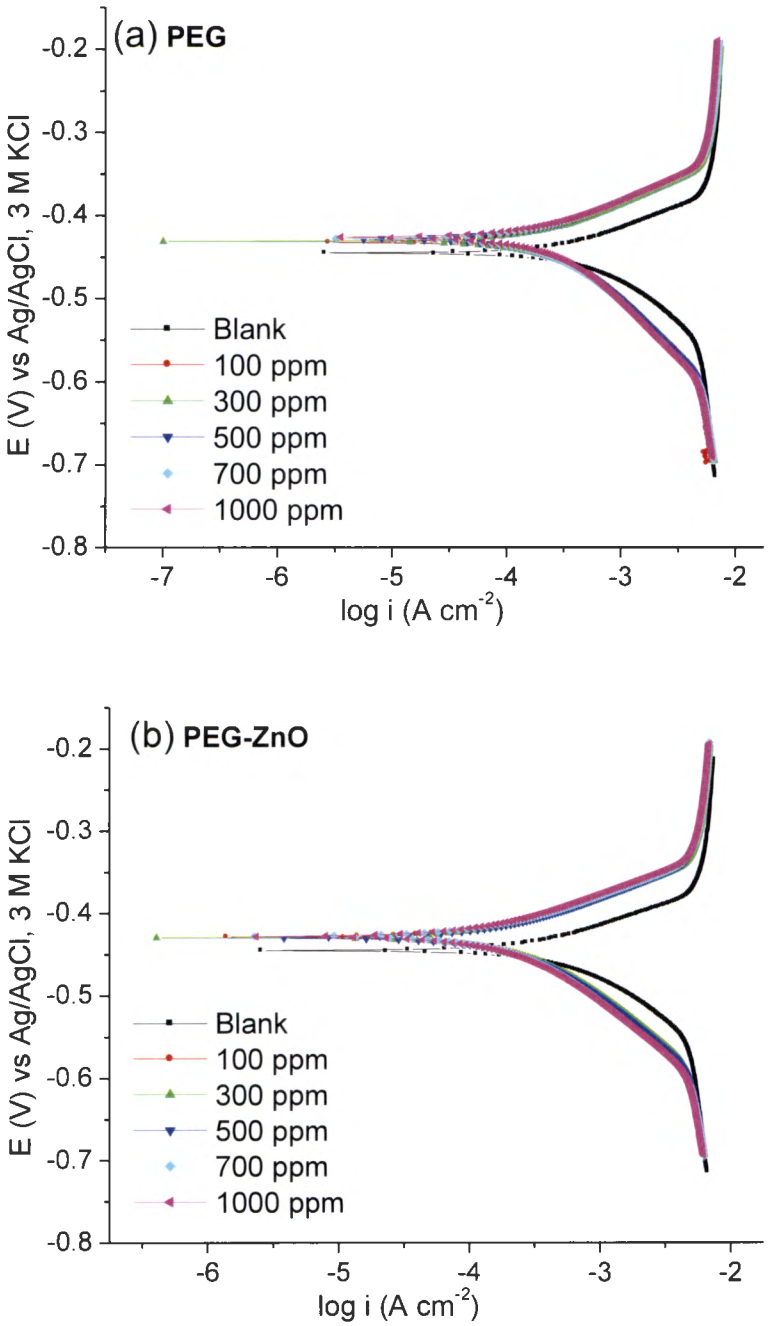

Figure 4.5: Potentiodynamic polarization curves of mild steel in 5 % HCl without and with various concentrations of (a) PEG and (b) PEG-ZnO

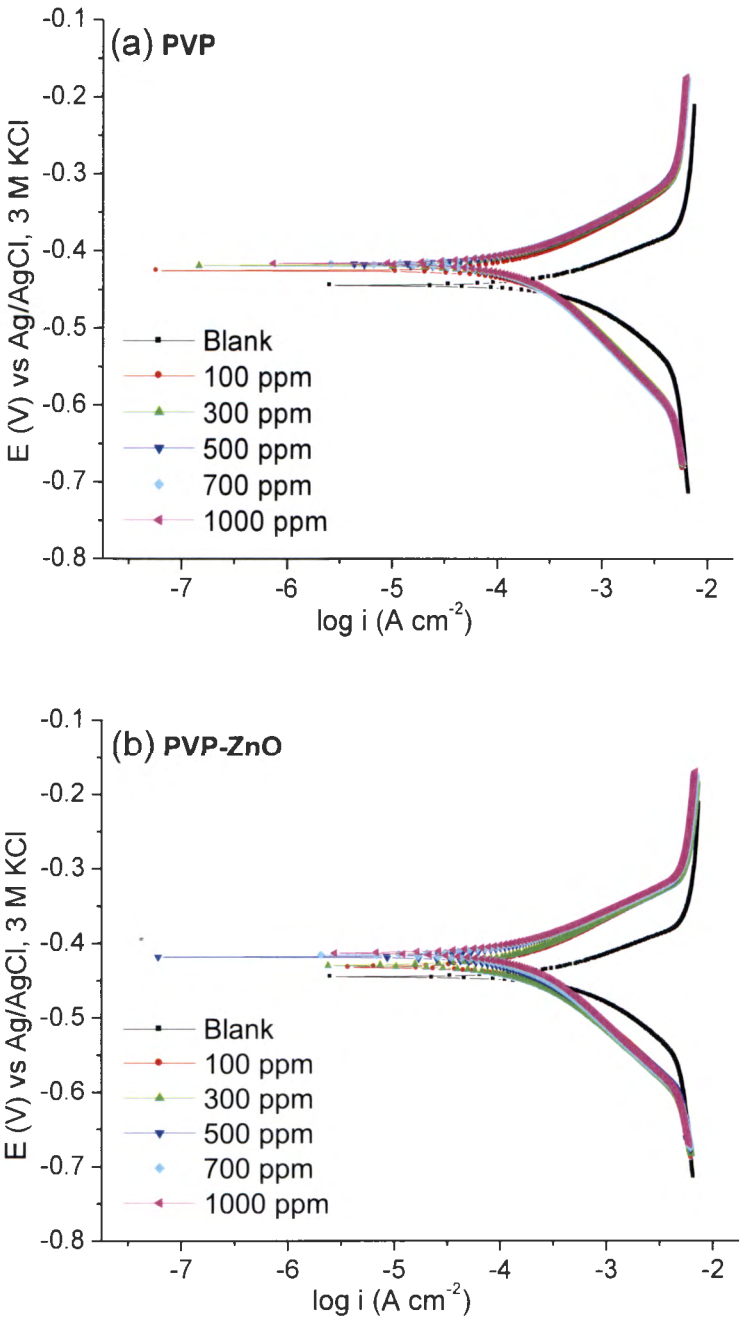

Figure 4.6: Potentiodynamic polarization curves of mild steel in 5 % HCl without and with various concentrations of (a) PVP and (b) PVP-ZnO

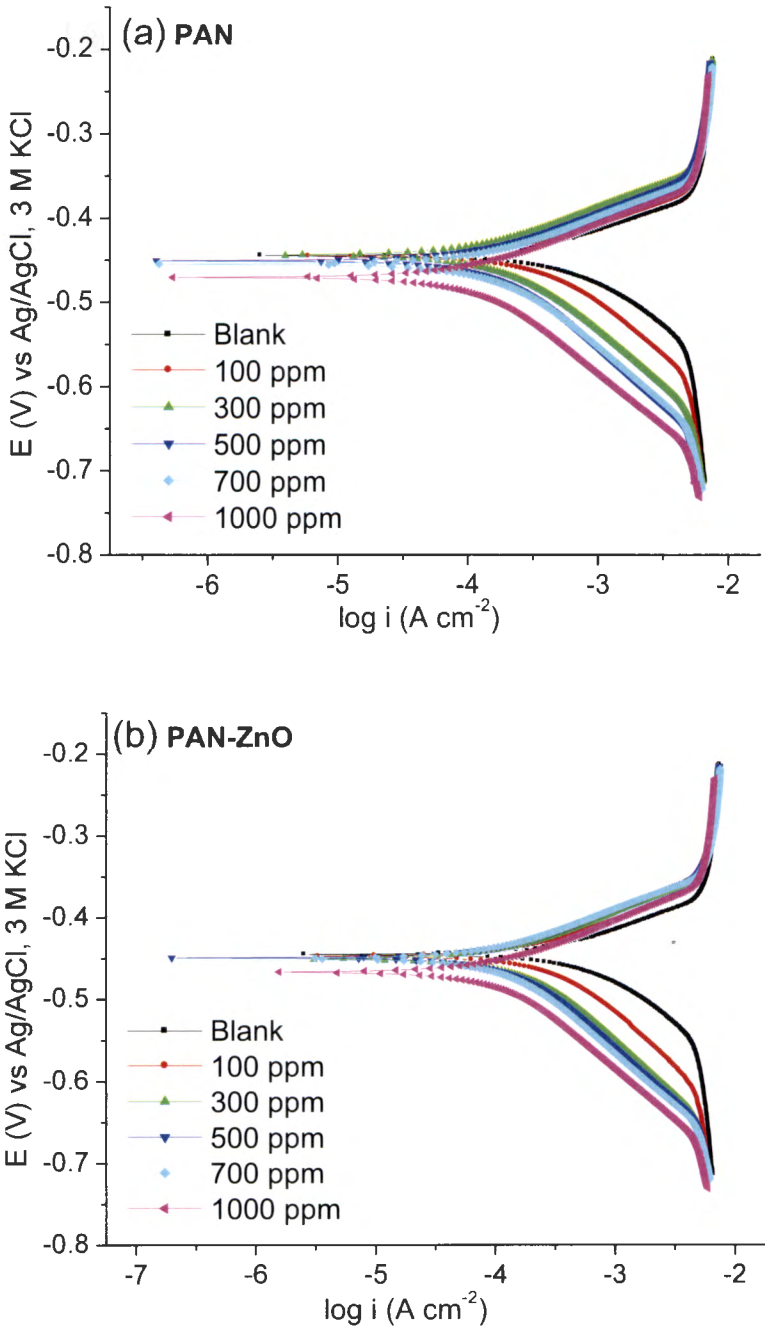

Figure 4.7: Potentiodynamic polarization curves of mild steel in 5 % HCl without and with various concentrations of (a) PAN and (b) PAN-ZnO

It can be seen from the plots that the addition of the studied inhibitors into the acidic medium reduced both the anodic and cathodic reactions and slightly shifted the corrosion potential to noble position except in the case of PAN and PAN-ZnO. The shift towards the noble position suggests that the inhibitors reduced the anodic dissolution of mild steel better than cathodic hydrogen ion reduction [45].

Table 4.1 below presents the values of electrochemical kinetic parameters such as the corrosion potential (E_{corr}), corrosion current density (i_{corr}), anodic Tafel slope (b_a) and cathodic Tafel slope (b_c) obtained from the potentiodynamic polarization curves.

Table 4.1: Electrochemical kinetic parameters obtained from polarization experiments for mild steel in 5 % HCl in the presence and absence of studied inhibitors

Inhibitor Conc. (ppm)	**$-E_{corr}$ (mV)**	**i_{corr} ($\mu A/cm^2$)**	**R_p (Ωcm^2)**	**b_a (mV/dec)**	**b_c (mV/dec)**	**%IE_i**	**%IE_P**
Blank (5 % HCl)	445.05	655.25	33.91	118.95	89.77	-	-
PEG (as inhibitor)							
100	433.28	271.77	72.85	122.29	72.68	58.52	53.45
300	432.12	255.53	74.14	118.89	68.90	61.00	54.26
500	429.25	238.86	78.67	118.83	68.04	63.55	56.90
700	428.88	224.75	81.63	119.03	65.48	65.70	58.46
1000	427.53	218.23	81.70	111.63	65.01	66.70	58.50
PEG-ZnO (as inhibitor)							
100	419.35	244.23	80.00	114.12	74.27	62.73	57.61
300	430.27	231.90	80.16	103.72	72.88	64.61	57.70
500	430.42	210.28	84.84	103.93	67.93	67.91	60.00
700	428.41	208.50	88.65	116.17	67.17	68.18	61.75
1000	428.53	200.31	94.40	115.31	69.95	69.43	64.08
PVP (as inhibitor)							
100	427.71	209.87	97.23	114.43	79.72	67.97	65.12
300	420.85	206.66	102.31	128.19	78.49	68.46	66.56
500	419.18	202.64	108.23	140.48	78.84	69.07	68.67
700	418.39	201.46	110.33	142.15	79.97	69.25	69.27
1000	418.16	183.23	110.54	121.63	75.64	72.04	69.32
PVP-ZnO (as inhibitor)							
100	433.27	205.52	100.50	106.23	86.12	68.64	66.26
300	430.95	204.38	106.98	125.80	83.94	68.81	68.30
500	419.66	184.11	110.20	125.83	74.31	71.90	69.23
700	416.66	176.04	113.34	130.37	71.04	73.13	70.08
1000	414.12	167.06	114.53	115.40	71.27	74.50	70.39
PAN (as inhibitor)							
100	447.57	508.89	44.62	152.48	79.57	22.30	24.00
300	445.87	281.63	89.84	150.91	94.90	57.02	62.26
500	452.63	243.36	93.78	160.02	78.25	62.86	63.84
700	456.59	207.91	100.44	142.17	72.66	68.27	66.24
1000	472.47	123.90	161.65	128.34	71.99	81.09	79.02
PAN-ZnO (as inhibitor)							
100	448.34	380.28	57.95	149.65	76.92	41.96	41.48
300	451.73	237.96	93.83	150.34	78.14	63.68	63.86
500	450.16	191.61	111.07	146.24	73.70	70.76	69.47
700	451.09	138.19	137.00	133.30	64.77	78.91	75.25
1000	467.79	108.67	168.82	123.13	64.30	83.42	79.91

The observed shifts in E_{corr} in the presence of the studied inhibitors do not follow a definite trend. The range of maximum displacement of E_{corr} as a result of the introduction of the various studied inhibitors into the acid solution is ± 27.42 mV. Since the E_{corr} displacement is less than 85 mV, it indicates the inhibitors function as mixed-type corrosion inhibitors with predominant anodic effect in all the studied inhibitors except PAN and PAN-ZnO, which acts predominantly as cathodic inhibitors [101, 102]. There is no remarkable effect of the addition of inhibitors on anodic and cathodic Tafel slopes, which suggests that adsorption of the polymers and the polymer nanocomposites on the metal surface is simply by geometrical blocking mechanism without any interference on the anodic dissolution and cathodic hydrogen ion reduction mechanisms [45]. It can be observed that increase in the concentration of the studied inhibitors leads to decrease in the corrosion current density, i_{corr} thereby leading to increase in inhibition efficiency.

4.2.2 LINEAR POLARIZATION RESISTANCE (LPR)

The values of the polarization resistance (R_p) and the calculated inhibition efficiency (IE_p) obtained for mild steel corrosion in the presence and absence of various concentrations of the studied inhibitors at 303 K are listed in Table 4.1.

It is observed that the values of R_p in the presence of inhibitors are higher than that of the uninhibited solution. This trend suggests that the studied inhibitors retarded corrosion by increasing the protective film on the mild steel surface [103].

The inhibition efficiency for the studied polymers and their ZnO nanocomposites was obtained from the values of the polarization resistance (R_p) in the absence and presence of the inhibitors using the equation:

$$IE_p = \frac{R_p - R^0{}_p}{R_p} \times 100 \qquad (4.2)$$

where, R^o_p and R_p are the polarization resistance values in the absence and presence of the studied inhibitors.

There is a good agreement between the results obtained from linear polarization measurements and potentiodynamic polarization experiments. The results further revealed that polymer-ZnO

nanocomposites generally showed higher inhibition efficiencies than the corresponding polymer alone. The synergistic effect of ZnO nanoparticles on the inhibition efficiency of the polymers is more obvious for PAN as its inhibition efficiency was nearly doubled by the addition of ZnO nanoparticles at 100 ppm concentration of the polymer.

4.2.3 ELECTROCHEMICAL IMPEDANCE SPECTROSCOPY (EIS)

Electrochemical impedance spectroscopy (EIS) is a reliable method widely used in the study of corrosion inhibition. It helps to gain knowledge of the kinetics of the electrode processes and the surface properties of the systems under investigation.

EIS measures the impedance of an electrochemical system over a range of frequencies from which the frequency response of the system including the energy storage and dissipation properties of the system can be determined. Impedance spectra can be represented in various ways including Nyquist, Bode modulus and Bode phase angle. Some scholars have suggested that Bode modulus is the easiest and most suitable of the three common impedance representation methods. This is because it minimizes the dispersion of the experimental data and gives a better insight into the frequency-dependent behaviour of the electrochemical system. Nevertheless some authors prefer to use the three representation methods and compare their spectra [103, 104].

The Nyquist and Bode plots of mild steel in 5 % HCl in the presence and absence of the various concentrations of PEG, PVP, PAN and their ZnO nanocomposites at 303 K are presented in Figures 4.8 – 4.12.

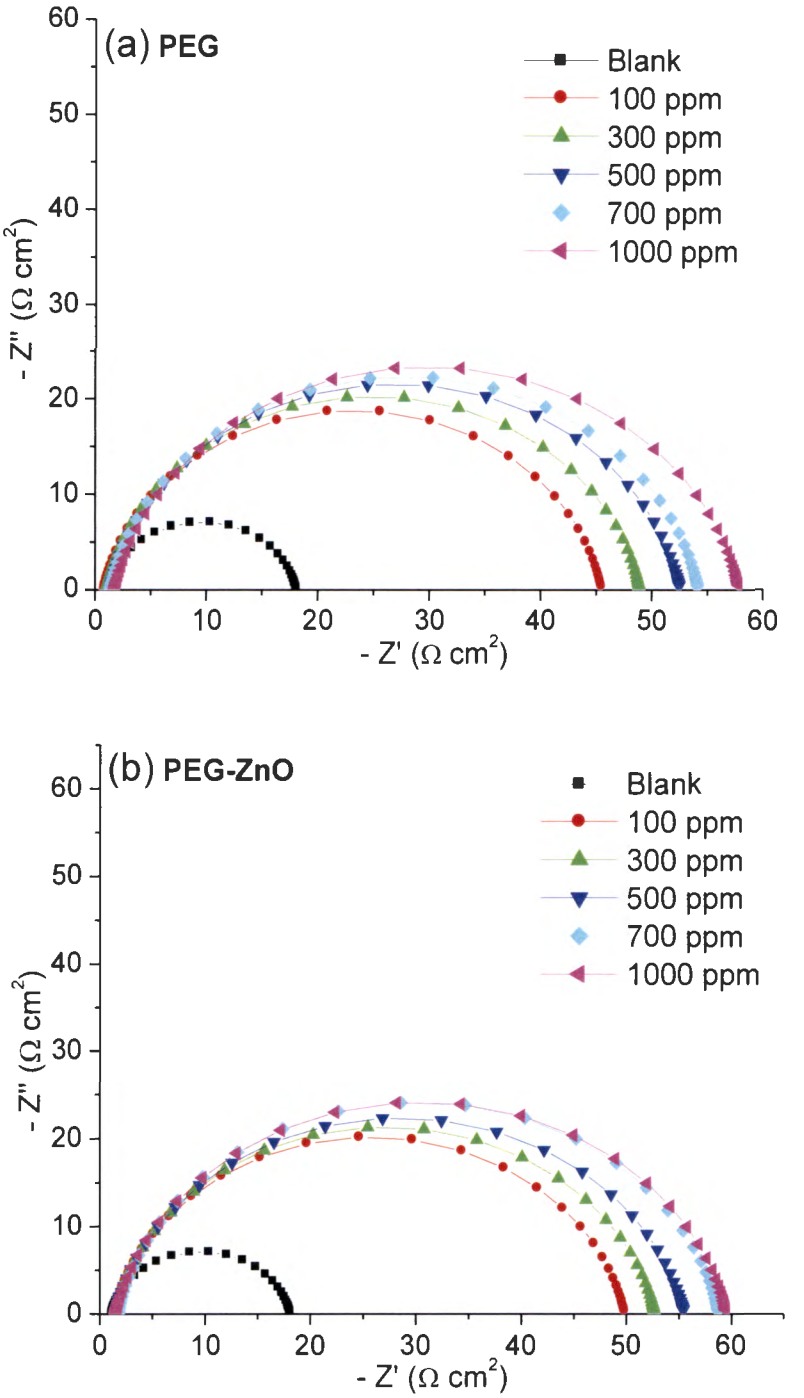

Figure 4.8: Nyquist plots for mild steel in 5 % HCl without and with various concentrations of (a) PEG and (b) PEG-ZnO

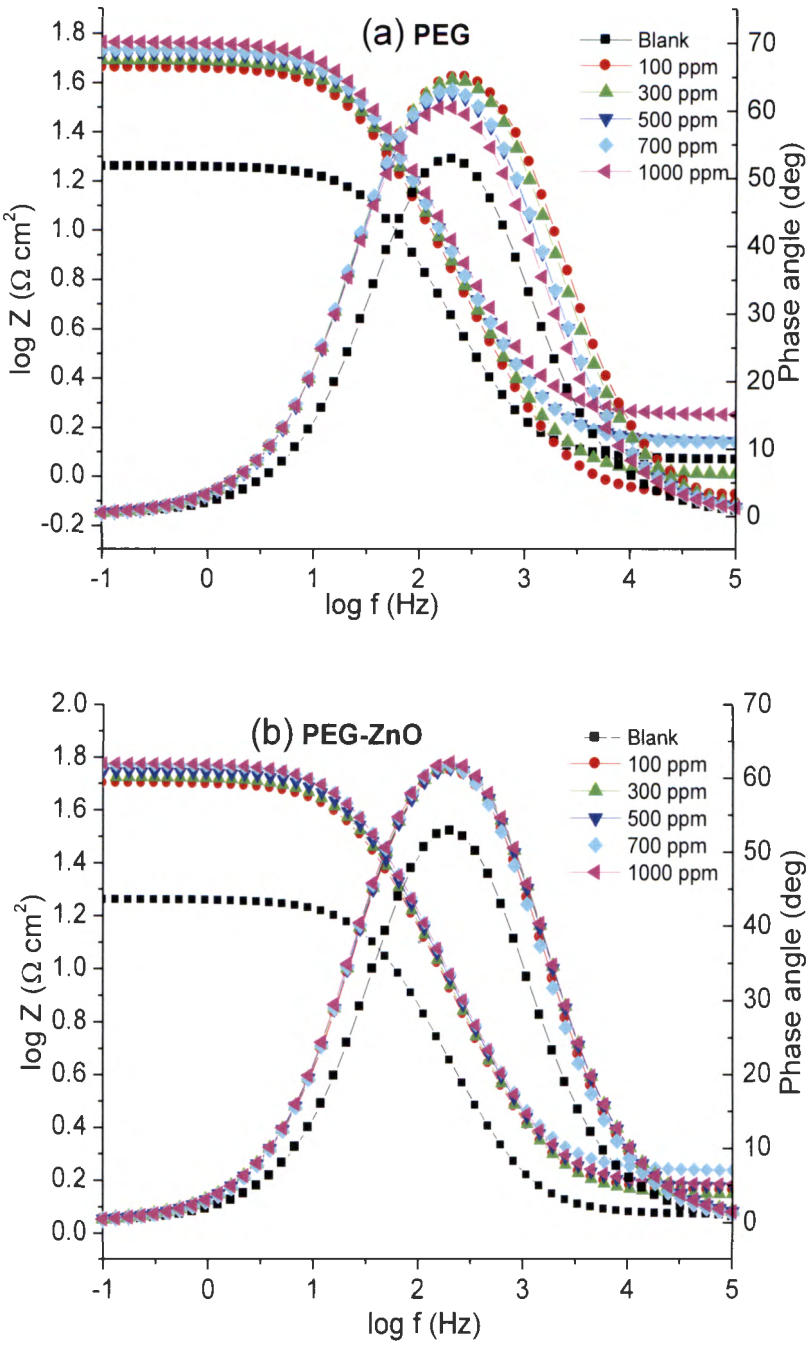

Figure 4.9: Bode plots for mild steel in 5 % HCl without and with various concentrations of (a) PEG and (b) PEG-ZnO

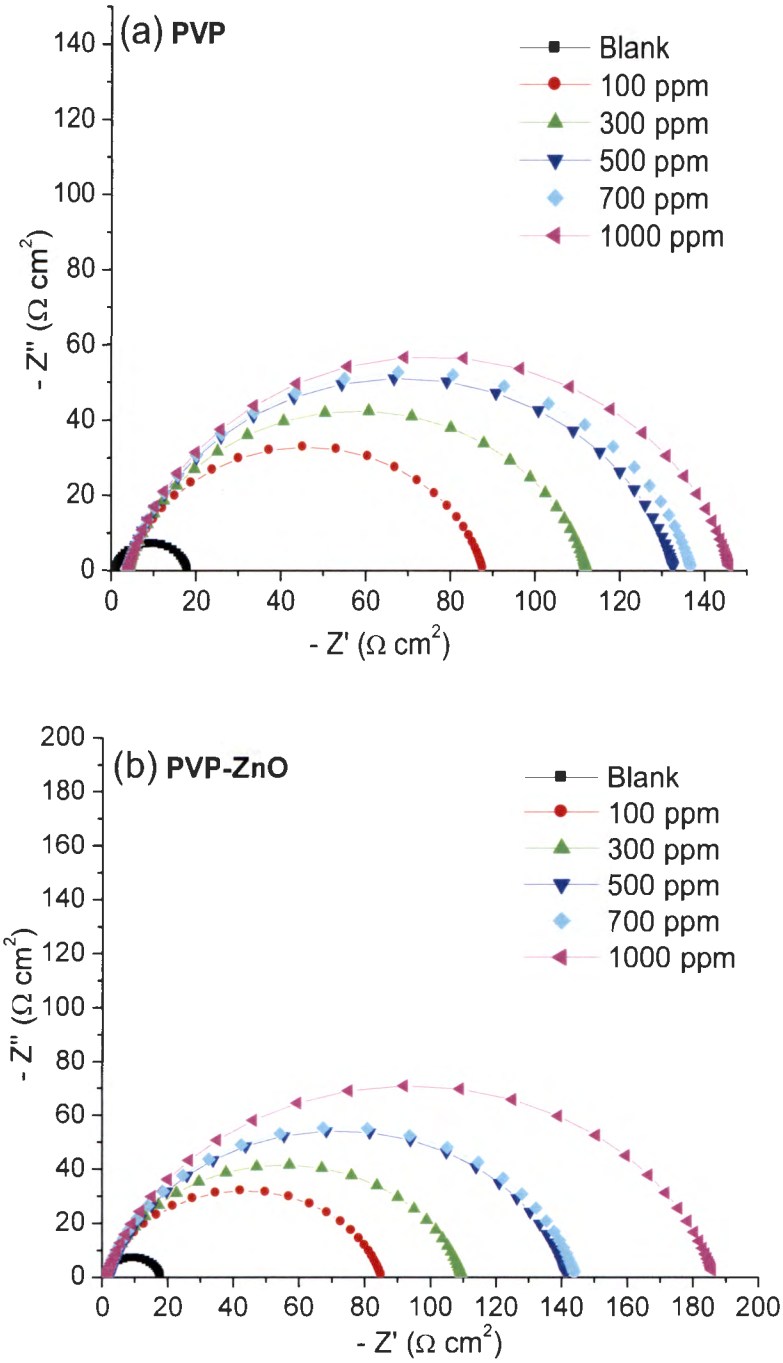

Figure 4.10: Nyquist plots for mild steel in 5 % HCl without and with various concentrations of (a) PVP and (b) PVP-ZnO

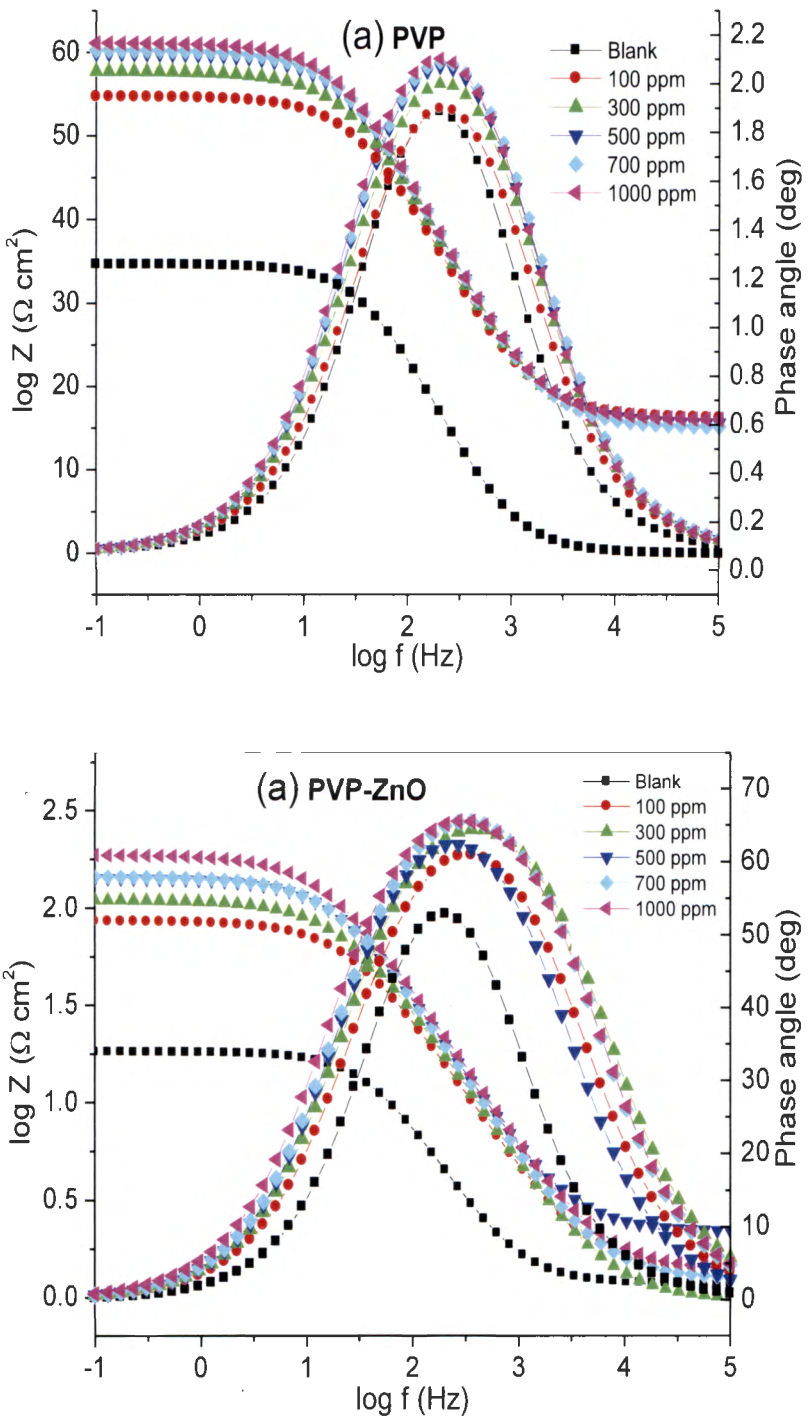

Figure 4.11: Bode plots for mild steel in 5 % HCl without and with various concentrations of (a) PVP and (b) PVP-ZnO

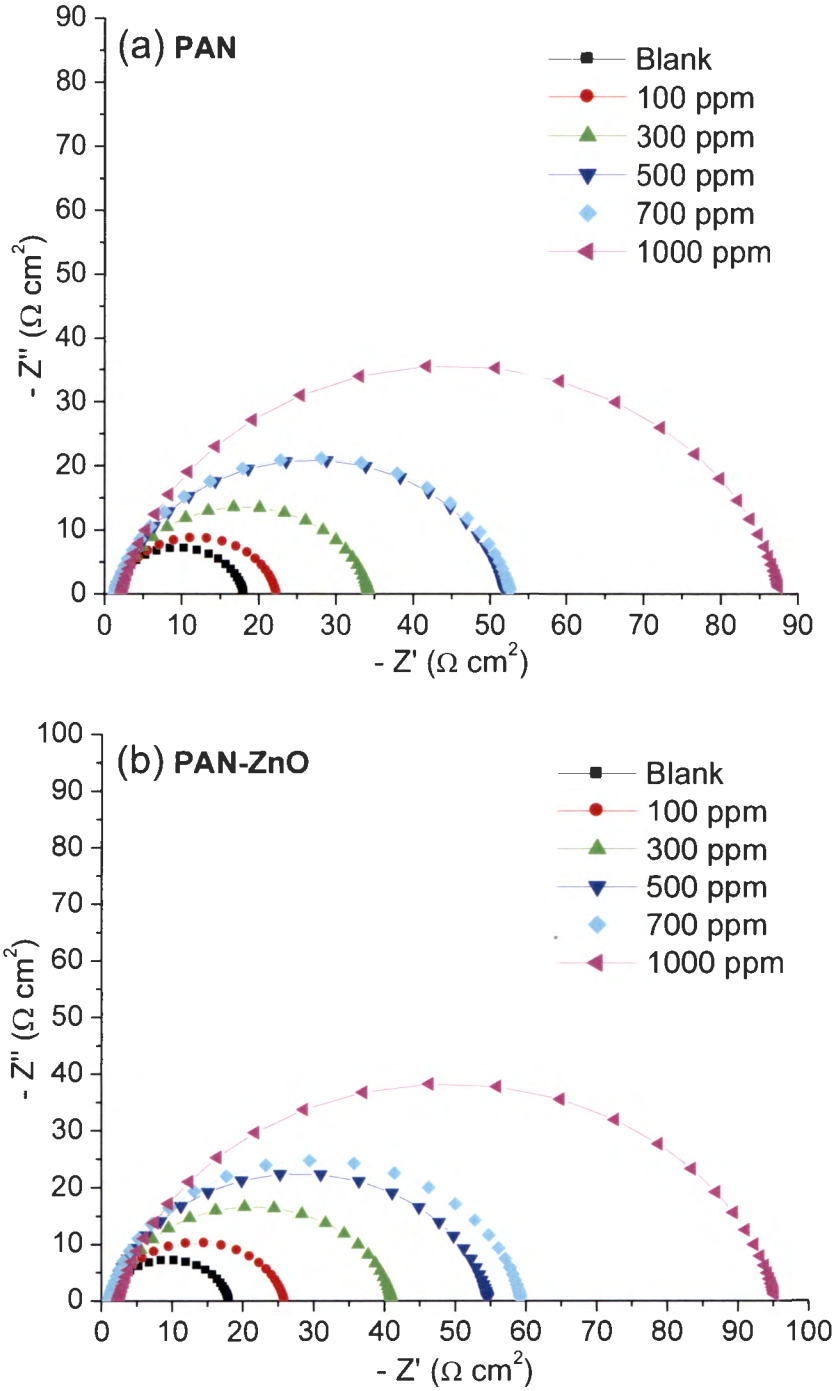

Figure 4.12: Nyquist plots for mild steel in 5 % HCl without and with various concentrations of (a) PAN and (b) PAN-ZnO

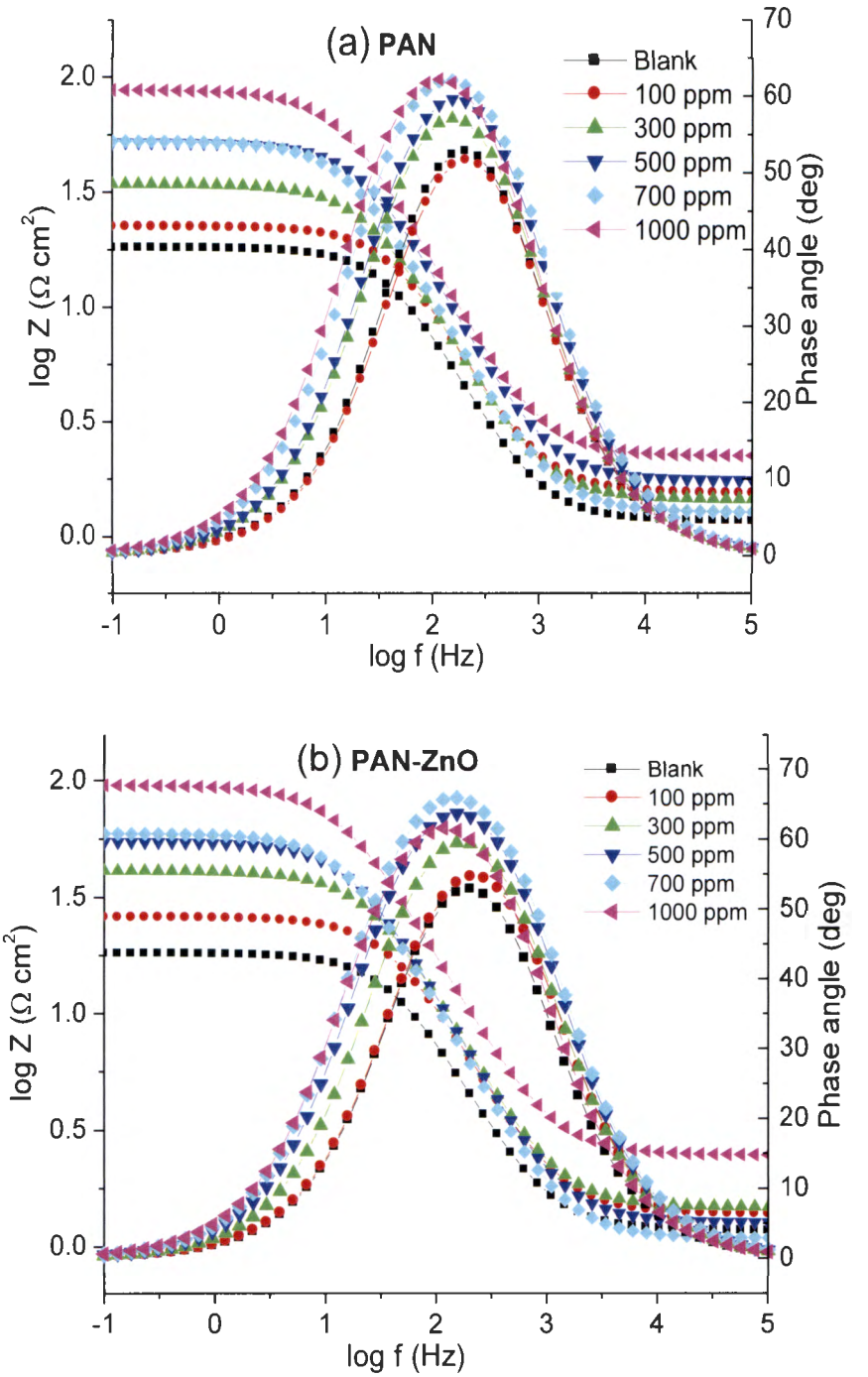

Figure 4.13: Bode plots for mild steel in 5 % HCl without and with various concentrations of (a) PAN and (b) PAN-ZnO

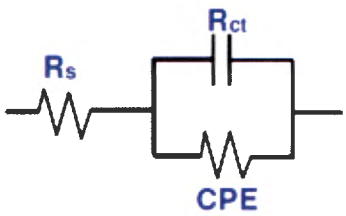

Figure 4.14: Randle's equivalent circuit

The Nyquist plots contain depressed and imperfect semicircles which are characteristic features of solid electrodes and are often referred to as the frequency dispersions of interfacial impedance. This feature is commonly attributed to different factors such as surface roughness, adsorption of inhibitors, impurities, discontinuity in the electrode and inhomogeneity of the electrode surface [75, 105]. The single depressed semicircles in the Nyquist plots correspond to one time constant in the Bode plots. This implies that the corrosion of mild steel is mainly controlled by a single charge transfer process. The existing similarity in the nature of the Nyquist and Bode plots obtained from the impedance studies suggest that the inhibitors do not alter the corrosion mechanism [106, 107]. The shape of the depressed semicircles in the absence and presence of the studied inhibitors follow the same trend showing that the addition of the inhibitors did not affect the mechanism of corrosion of the mild steel substrate in the acidic medium.

The Nyquist plots presented in Figures 4.8, 4.10 and 4.12 exhibit both large capacitive loops and inductive loops at high frequencies and low frequencies, respectively. The high frequency capacitive loop is attributed to the charge transfer reaction and double layer capacitance (C_{dl}) while the low frequency inductive loop is attributed to relaxation process due to the adsorption of charged species on the working electrode surface [109, 110]. The diameter of the capacitive loop is found to increase with increase in the concentration of the studied inhibitors which reduces the rate of electrochemical corrosion. The Bode plots exhibited increased area under the phase angle curves in the presence of the studied inhibitors compared to the uninhibited solution [108]. This suggests the adsorption of the inhibitor molecules on the mild steel surface and the formation of protective film.

Figure 4.14 shows the electrical equivalent circuit used to analyze the impedance spectra. The Randle's equivalent circuit used for all the studied inhibitors is one having a resistor of solution resistance (R_s), and a resistor of charge transfer resistance (R_{ct}) in parallel connection with the

constant phase element (CPE). For the description of a frequency independent phase shift between an applied alternating current (ac) potential and its current response, a constant phase element (CPE) is used which is defined in impedance representation as seen in Equation 4.3 below;

$$Z_{CPE} = Y_0^{-1}(i\omega)^{-n} \tag{4.3}$$

where; Y_0 is the CPE constant, ω is the angular frequency (in rad s^{-1}), $i^2 = -1$ is the imaginary number and n is a CPE exponent which can be used as a gauge of the heterogeneity or roughness of the surface. Depending on the value of n, CPE can represent resistance (n = 0, Y_0 = R), capacitance (n = 1, Y_0 = C), inductance (n = −1, $Y_0 = L$) or Warburg impedance (n = 0.5, $Y_0 = W$) [111].

Equation 4.4 below was used to calculate the values of double-layer capacitance, C_d

$$C_{dl} = (Y_0 R_{ct}^{1-n})^{1/n} \tag{4.4}$$

where, Y_0 is the CPE (constant phase element) constant, R_{ct} the charge-transfer resistance and n is a CPE exponent which can be used as a gauge of the heterogeneity or roughness of the surface [112].

The inhibition efficiency was determined from the values obtained from the electrochemical impedance spectroscopic measurement according to Equation 4.5 [113];

$$IE_z = \frac{R_{ct} - R^0_{ct}}{R_{ct}} \times 100 \tag{4.5}$$

where, IE_z is the inhibition efficiency, R_{ct} and R^0_{ct} are the charge transfer resistances in the presence and absence of studied inhibitors respectively.

The surface coverage values (θ) are obtained for all concentrations using Equation 4.6

$$\theta = 1 - \frac{R^0_{ct}}{R_{ct}} \tag{4.6}$$

The electrochemical impedance parameters such as solution resistance (R_s), charge transfer resistance (R_{ct}), double layer capacitance (C_{dl}), and the calculated inhibition efficiency obtained from the analysis of the impedance spectra are presented in Table 4.2.

Table 4.2: Electrochemical impedance parameters obtained for mild steel in 5 % HCl in the presence and absence of studied inhibitors

Concentration	**R_s (Ω cm^2)**	**R_{ct} (Ω cm^2)**	**n**	**Y_0 (μFcm^{-2})**	**C_{dl} (μFcm^{-2})**	**%IE$_z$**
Blank (5 % HCl)	1.17	17.0	0.886	425	225.31	-
PEG (as inhibitor)						
100 ppm	0.83	44.7	0.886	258	146.51	61.97
300 ppm	1.01	47.9	0.891	233	134.48	64.51
500 ppm	1.38	51.1	0.890	219	125.68	66.73
700 ppm	1.37	52.8	0.892	215	124.99	67.80
1000 ppm	1.78	56.1	0.882	210	115.91	69.70
PEG-ZnO (as inhibitor)						
100 ppm	1.44	48.5	0.882	226	123.54	64.95
300 ppm	1.39	51.3	0.880	221	119.94	66.86
500 ppm	1.49	54.0	0.879	211	113.93	68.52
700 ppm	1.72	57.0	0.892	186	107.24	70.18
1000 ppm	1.52	58.0	0.882	197	108.29	70.69
PVP (as inhibitor)						
100 ppm	4.19	83.6	0.844	122	52.29	79.67
300 ppm	3.99	108.0	0.845	110	48.79	84.26
500 ppm	3.98	129.0	0.851	98	45.59	86.82
700 ppm	3.85	133.0	0.851	96	44.73	87.22
1000 ppm	4.13	142.0	0.857	93	45.16	88.03
PVP-ZnO (as inhibitor)						
100 ppm	1.37	83.9	0.826	171	69.91	79.74
300 ppm	0.97	109.0	0.828	154	65.90	84.40
500 ppm	2.16	139.0	0.839	126	57.98	87.77
700 ppm	1.24	143.0	0.839	127	57.52	88.11
1000 ppm	1.38	185.0	0.831	120	55.31	90.81
PAN (as inhibitor)						
100 ppm	1.53	20.8	0.880	338	171.87	18.27
300 ppm	1.45	32.9	0.877	354	189.51	48.33
500 ppm	1.74	50.2	0.881	245	135.23	66.14
700 ppm	1.27	51.4	0.877	325	183.01	66.93
1000 ppm	2.23	85.4	0.883	218	128.60	80.09
PAN-ZnO (as inhibitor)						
100 ppm	1.38	24.6	0.879	308	157.22	30.89
300 ppm	1.47	39.6	0.888	271	152.99	57.07
500 ppm	1.26	53.3	0.891	270	160.75	68.11
700 ppm	1.08	58.2	0.897	284	177.34	70.79
1000 ppm	2.47	93.0	0.877	202	143.25	81.72

From the table, it is clearly seen that there was increase in the charge transfer resistance (R_{ct}) values due to increase in the number of the inhibitor molecules added to the system to reduce the surface area exposed to the corrosion medium. This consequently increased the calculated inhibition efficiency. The increased inhibition efficiency implies that the studied polymers and polymer nanocomposites are effective corrosion inhibitors of mild steel in 5 % HCl. No significant change was observed in the values of n. The n value stabilized in the range of 0.826 – 0.897 which reveals that the corrosion of mild steel is controlled by a single charge transfer process with and without the studied inhibitors The n values are also close to 1, indicating the pseudo-capacitive characteristics of the electrode/electrolyte systems [114, 115].

The thickness of the protective layer (d) is evaluated from the Helmholtz model and is mathematically related to the double layer capacitance (C_{dl}) using Equation 4.7;

$$C_{dl} = \frac{\varepsilon\varepsilon_o}{d} \qquad (4.7)$$

where, ε is the dielectric constant of the protective layer and ε_o is the permittivity of free space, C_{dl} is the double layer capacitance.

The C_{dl} values for the studied inhibitors reduced when compared to the uninhibited system which suggests the gradual substitution of water molecules on the metal surface by the studied inhibitors. The initial decrease in C_{dl} value from the uninhibited solution to the inhibited solutions is mainly ascribed to a decrease in the local dielectric constant, while the observed further decrease in C_{dl} with increasing concentrations of the studied inhibitors is attributed to increase in the thickness of the electrical double layer [71].

The results from the impedance spectra also corroborate those obtained from polarization measurements.

4.2.4 EFFECT OF ZnO NANOPARTICLES IN NANOCOMPOSITES ON INHIBITION EFFICIENCY

In order to examine the effect of the ZnO nanoparticles on the inhibitive ability of the polymers, potentiodynamic polarization curves and Nyquist plots of the polymers and their respective ZnO nanocomposites were plotted and presented in Figures 4.15 and 4.16.

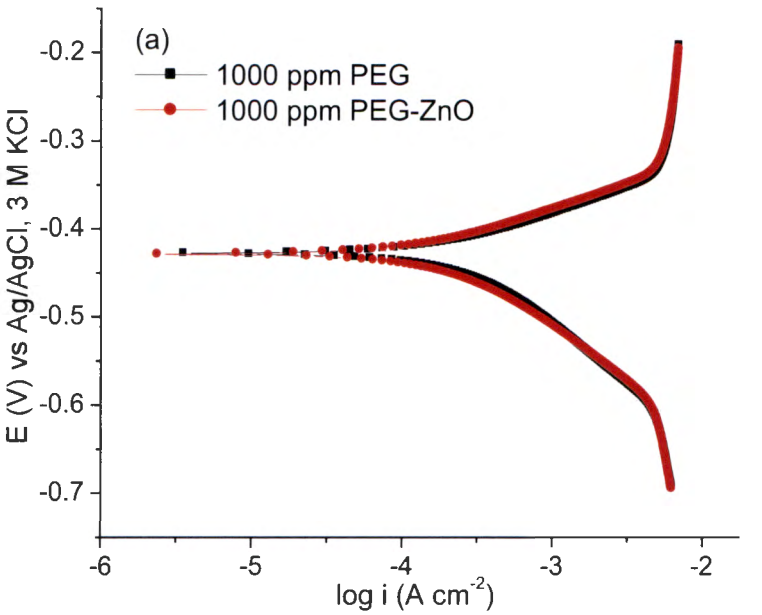
(a)
1000 ppm PEG
1000 ppm PEG-ZnO
E (V) vs Ag/AgCl, 3 M KCl
-0.2
-0.3
-0.4
-0.5
-0.6
-0.7
-6
-5
-4
-3
-2
log i (A cm-2)

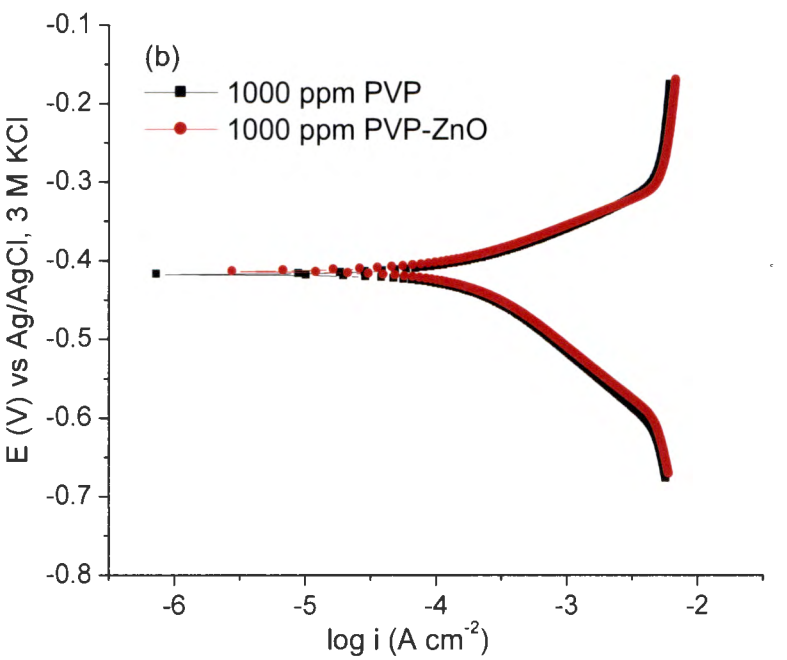
(b)
1000 ppm PVP
1000 ppm PVP-ZnO
E (V) vs Ag/AgCl, 3 M KCl
-0.1
-0.2
-0.3
-0.4
-0.5
-0.6
-0.7
-0.8
-6
-5
-4
-3
-2
log i (A cm-2)

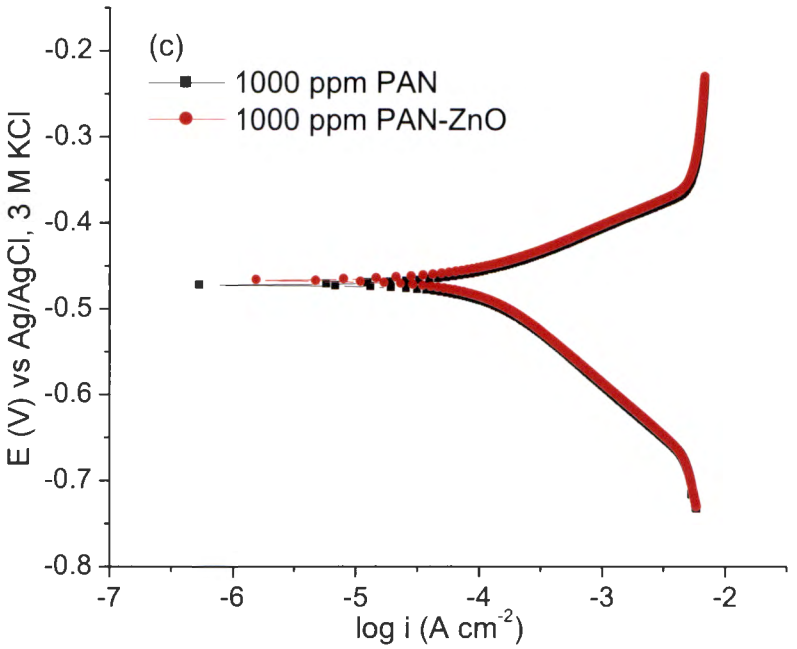

Figure 4.15: Potentiodynamic polarization curves of mild steel in 5% HCl with maximum concentrations of 1000 ppm of (a) PEG and PEG-ZnO (b) PVP and PVP-ZnO (c) PAN and PAN-ZnO

The potentiodynamic polarization curves in Figure 4.15(a-c) revealed that the addition of the polymers and polymer nanocomposites reduced the current densities for both anodic and cathodic half-reactions [116]. However, systems containing polymer-ZnO nanocomposites exhibited lower current densities than the polymers alone. This can be attributed to the presence of ZnO nanoparticles in the polymer nanocomposites which improved the corrosion resistance of the polymers. The ZnO nanoparticles improved the barrier and the anticorrosion potentials of the selected polymers [47, 117].

The order of inhibition efficiency of the ZnO polymer nanocomposites is PVP-ZnO > PAN-ZnO > PEG-ZnO. The effect of ZnO on corrosion inhibition efficiency of the polymers was more noticeable in the case of PAN especially at low concentration of the polymer. In general, PVP-ZnO showed highest inhibition efficiency for mild steel in 5 % HCl.

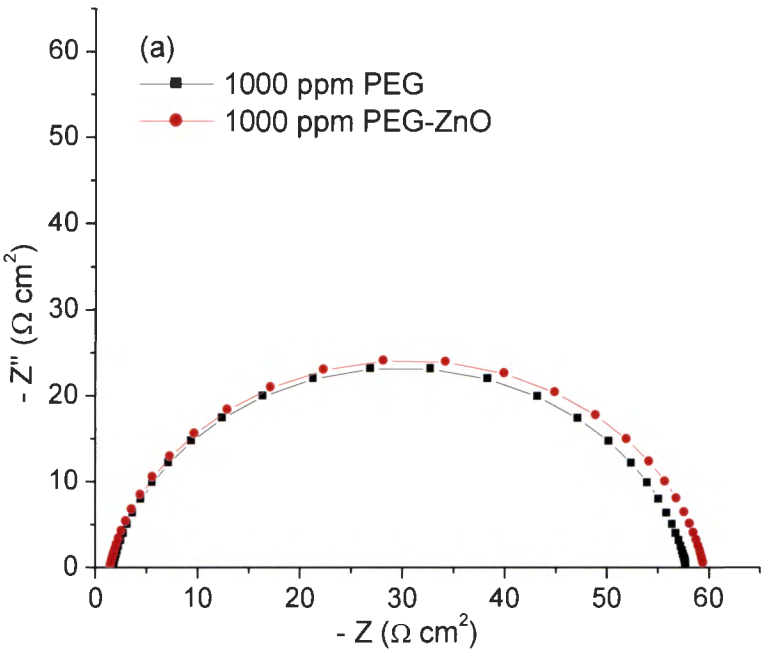
(a)
1000 ppm PEG
1000 ppm PEG-ZnO
- Z'' (Ω cm²)
- Z (Ω cm²)
0
10
20
30
40
50
60

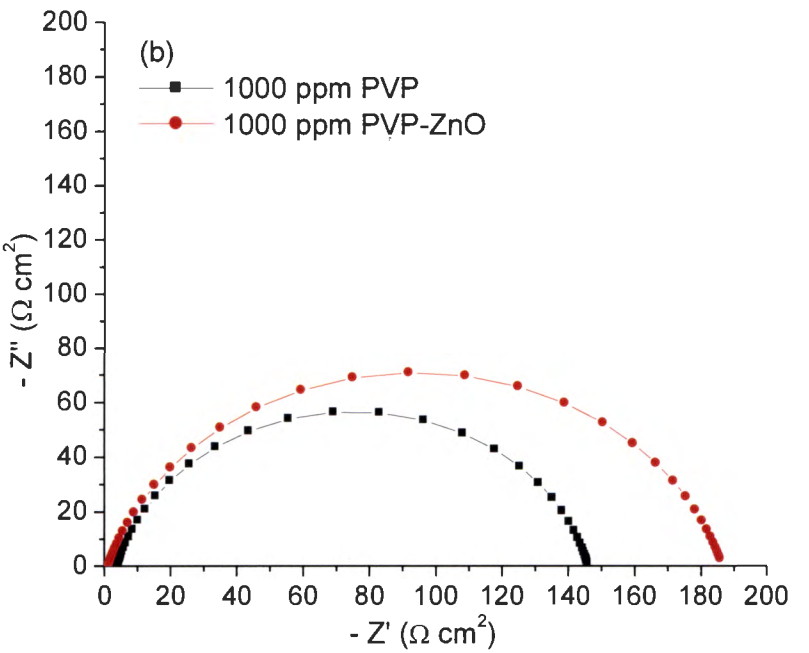
(b)
1000 ppm PVP
1000 ppm PVP-ZnO
- Z'' (Ω cm²)
- Z' (Ω cm²)
0
20
40
60
80
100
120
140
160
180
200

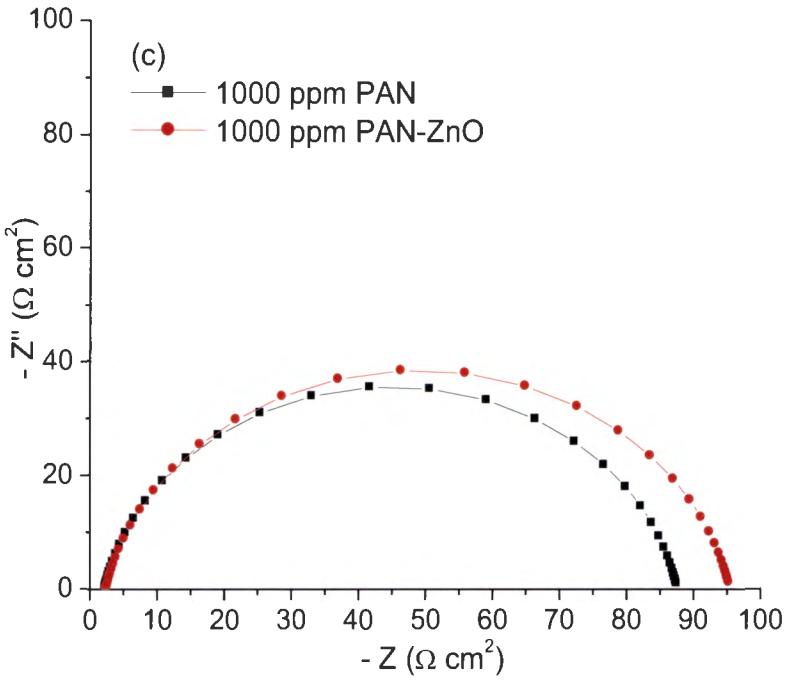

Figure 4.16: Nyquist plots for mild steel in 5% HCl with maximum concentrations of 1000 ppm of: (a) PEG and PEG-ZnO (b) PVP and PVP-ZnO (c) PAN and PAN-ZnO

The ZnO nanocomposites had higher R_{ct} values compared to the polymers alone. This implies that the ZnO nanocomposites adsorbed on the mild steel surface better than the polymers. The higher inhibition efficiency obtained from the Nyquist plot for PVP and PVP-ZnO compared to other studied inhibitors can be attributed to the presence of more heteroatoms with electronegativity (N, O) in its anions making it better adsorbed on the mild steel surface and improving its inhibition efficiency [118]. PVP-ZnO gave a better R_{ct} value at the maximum studied concentration than the PAN-ZnO and PEG-ZnO. The observed order of inhibition efficiency agrees with those obtained from polarization measurements and linear polarization resistance except in a few cases.

4.3 ADSORPTION ISOTHERM AND THERMODYNAMIC PARAMETERS

Adsorption isotherms are used to explain the mechanisms followed by inhibitor molecules in protecting metal surface [43]. The experimental data were tested with several frequently used adsorption isotherms. Langmuir adsorption isotherm was found to give the best line of fit for the polymer and the polymer nanocomposites adsorbed on the mild steel in 5 % HCl.

Langmuir adsorption isotherm is given by Equation 4.8:

$$\theta = \frac{K_{ads}C_{inh}}{1 + K_{ads}C_{inh}} \quad (4.8)$$

where, θ is the degree of surface coverage, K_{ads} is the equilibrium constant for the adsorption process, and C_{inh} is the concentration of the inhibitors [118].

The equation can be rearranged to Equation 4.9:

$$\frac{C_{inh}}{\theta} = \frac{1}{K_{ads}} + C_{inh} \quad (4.9)$$

The values of linear regression coefficient (R^2) of Langmuir adsorption isotherm for all the studied inhibitors were close to unity, thus validating this approach [119].

The Gibb's Free energies of adsorption ($\Delta G°_{ads}$) were calculated using Equation 4.10 [120];

$$\Delta G°_{ads} = -RT\, ln(55.5K_{ads}) \quad (4.10)$$

where, 55.5 represents the concentration of water in the solution (mol/dm^3), T is the absolute temperature, and R is the universal gas constant.

The values of K_{ads} and ΔG°_{ads} obtained using the Langmuir absorption isotherm for the studied inhibitors on mild steel in the acid medium are presented in Table 4.3.

Table 4.3: Adsorption parameters obtained from the Langmuir adsorption isotherm plots for the studied inhibitors on mild steel in 5 % HCl at 303 K.

Inhibitor	**K_{ads} (x 10^4 mol^{-1})**	**$-\Delta G^{\circ}_{ads}$ (kJ mol^{-1})**
PEG	9.87	15.89
PVP	61.88	20.51
PAN	79.39	21.14

Generally, the calculated values of $\Delta G°_{ads}$ around –20 kJ mol^{-1} or less are associated with physical adsorption (physiosorption process) which involves electrostatic interaction between the charged inhibitor molecules and the charged metal surface, while those around –40 kJ mol^{-1} and more negative indicate charge sharing or transfer from the organic molecules to the metal

surface to form co-ordinate bond (chemisorption process) [21, 22, 121]. The obtained values of $\Delta G°_{ads}$ showed that the adsorption process of the studied inhibitors on mild steel is predominantly by physiosorption process. The obtained negative values of $\Delta G°_{ads}$ indicate the spontaneity of the adsorption of the studied inhibitors on the mild steel surface and the stability of the adsorbed layer on the surface of the mild steel.

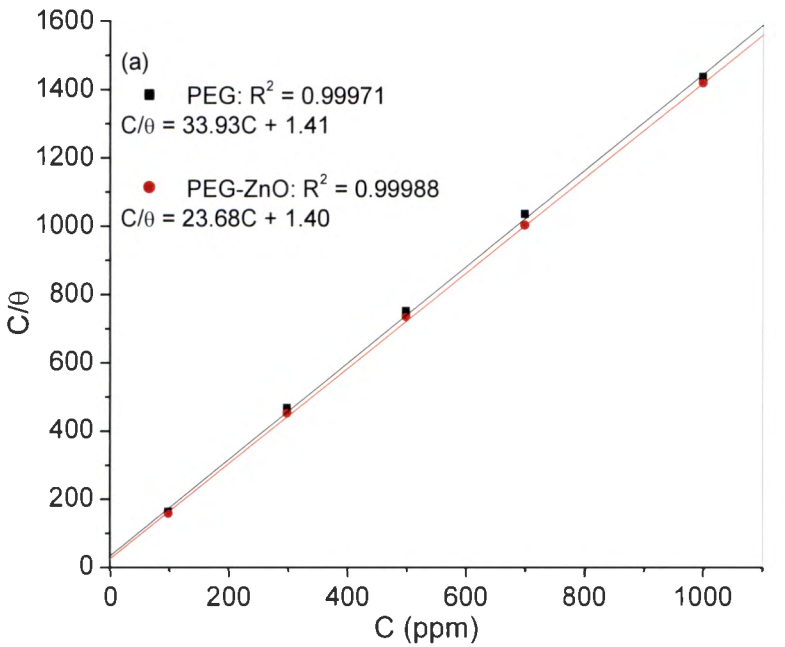

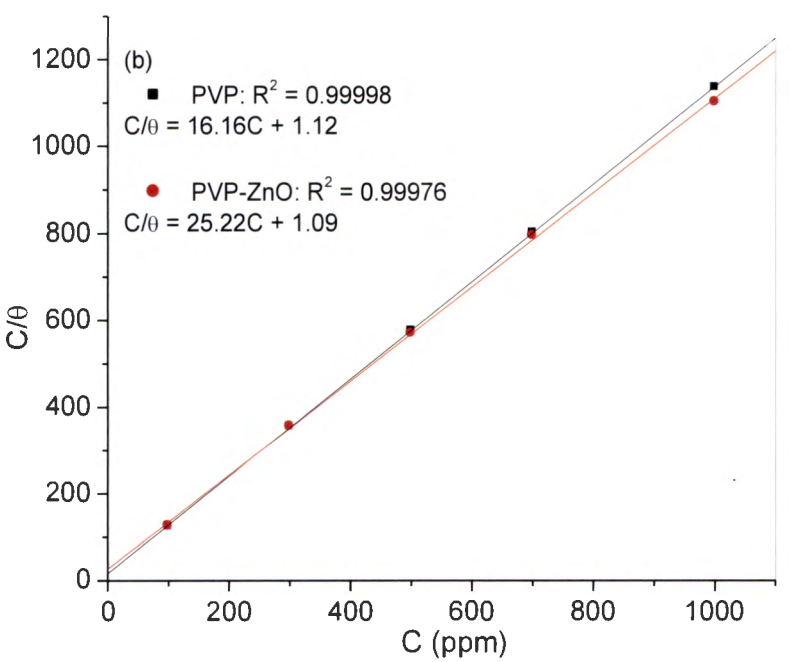

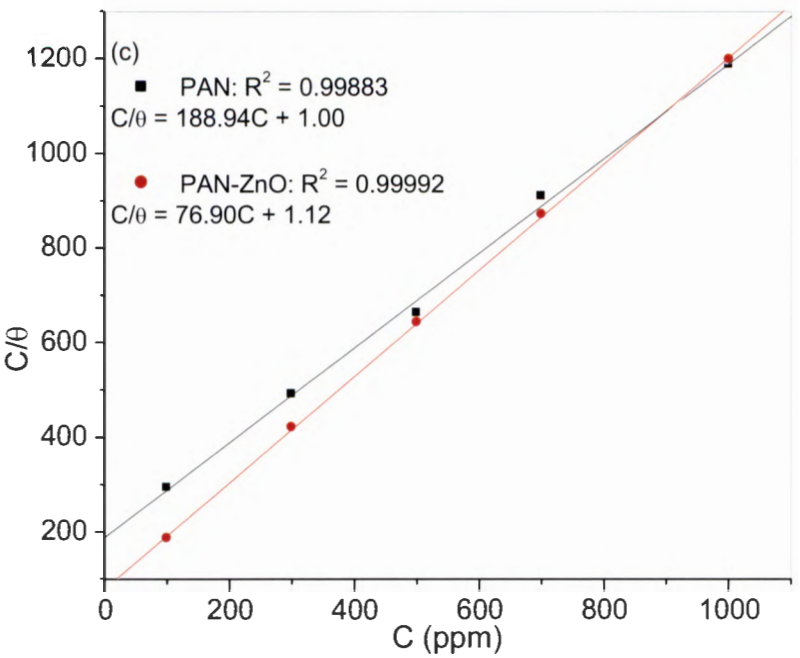

Figure 4.17: Langmuir adsorption plots for mild steel corrosion in 5 % HCl in the presence of various concentrations of (a) PEG and PEG-ZnO (b) PVP and PVP-ZnO (c) PAN and PAN-ZnO

4.4 MECHANISM OF INHIBITION

The adsorption of organic inhibitors on mild steel surface can be represented as a substitution adsorption process between the molecules of the organic inhibitors and the water molecules on the metallic surface $H_2O_{(ads)}$ [56]:

$$Org_{(sol)} + xH_2O_{(ads)} \rightleftharpoons Org_{(ads)} + xH_2O_{(sol)} \qquad (4.11)$$

in which $Org_{(sol)}$ and $H_2O_{(sol)}$ and $Org_{(ads)}$ and $H_2O_{(ads)}$ are the polymers and polymer nanocomposites) and water molecules in the aqueous solution and the adsorbed organic and water molecules on the surface, respectively. x is the size ratio representing the number of water molecules replaced by a molecule of organic adsorbate [122, 123].

Corrosion inhibition of mild steel in 5 % HCl increases with increase in the concentration of the inhibitor molecules. This implies that more inhibited molecules were adsorbed onto the mild steel surface at higher concentration, leading to greater surface coverage. The order of inhibition efficiency achieved by the studied inhibitors for mild steel corrosion in 5 % HCl at the maximum concentration of 1000 ppm from the EIS result follows the order:

PVP-ZnO > PAN-ZnO > PEG-ZnO

Adsorption of the inhibitor molecules takes place through heteroatoms such as O, N, S and P, double or triple bonds, or aromatic rings [31, 71, 74]. The inhibition efficiency is expected to increase in the order P > S > N > O [124]. Other factors such as molecular weight, solubility and structure of the inhibitors also determine how well inhibitors adsorb and form protective layer on the mild steel [32, 38, 43]. The chemical structure of PEG, PVP and PAN reveals that PEG contains only oxygen heteroatom, PVP contains nitrogen and oxygen atoms, while PAN contains only nitrogen atom. It has been reported that nitrogen-containing inhibitors tend to perform optimally as corrosion inhibitors in hydrochloric acid [124, 125]. Also, the presence of chelating rings in PVP leads to increased electron density on nitrogen atom. This might inform the higher inhibition potential of PVP compared to PEG and PAN. PAN acts as a better corrosion inhibitor of mild steel than PEG because of its high molecular weight, possession of triple bond and presence of nitrogen atom. The major setback with PAN is its relative insolubility in the corrosive medium. For their respective nanocomposites, the incorporation of ZnO nanoparticles results in the reinforcement of the properties of the polymers and acts as a physical barrier against attacking ions in the corrosive medium [46, 47, 117].

It could be proposed that the studied polymers and polymer-ZnO nanocomposites adsorb onto the mild steel surface by:

(a) Electrostatic interaction between the charged molecules and charged metal surface;

(b) Interaction of π-electrons with the metal;

(c) Interaction of unshared electron pair in the molecule with the metal surface; and

(d) The combination of all the effects [70, 126, 127].

4.5 SCANNING ELECTRON MICROSCOPY (SEM)

Scanning electron microscopy (SEM) is a very powerful investigative technique employed to gain information about the adsorbed film of the inhibitors on the metal and the extent of corrosion in the mild steel [128]. Surface morphology of mild steel immersed in 5 % HCl for 24 h in the presence and absence of the maximum concentration of the studied inhibitors was conducted using scanning electron microscopy (SEM). The surface micrographs provide information on the extent of surface damage caused by corrosion in each case of the studied inhibitors which can be correlated to the inhibition efficiency.

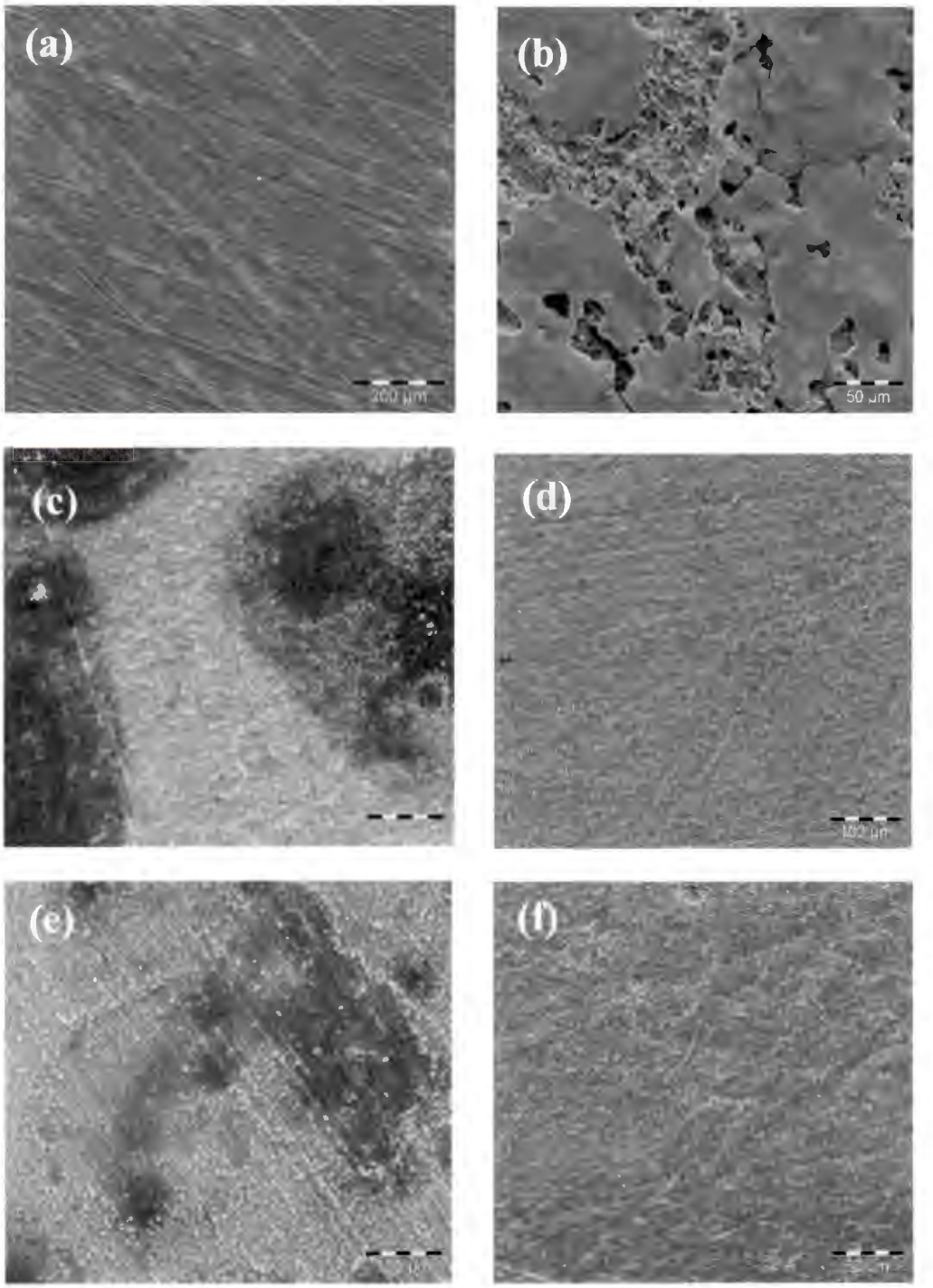
(a)
200 µm
(b)
50 µm
(c)
(d)
(e)
(f)

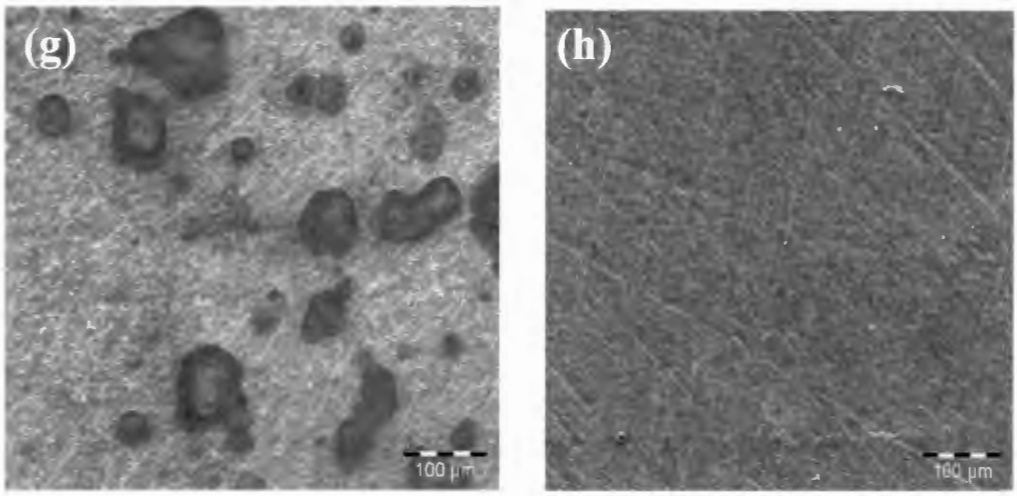

Figure 4.18: SEM images of mild steel surface (a) in the polished state (b) mild steel in 5 % HCl and with 1000 ppm of (c) PEG (d) PEG-ZnO (e) PVP (f) PVP-ZnO (g) PAN and (h) PAN-ZnO after 24 h

Figure 4.18(a) shows micrograph image of freshly polished plain mild steel, which shows polishing scratches due to surface pre-treatment. Figure 4.18 (b) showed that the surface of mild steel immersed in 5 % HCl for 24 h without the inhibitors is severely damaged. Cracks, pits and oxides due to corrosion process are observed. However, in the presence of the polymers and polymer nanocomposites the mild steel surface in 5 % HCl exhibited drastic reduction in surface damage, leading to relatively smoother surface (Figure 4.18(c-h)). This is attributed to the formation of protective films and adsorption of inhibitor molecules on the surface of the steel substrate [129, 130]. The surfaces of the mild steel in the presence of the polymer nanocomposites (Figure 4.18d, f, h) showed better smoothness than those in the presence of the polymers (Figure 4.18c, e, g). This confirms that all the studied inhibitors retard corrosion in mild steel immersed in 5 % HCl by forming a protective film on the mild steel surface with the polymer nanocomposites providing a better protection than the polymers.

CHAPTER 5

CONCLUSION

5.1 CONCLUSION

Three polymers (PEG, PVP and PAN) and their respective ZnO nanocomposites have been studied for their corrosion inhibition potentials for mild steel in 5 % HCl solution using different characterization and electrochemical techniques. The following conclusions can be drawn based on the results obtained from the study:

1. Successful synthesis of polymer-ZnO nanocomposites of PEG, PVP and PAN was confirmed using FTIR, UV-vis, TGA and TEM techniques.
2. The polymers and polymer-ZnO nanocomposites effectively inhibited corrosion of mild steel in 5 % HCl and the inhibition efficiency increased with increase in concentration of the inhibitors.
3. Potentiodynamic polarization revealed that the inhibitors retard both anodic and cathodic reactions involved in the corrosion of mild steel in 5 % HCl. PEG and PVP, and their ZnO nanocomposites showed more anodic inhibitive effect, while PAN and PAN-ZnO exhibited more cathodic effects in their inhibitive actions.
4. The results obtained from potentiodynamic polarization measurements and electrochemical impedance spectroscopic measurements revealed the same trend for the inhibitive actions of the studied compounds. The order of inhibition efficiency is PVP-ZnO > PAN-ZnO > PEG-ZnO.
5. The adsorption mechanism of the polymers and their ZnO nanocomposites on the surface of the mild steel followed Langmuir adsorption isotherm model.
6. SEM images showed that the inhibitors provided adequate surface protection for the mild steel surface from the corrosive ions in the environment. The polymer nanocomposites however gave better protection to mild steel surface.
7. The mode of absorption is essentially by physiosorption and the negative sign of $\Delta G°_{ads}$ indicates that adsorption of the studied inhibitors on the metal surface in 5 % HCl is spontaneous.

5.2 FUTURE WORK

The anticorrosion potentials of the selected polymers (PEG, PVP and PAN) and their ZnO nanocomposites will be investigated for mild steel corrosion in 3.5 % NaCl solution.

REFERENCES

1. Z. Ahmad, Principles of corrosion engineering and corrosion control. Butterworth Heinemann, ISBN-10: 0750659246. (2006) 1–10.
2. V.S. Sastri, Corrosion inhibitors: theory and practice, John Wiley & Sons, Inc., Hoboken, New Jersey. (2011) 1–27.
3. R. Govindasamy, S. Ayappan, Study of corrosion inhibition properties of novel semicarbazones on mild steel in acidic solutions, J. Chil. Chem. Soc. 60 (2015) 2786–2798.
4. S.I. Durowaye, V.O. Durowaye, B.M. Begusa, Corrosion inhibition of mild steel in acidic medium by methyl red (2,4-dimethylamino-2'-carboxylazobenzene), IJERT. 4 (2014) 469–475.
5. F.G. Fontana, Corrosion engineering. McGraw Hill, New York. (1986) 1–75.
6. https://www.shutterstock.com/image-photo/corroded-casing-pipes-situated-near-oil-105811433. (accessed 20 February 2018).
7. https://www.pinterest.com/pin/487796203371378349. (accessed 20 February 2018).
8. N. Krishnamurthy, N.P. Vallinayagam, D. Madhavan. Engineering Chemistry. PHI Learning Pvt. Ltd. (2014) 184.
9. K. Nisancioglu, Corrosion of aluminium alloys, Proceedings of ICAA3. 3(1992) 239–259.
10. J.R. Davis, Corrosion: Understanding the Basics, ASM International. (2000) 1–13.
11. N.A. Negm, M.A. Yousef, S.M. Tawfik, Impact of synthesized and natural compounds in corrosion inhibition of carbon steel and aluminium in acidic media, Recent Patents on Corrosion Science, 3 (2013) 58–68.
12. G.H. Koch, M.P.H. Brongers, N.G. Thompson, Y.P. Virmani, J. H. Payer, Corrosion costs and preventive strategies in the United States, FHWA-RD-01-156, C. C. Technologies Laboratories, Inc, USA. (2001).
13. J.J. McEwan, Corrosion control in Southern Africa, Corrosion Institute of Southern Africa, Kelvin, RSA. (2004) 1–135.
14. G.S. Frankel, N. Sridhar, Understanding localized corrosion. Mater. Today. 11(2008) 38–44.
15. P.R. Roberge, Corrosion Engineering Principles and Practice, McGraw-Hill, New York. (2008).

16. K.A. Adedeji, E.O. Sangotayo, O. Adekunle, O.M. Odeniyi, Investigation of some factors influencing corrosion on refrigerator, CER. 9 (2017) 24–33.
17. P.R. Roberge, Handbook of Corrosion Engineering, McGraw-Hill, New York. (1999).
18. P.P. Deshpande, N.G. Jadhav, V.J. Gelling, D. Sazou, Conducting polymers for corrosion protection: a review, J. Coat. Technol. Res. 11 (2014) 473–494.
19. A.M. Badiea, K.N. Mohana, Corrosion mechanism of low-carbon steel in industrial water and adsorption thermodynamics in the presence of some plant extracts, J. Mater. Engr. Perform. 18 (2008) 1264–1271.
20. E.A. Noor, A.H. Al-Moubaraki, Corrosion behaviour of mild steel in hydrochloric acid solutions, Int. J. Electrochem. Soc. 3 (2008) 806–818.
21. A. Zarrouk, I. Warad, B. Hammonuti, A. Dafali, S.S.A. Al-Deyab, N. Benchat, The effect of temperature on the corrosion of Cu/HNO_3 in the presence of organic inhibitor: Part-2, Int. J. Electrochem. Sci. 5 (2010) 1516–1526.
22. I. Dehri, M. Ozcan, The effect of temperature on the corrosion of mild steel in acidic media in the presence of some sulphur-contaning organic compounds, Mater. Chem. Phys. 98 (2006) 316–323.
23. L.L. Shreir, Basic concepts of corrosion, Elsevier B.V. 1 (2010) 89–95.
24. D. Kesavan, M. Gopiraman, N. Sulochana, Green inhibitors for corrosion of metals: a review, Che. Sci. Rev. Lett. 1 (2012) 1–8.
25. B.E. Amitha Rani, B.J. Basu, Green inhibitors for corrosion protection of metals and alloys: an overview, Int. J. Corros. 12 (2015) 300–315.
26. J.J. Fu, H.S. Zang, Y. Wang, S.N. Li, T. Chen, X.D. Liu, Experimental and theoretical study on the inhibition performances of quinoxaline and its derivatives for the corrosion of mild steel in hydrochloric acid, Ind. Eng. Chem. Res. 51 (2012) 6377–6386.
27. M. Soukieh, F. Nassr-Allah, M. Kakhia, H. Jabboli, Physical-chemical principles of corrosion inhibitors for metals and metallic alloys and the inhibition mechanisms, Aalam Al-Zarra. 102 (2006) 77.
28. E.H. Norman, NACE glossary of corrosion terms, Mat. Pro. 4 (1965) 79–80.
29. N. Hackerrman., in "Fundamentals of Inhibitors," NACE Basic Corrosion Course, Houston, TX: NACE. (1965).
30. A. Rustandi, J.W. Soedarsono, B. Suharno, The use of mixture of piper betle and green tea as a green corrosion inhibitor for API X-52 steel in aerated 3.5 % NaCl solution at various rotation rates, Adv. Mat. Res. 383 (2012) 5418–5425.

31. E.E. Ebenso, I.B. Obot, L.C. Murulana, Quinoline and its derivatives as effective corrosion inhibitors for mild steel in acidic medium, Int. J. Electrochem. Sci. 5 (2010) 1574–1586.
32. N.O. Eddy, F. Awe, E.E. Ebenso, Adsorption and inhibitive properties of ethanol extracts of leaves of solanum melongena for the corrosion of mild steel in 0.1 M HCl, Int. J. Electrochem. Sci. 5 (2010) 1996–2011.
33. S. Muralidharan, M.A. Quraishi, S.V.K. Iyer, The effect of molecular structure on hydrogen permeation and the corrosion inhibition of mild steel in acidic solutions, Corros. Sci. 37 (1995) 1739–1750.
34. P.M. Niamien, H.A. Kouassi, A. Trokourey, F.K. Essy, D. Sissouma, Y. Bokra. Copper corrosion inhibition in 1 M HNO_3 by two benzimidazole derivatives, ISRN Mater. Sci. 2012 (2012) 1–15.
35. Development in corrosion protection, Edited by M. Aliofkhazraei. ISBN 978-935-51-1223-5, InTech. (2014).
36. R.B. Faltermeier, A corrosion inhibitor test for copper-based artifacts, Stud. Conserv. 44 (1999) 121–128.
37. S.A. Umoren, Z.M. Gasem, I.B. Obot, Natural products for material protection: inhibition of mild steel corrosion by date palm seed extracts in acidic media, Ind. Eng. Chem. Res. 52 (2013) 14855–14865.
38. S.A. Abo El-Enin, A. Amin, Review of corrosion inhibitors for industrial applications, IJERR. 3 (2015) 127–145.
39. Uhlig's corrosion handbook, Edited by R. Winston Revie. ISBN 0-471-15777-5 John Wiley & Sons, Inc (2000).
40. S. Paul, I. Koley, Corrosion inhibition of carbon steel in acidic environment by papaya seed as green inhibitor, J. Bio. Tribo. Corros. 2 (2016) 6–14.
41. G. Vijayakumar, R. Tamilarasana, M. Dharmendirakumar, Adsorption, kinetic, equilibrium and thermodynamic studies on the removal of basic dye Rhodamine-B from aqueous solution by the use of natural adsorbent perlite, J. Mater. Environ. Sci. 3 (2012) 157–170.
42. P. Pandey, S.S. Sambi, S.K. Sharma, S. Singh, Batch adsorption studies for the removal of Cu (II) ions by ZeoliteNaX from aqueous stream, WCECS. 1 (2009) 1–6.

43. I. B. Obot, N.O. Obi-Egbedi, S.A. Umoren, E.E. Ebenso, Adsorption and kinetic studies on the inhibition potential of fluconazole for the corrosion of Al in HCl solution, Chem. Eng. Commun. 198 (2011) 711–725.
44. R. Kalaivani, P.T. Arasu, S. Rajendran, Corrosion inhibition by polymers – bird's eye view, Eur. Chem. Bull. 2 (2013) 807–815.
45. M.M. Solomon, S.A. Umoren, In-situ preparation, characterization and anticorrosion property of polypropylene glycol/silver nanoparticles composite for mild steel corrosion in acid solution, J. Colloid Interf. Sci. 462 (2016) 29–41.
46. S.A. Kumar, H. Bhandari, C. Sharma, F. Khatoon, S.K. Dhawan, A new smart coating of polyaniline–SiO_2 composite for protection of mild steel against corrosion in strong acidic medium, Polym. Int. 62 (2013) 1192–1201.
47. R.E. Morsi, A. Labena, E.A. Khamis, Core/shell (ZnO/polyacrylamide) nanocomposite: in-situ emulsion polymerization, corrosion inhibition, anti-microbial and anti-biofilm characteristics, J. Taiwan Inst. Chem. Eng. 63 (2016) 512–522.
48. J.R. Fried, Polymer science and technology, ISBN 978-0-13-703955-5 (2014).
49. Chemistry Part II (NCERT XII) Unit-15. 425–428.
50. K. Leja, G. Lewandowicz, Polymer biodegradation and biodegradable polymers - a review, Polish J. of Environ. Stud. 19 (2010) 255–266. .
51. Y. Jianguo, W. Lin, V. Otieno-Alego, D.P. Schweinsberg, Polyvinylpyrrolidone and polyethylenimine as inhibitors for the corrosion of a low carbon steel in phosphoric acid, Corros. Sci. 37 (1995) 975–985.
52. A. Yurt, V. Bütün, B. Duran, Effect of the molecular weight and structure of some novel water-soluble triblock copolymers on the electrochemical behaviour of mild steel, Mater. Chem. Phys. 105 (2007) 114–121.
53. S. Rajendran, S.P. Sridevi, N. Anthony, A.A. John, M. Sundaravadivelu, Corrosion behaviour of carbon steel in polyvinyl alcohol, Anti-Corr. Meth. Mater. 52 (2005) 102–107.
54. V.G. Kadajji, G.V. Betageri, Water soluble polymers for pharmaceutical applications, Polymers. 3 (2011) 1972–2009.
55. M. Liang, H. Zhou, Q. Huang, S. Hu, W. Li, Synergistic effect of polyethylene glycol 600 and polysorbate on corrosion inhibition of zinc anode in alkaline batteries, J. Appl. Electrochem. 41 (2011) 991–997.

56. M.A. Deyab, S.S.A. El-Rehim, Influence of polyethylene glycols on the corrosion inhibition of carbon steel in butyric acid solution: weight loss, EIS and theoretical studies, Int. J. Electrochem. Sci. 8 (2013) 12613–12627.
57. K.M. Koczkur, S. Mourdikoudis, L. Polavarapu, S.E. Skrabalak, Polyvinylpyrrolidone (PVP) in nanoparticle synthesis, Dalton Trans. 44 (2015) 17883–17905.
58. L.A. Al Juhaiman, A. Abu Mustafa, W.K. Mekhamer, Polyvinylpyrrolidone as a green corrosion inhibitor of carbon steel in neutral solutions containing NaCl: electrochemical and thermodynamic study, Int. J. Electrochem. Sci. 7 (2012) 8578–8596.
59. T. An, G. Panthi, M. Park, S. Park, H. Kim, Polyacrylonitrile composite nanofibers encapsulated with Ag_2CO_3 nanoparticles: a study on the effect of photocatalytic performances of composite nanofibers electrospun at different applied electric voltages, ICBNE. (2015) 37–41.
60. S. Chouhan, A.K. Bajpai, J. Bajpai, R. Katare, S.J. Dhoble, Mechanical and UV absorption behaviour of zinc oxide nanoparticles: reinforced poly(vinylalcohol-g-acrylonitrile) nanocomposite films, Polym. Bull. (2017) 1–23.
61. S. Chouhan, R. Bhatt, A.K. Bajpai, J. Bajpai, R. Katare, Investigation of UV absorption and antibacterial behaviour of zinc oxide containing poly(vinyl alcohol-g-acrylonitrile) (PVA-g-PAN) nanocomposites films, Fibers Polym. 16 (2015) 1243–1254.
62. P.J. Lee, E. Saion, N.M. Al-Hada, N. Soltani, A simple up-scalable thermal treatment method for synthesis of ZnO nanoparticles, Metals 5 (2015) 2383–2392.
63. Q. Luo, X. Yang, X. Zhao, D. Wang, R. Yin, X. Li, J. An, Facile preparation of well-dispersed ZnO/cyclized polyacrylonitrile nanocomposites with highly enhanced visible-light photocatalytic activity, Appl. Catal., B. 204 (2017) 304–315.
64. T. Kaehler, Nanotechnology: basic concepts and definitions. Clin. Chem. 40 (1994) 1797–1799.
65. D.R. Paul, L.M. Robeson, Polymer nanotechnology: nanocomposites, Polymer. 49 (2008) 3187–3204.
66. M.M. Solomon, S.A. Umoren, A.U. Israel, E.E. Ebenso, Polypropylene glycol-silver nanoparticle composites: a novel anticorrosion material for aluminium in acid medium, JMEPEG. 24 (2015) 4206–4218.
67. P.R. Solanki, A. Kaushik, A.A. Ansari, G. Sumana, B.D. Malhotra, Zinc oxide-chitosan nanobiocomposite for urea sensor, Appl. Phys. Lett. 93 (2008) 163903–163905.
68. S.A. Umoren, M.J. Banera, T. Alonso-Garcia, C.A. Gervasi, M.V. Mirífico, Inhibition of mild steel corrosion in HCl solution using chitosan, Cellulose. 20 (2013) 2529–2545.

69. S. Kumar, H. Vashisht, L.O. Olasunkanmi, I. Bahadur, H. Verma, G. Singh, I.B. Obot, E.E. Ebenso, Experimental and theoretical studies on inhibition of mild steel corrosion by some synthesized polyurethane tri-block co-polymers, Sci. Rep. 6 (2016) 30937–30954.

70. C.B. Verma, M.A. Quraishi, E.E. Ebenso, Application of some oligopolymers as effective corrosion inhibitors for mild steel in 1 M HCl: gravimetric, thermodynamic and electrochemical analysis, Int. J. Electrochem. Sci. 9 (2014) 5507–5519.

71. S. John, M. Kuruvilla, A. Joseph, Surface morphological and impedance spectroscopic studies on the interaction of polyethylene glycol (PEG) and polyvinylpyrrolidone (PVP) with mild steel in acid Solutions, Res Chem Intermed. 39 (2013) 1169–1182.

72. S.A. Umoren, E.E. Ebenso, Blends of polyvinylpyrrolidone and polyacrylamide as corrosion inhibitors for aluminium in acidic medium, IJCT. 15 (2008), 355–363.

73. K. Alaoui, Y. El Kacimi, M. Galai, R. Touir, K. Dahmani, A. Harfi, M. Ebn Touhami, Anti-corrosive properties of polyvinyl alcohol for carbon steel in hydrochloric acid media: electrochemical and thermodynamic investigation, J. Mater. Environ. Sci. 7 (2016) 2389–2403.

74. M. Mobin, M.A. Khan, Adsorption and corrosion inhibition behaviour of polyethylene glycol alone and surfactants additives on mild steel in H_2SO_4, JMEPEG. 23 (2014) 222–229.

75. G.A. El-Mahdy, A.M. Atta, H.A. Al-Lohedan, A.M. Tawfik, A.A. Abdel-Khalek, Application of silica/polyacrylamide nanocomposite as anticorrosive layer for steel, Int. J. Electrochem. Sci. 10 (2015) 151–161.

76. R. Geethanjali, S. Subhashini, Synthesis of magnetite-containing polyaniline-polyacrylamide nanocomposite, characterization and corrosion inhibition behaviour on mild steel in acid media, Chem. Sci. Trans. 2 (2013) 1148–1159.

77. V.Q. Trung, D.N. Huyen, Synthesis, properties and application of polyindole/TiO_2 nanocomposites, J. Phys. Conf. Ser. 187 (2009) 012058–012063.

78. Y. Sasikumar, A.M. Kumar, Z.M. Gasem, E.E. Ebenso, Hybrid nanocomposite from aniline and CeO_2 nanoparticles: surface protective performance on mild steel in acidic environment, Appl. Surf. Sci. 330 (2015) 207–215.

79. O.E. Fayemi, A.S. Adekunle, E.E. Ebenso, Metal oxide nanoparticles/multi-walled carbon nanotube nanocomposite modified electrode for the detection of dopamine: comparative electrochemical study, J. Biosens. Bioelectron. 6 (2015) 190–203.

80. D. Dwivedi, K. Lepkova´, T. Becker, Carbon steel corrosion: a review of key surface properties and characterization methods, RSC Adv. 7 (2017) 4580–4610.
81. J.A. Alvarado, A. Maldonado, H. Juarez, M. Pacio, Synthesis of colloidal ZnO nanoparticles and deposit of thin films by spin coating technique, J. Nanomater. 2013 (2013), 1–9.
82. N.S. Rao, M.V.B. Rao, Structural and optical investigation of ZnO nanopowders synthesized from zinc chloride and zinc nitrate, Am. J. Mater. Sci. 5 (2015) 66–68.
83. T. Thirugnanam, Effect of polymers (PEG and PVP) on sol-gel synthesis of microsized zinc oxide, J. Nanomater. 2013 (2013) 43–49.
84. S. Liufu, H. Xiao, Y. Li, Investigation of PEG adsorption on the surface of zinc oxide nanoparticles, Powder Technol. 145 (2004) 20–24.
85. C.R. Martinez, P. Joshi, J.L. Vera, J.E. Ramirez-Vick, O. Perales, S.P. Singh, Cytotoxic studies of PEG functionalized ZnO nanoparticles on MCF-7 cancer cells, NSTI-Nanotech. 3 (2011) 420–423.
86. T. Gutul, E. Rusu, N. Condur, V. Ursaki, E. Goncearenco, P. Vlazan, Preparation of poly(N-vinylpyrrolidone)-stabilized ZnO colloid nanoparticles, Beilstein J. Nanotechnol. 5 (2014) 402–406.
87. D. Shao, D. Gao, Q. Wei, L. Tao, H. Zhu, M. Ge, Deposition of ZnO on polyacrylonitrile fiber by thermal solvent coating, Fib. Polymers. 12 (2011) 214–219.
88. R.F. Ribeiro, L.C. Pardini, N.P. Alves, B. Júnior, C.A. Rios, Thermal stabilization study of polyacrylonitrile fiber obtained by extrusion, Polímeros. 25 (2015) 523–530.
89. S. Talam, S.R. Karumuri, N. Gunnam, Synthesis, characterization, and spectroscopic properties of ZnO nanoparticles, ISRN Nanotechnology. 2012 (2012) 1–6.
90. R. Sedghi, M.R. Nabid, M. Shariati, M. Behbahani, H.R. Moazzami, Preparation of PAN-based electrospun nanofiber webs containing Ni-ZnO as high performance visible light photocatalyst, Fib. Polym. 17 (2016) 1969–1976.
91. I. Bahadur, Mehbub I.K Momin, N.A. Koorbanally, M. Sattari, E.E. Ebenso, L.M. Katata-Seru, S. Singh, D. Ramjugernath, Interactions of polyvinylpyrrolidone with imidazolium based ionic liquids: spectroscopic and density functional theory studies, J. Mol. Liq. 213 (2016) 13–16.
92. H. Zhang, L. Xu, F. Yang, L. Geng, The synthesis of polyacrylonitrile/carbon nanotube microspheres by aqueous deposition polymerization under ultrasonication, Carbon. 48 (2010) 688–695.

93. G. Prusty, S.K. Swain, Synthesis and characterization of conducting gas barrier polyacrylonitrile/graphite nanocomposites, Polym. Compos. 32 (2011) 1336–1342.
94. V. Muşat, A. Tăbăcaru, B.S. Vasile, V.A. Surdu, Size-dependent photoluminescence of zinc oxide quantum dots through organosilane functionalization, RSC Adv. 4 (2014) 63128–63136.
95. A.K. Arora, S. Devi, V.S. Jaswal, J. Singh, M. Kinger, V.D. Gupta, Synthesis and characterization of ZnO nanoparticles, Orient. J. Chem. 30 (2014) 1671–1679.
96. M.A. Hussein, B.M. Abu-Zied, A.M. Asiri, Preparation, characterization, and electrical properties of ZSM-5/PEG composite particles, Polym. Compos. 35 (2014) 1160–1168.
97. S.S. Mali, H. Kim, W.Y. Jang, H.S. Park, P.S. Patil, C.K. Hong, Novel synthesis and characterization of mesoporous zno nanofibers by electrospinning technique, ACS Sustain. Chem. Eng. 1 (2013) 1207–1213.
98. S.K. Nataraj, B.H. Kim, J.H. Yun, D.H. Lee, T.M. Aminabhavi, K.S. Yang, Electrospun nanocomposite fiber mats of zinc-oxide loaded polyacrylonitrile, Carbon Lett. 9 (2008) 108–114.
99. A. Yar, B. Haspulat, T. Üstün, V. Eskizeybek, A. Avcı, H. Kamış, S. Achour, Electrospun TiO_2/ZnO/PAN hybrid nanofiber membranes with efficient photocatalytic activity, RSC Adv. 7 (2017) 29806–29814.
100. D. Yiamsawas, K. Boonpavanitchakul, W. Kangwansupamonkon, Synthesis and characterization of ZnO nanostructures with antimicrobial properties, ICONN IEEE. (2008) 133–136.
101. M. Sikine, H. Elmsellem, Y.K. Rodi, H. Steli, A. Aouniti, B. Hammouti, Y. Ouzidan, F.O. Chahdi, M. Bourass, E.M. Essassi, Corrosion inhibition of mild steel by 6-bromo-1H-imidazo [4, 5-b] pyridin-2 (3H)-one in 1 M HCl: experimental and computational study, J. Mater. Environ. Sci. 7 (2016) 4620–4632.
102. A.S. Fouda, A.A. Al-Sarawy, E.E. El-Katori, Pyrazolone derivatives as corrosion inhibitors for C-steel in hydrochloric acid solution, Desalination. 201 (2006) 1–13.
103. S. Umoren, M.M. Solomon, A.U. Israel, U.M. Eduok, A.E. Jonah, Comparative study of the corrosion inhibition efficacy of polypropylene glycol and poly (methacrylic acid) for mild steel in acid solution, J. Dispers. Sci. Technol. 36 (2015) 1721–1735.
104. M. Ates, Review study of electrochemical impedance spectroscopy and equivalent electrical circuits of conducting polymers on carbon surfaces, Prog. Org. Coat. 71 (2011) 1–10.

105. L.O. Olasunkanmi, I.B. Obot, M.M. Kabanda, E.E. Ebenso, Some quinoxalin-6-yl derivatives as corrosion inhibitors for mild steel in hydrochloric acid: experimental and theoretical studies, J. Phys. Chem. C. 119 (2015) 16004–16019.

106. M. Manssouri, Y. El Ouadi, M. Znini, J. Costa, A. Bouyanzer, J. M. Desjobert, L. Majidi, Adsorption properties and inhibition of mild steel corrosion in HCl solution by the essential oil from fruit of moroccan ammodaucus leucotrichus, J. Mater. Environ. Sci. 6 (2015) 631–646.

107. X. Zhang, Y. Zheng, X. Wang, Y. Yan, and W. Wu, Corrosion inhibition of N80 steel using novel diquaternary ammonium salts in 15 % hydrochloric acid, Ind. Eng. Chem. Res. 53 (2014) 14199–14207.

108. M.E. Mashuga, L.O. Olasunkanmi, E.E. Ebenso, Experimental and theoretical investigation of the inhibitory effect of new pyridazine derivatives for the corrosion of mild steel in 1 M HCl, J. Mol. Struct. 1136 (2017) 127–139.

109. L.C. Murulana, M.M. Kabanda, E.E. Ebenso, Experimental and theoretical studies on the corrosion inhibition of mild steel by some sulphonamides in aqueous HCl, RSC Adv. 5 (2015) 28743–28761.

110. G. Karthik, M. Sundaravadivelu, Studies on the inhibition of mild steel corrosion in hydrochloric acid solution by atenolol drug, Egypt. J. of Petrol. 25 (2016) 183–191.

111. L.C. Murulana, A.K. Singh, S.K. `Shukla, M.M. Kabanda, E.E. Ebenso, Experimental and quantum chemical studies of some bis(trifluoromethyl-sulfonyl) imide imidazolium-based ionic liquids as corrosion inhibitors for mild steel in hydrochloric acid solution, Ind. Eng. Chem. Res. 51 (2012) 13282–13299.

112. A.K. Singh, M.A. Quraishi, Adsorption properties and inhibition of mild steel corrosion in hydrochloric acid solution by ceftobiprole, J. Appl. Electrochem. 41 (2011) 7–18.

113. O. El Khattabi, B. Zerga, M. Sfaira, M. Taleb, M. Ebn Touhami, B. Hammouti, L. Herrag, M. Mcharfi, On the adsorption properties of an imidazole-pyridine derivative as corrosion inhibitor of mild steel in 1 M HCl, Der. Pharma Chem. 4 (2012) 1759–1768.

114. D.K. Yadav, M.A. Quraishi, B. Maiti, Inhibition effect of some benzylidenes on mild steel in 1 M HCl: an experimental and theoretical correlation, Corros. Sci. 55 (2012) 254–266.

115. L.O. Olasunkanmi, I.B. Obot, E.E. Ebenso, Adsorption and corrosion inhibition properties of N-{n-[1-R-5-(quinoxalin-6-yl)-4, 5-dihydropyrazol-3-yl] phenyl}

methanesulfonamides on mild steel in 1 M HCl: experimental and theoretical studies, RSC Adv. 6 (2016) 86782–86797.

116. M.A. Chidiebere, C.E. Ogukwe, K.L. Oguzie, C.N. Eneh, E.E. Oguzie, Corrosion inhibition and adsorption behaviour of punica granatum extract on mild steel in acidic environments: experimental and theoretical studies, Ind. Eng. Chem. Res. 51 (2012) 668–677.
117. M.J. Palimi, M. Rostami, M. Mahdavian, B. Ramezanzadeh, A study on the corrosion inhibition properties of silane-modified Fe_2O_3 nanoparticle on mild steel and its effect on the anticorrosion properties of the polyurethane coating, J. Coat. Technol. Res. 12 (2015) 277–292.
118. M.E. Mashuga, L.O. Olasunkanmi, A.S. Adekunle, S. Yesudass, M.M. Kabanda, E.E. Ebenso, Adsorption, thermodynamic and quantum chemical studies of 1-hexyl-3-methylimidazolium based ionic liquids as corrosion inhibitors for mild steel in HCl, Materials. 8 (2015) 3607–3632.
119. R. Karthikaiselvi, S. Subhashini, Study of adsorption properties and inhibition of mild steel corrosion in hydrochloric acid media by water soluble composite poly (vinyl alcohol-o-methoxy aniline), J. Assoc. Arab Univ. Basic Appl. Sci. 16 (2014) 74–82.
120. H.U. Nwankwo, L.O. Olasunkanmi, E.E. Ebenso, Experimental, quantum, chemical and molecular dynamic simulations studies on the corrosion inhibition of mild steel by some carbazole derivatives, Sci. Rep. 7 (2017) 1–18.
121. J. Dahdele, I. Danaee, G.R. Rashed, Thermodynamic and adsorption isotherm of N, N'-bis (2, 4, 6-trihydroxyacetophenone)-2, 2-dimethylpropandiimine as a corrosion inhibitor on SA-210 steel in alkaline NaCl solution, J. Chil. Chem. Soc. 61 (2016) 3025–3030.
122. D. Daoud, T. Douadi, S. Issaadi, S. Chafaa, Adsorption and corrosion inhibition of new synthesized thiophene schiff base on mild steel X52 in HCl and H_2SO_4 solutions, Corros. Sci. 79 (2014) 50–58.
123. O.O. Fadare, A.E. Okoronkwo, E.F. Olasehinde, Assessment of anti-corrosion potentials of extract of ficus asperifolia-miq (moraceae) on mild steel in acidic medium, Afr. J. Pure Appl. Chem. 10 (2016) 8–22.
124. S. John, A. Joseph, Electroanalytical and theoretical investigations of the corrosion inhibition behaviour of Bis-1, 2, 4-Triazole precursors EBATT and BBATT on mild steel in 0.1 N HNO_3, Ind. Eng. Chem. Res. 51 (2012) 16633–16642.

125. A. Zarrouk, B. Hammouti, A. Dafali, M. Bouachrine, H. Zarrok, S. Boukhris, S.S.A. Al-Deyab, A theoretical study on the inhibition efficiencies of some quinoxalines as corrosion inhibitors of copper in nitric acid, J. Saudi Chem. 18 (2014) 450–455.
126. A.K. Dubey, G. Singh, Corrosion inhibition of mild steel in sulphuric acid solution by using polyethylene glycol methyl ether (PEGME), Port. Electrochim. Acta. 25 (2007) 221–235.
127. N.A. Negm, N.G. Kandile, E.A. Badr, M.A. Mohammed, Gravimetric and electrochemical evaluation of environmentally friendly non-ionic corrosion inhibitors for carbon steel in 1 M HCl, Corros. Sci. 65 (2012) 94–103.
128. A.S. Raja, S. Rajendran, P. Satyabama, Inhibition of corrosion of carbon steel in well water by DL-phenylalanine-Zn^{2+}, J. Chem. 2013 (2012) 1–8.
129. S. Bourichi, Y.K. Rodi, M.E. Azzouzi, Y. Kharbach F.O. Chahdi, A. Aouniti, Inhibitive effect of new synthetized imidazopyridine derivatives for the mild steel corrosion in hydrochloric acid medium, JMES. 8 (2017) 1696–1807.
130. A. Singh, Y. Lin, M.A. Quraishi, L.O. Olasunkanmi, O.E. Fayemi, Y. Sasikumar, B. Ramaganthan, I. Bahadur, I.B. Obot, A.S. Adekunle, M.M. Kabanda, Porphyrins as corrosion inhibitors for N80 steel in 3.5 % NaCl solution: electrochemical, quantum chemical, QSAR and monte carlo simulations studies, Molecules 20 (2015) 15122–15146.

APPENDIX: FORMULAE USED

1. **Potentiodynamic polarization inhibition efficiency:**

$$IE_i = \frac{i^0_{corr} - i^i_{corr}}{i^0_{corr}} \times 100$$

2. **Electrochemical impedance spectroscopy inhibition efficiency:**

$$IE_z = \frac{R_{ct} - R^0_{ct}}{R_{ct}} \times 100$$

3. **Linear polarization resistance inhibition efficiency:**

$$IE_p = \frac{R_p - R^0_p}{R_p} \times 100$$

4. **Surface coverage (EIS):**

$$\theta = 1 - \frac{R^0_{ct}}{R_{ct}}$$

5. **Current response, constant phase element (CPE):**

$$Z_{CPE} = Y_0^{-1}(i\omega)^{-n}$$

6. **Double layer resistance (C_{dl}):**

$$C_{dl} = (Y_0 R_{ct}^{1-n})^{1/n}$$

7. **Thickness of the protective layer:**

$$C_{dl} = \frac{\varepsilon\, \varepsilon_o}{d}$$

8. **Surface coverage (with thermodynamic parameters):**

$$\theta = \frac{K_{ads} C_{inh}}{1 + K_{ads} C_{inh}}$$

9. **Surface coverage (with thermodynamic parameters) rearranged:**

$$\frac{C_{inh}}{\theta} = \frac{1}{K_{ads}} + C_{inh}$$

10. **Equilibrium constant (K_{eq}):**

$$RT \ln K_{eq} = -\Delta G^0 = nF\Delta E^0$$

11. **Gibb's free energy of adsorption:**

$$\Delta G°_{ads} = -RT\ ln(55.5K_{ads})$$